Experimental and Numerical Investigation on Wave Interaction with Submerged Breakwater

M.Sc. Engineering Thesis

by

Silwati Al Womera

Department of Water Resources Engineering
Bangladesh University of Engineering and Technology (BUET)
Dhaka

January 2011

Experimental and Numerical Investigation on Wave Interaction with Submerged Breakwater

M.Sc. Engineering Thesis

by
Silwati Al Womera

Submitted to

Department of Water Resources Engineering,
Bangladesh University of Engineering and Technology, Dhaka
in partial fulfillment of the requirement for the degree of
Master of Science in Water Resources Engineering

Department of Water Resources Engineering
Bangladesh University of Engineering and Technology (BUET)
Dhaka

January 2011

Bangladesh University of Engineering and Technology, Dhaka

Department of Water Resources Engineering

Certification of Thesis

The thesis titled "**Experimental and Numerical Investigation on Wave Interaction with Submerged Breakwater**", submitted by Silwati Al Womera, Roll No. 100716008P, Session October 2007, to the Department of Water Resources Engineering, Bangladesh University of Engineering and Technology, has been accepted as satisfactory in partial fulfillment of the requirements for the degree of Master of Science in Water Resources Engineering and approved as to its style and content. Examination held on January 3, 2011.

_____

Dr. Md. Ataur Rahman — Chairman (Supervisor)
Associate Professor
Department of Water Resources Engineering
Bangladesh University of Engineering and Technology
Dhaka

_____

Dr. Md. Abdul Matin — Member (Ex-officio)
Professor
Department of Water Resources Engineering
Bangladesh University of Engineering and Technology
Dhaka

_____

Dr. M. F. Bari — Member
Professor
Department of Water Resources Engineering
Bangladesh University of Engineering and Technology
Dhaka

_____

Mr. Abu Saleh Khan — Member (External)
Deputy Executive Director
Institute of Water Modelling
Mohakhali, Dhaka

Candidate's Declaration

It is hereby declared that this thesis or any part of it has not been submitted elsewhere for the award of any degree or diploma.

Supervisor

_____

Dr. Md. Ataur Rahman
Associate Professor
Department of Water Resources Engineering
Bangladesh University of Engineering and Technology, Dhaka.

Candidate

_____

Silwati Al Womera
Roll No. 100716008P

TABLE OF CONTENTS

LIST OF FIGURES

PAGE NO.

ACKNOWLEDGEMENT

First of all, I must express gratitude and homage to the Almighty Allah for providing me the knowledge and capability to successfully complete the thesis. Then I would like to acknowledge my gratefulness and reverence to Dr. Md. Ataur Rahman, Associate Professor, Department of Water Resources Engineering (WRE), Bangladesh University of Engineering and Technology (BUET). His constant supervision, vast experience and in-depth knowledge in wave theory, scholarly guidance with precious advice and witty encouragement have been a great impetus to the accomplishment of this thesis work.

Sincere thanks are due to the other members of the Board of Examiners: Professor Dr. Md. Abdul Matin, Head of the Department of WRE, BUET, Professor Dr. M. Fazlul Bari, Department of WRE, BUET and Mr. Abu Saleh Khan, Deputy Executive Director, Institute of Water Modelling, Dhaka. Their valuable comments, careful review, constructive criticism and suggestions on this study are duly appreciated.

Special thanks go to Mr. Musfique Ahmed, undergraduate student, Department of WRE, BUET, for his sincere assistance in the collection of data during the laboratory experiments. I also like to thank the laboratory Assistants of the Hydraulics and River Engineering Laboratory of Bangladesh University of Engineering and Technology and all those who have helped me in conducting the laboratory experiments.

Last but not the least, I would like to express my gratitude to my parents, father-in-law and mother-in-law for their incessant inspiration and encouragement. The sacrifices, patience, moral support and help given to me from my husband Mr. Tanveer Awal, Assistant Professor, Department of Computer Science and Engineering, BUET, are really invaluable and will never be forgotten.

Silwati Al Womera

ABSTRACT

In this research work the interaction between waves and rectangular submerged breakwater has been investigated. To investigate the performance of proposed rectangular type submerged breakwater, experimental studies are carried out in a two-dimensional wave flume (21.3 m long, 0.76 m wide and 0.74 m deep) at the Hydraulics and River Engineering Laboratory of Bangladesh University of Engineering and Technology. A set of experiments are carried out at 50 cm still water depth with fixed submerged breakwaters of three different heights (30 cm, 35 cm and 40 cm) for five different wave periods (1.5 sec, 1.6 sec, 1.7 sec, 1.8 sec and 2.0 sec) in the same wave flume. For 15 run conditions, data of water surface at different locations are collected manually by providing a vertical scale on the flume side made of glass. Six different locations both in front of and behind the breakwater are selected for data collection. Also the type of wave breaking and position of wave breaking are simultaneously recorded with a digital video camera. Effects of breakwater height and length along the wave direction on wave height reduction are analyzed.

Two-dimensional numerical model based on the SOLA-VOF method developed for wave interaction with floating breakwater has been updated in this research to study the wave interaction with fixed submerged breakwater. The SOLA-VOF model allows an efficient tracking of the free surface. It is based on the concept of a fractional Volume Of Fluid (VOF) for tracking free surface boundaries using the donor–acceptor approximation algorithm. The treatment of the free surface configuration using a single VOF function F is computationally very efficient. The SOLA scheme is employed to calculate the pressure and velocities in each time step and the added dissipation zone method is adopted to treat the open boundary. The basic equations used for VOF method are the continuity equation, the Navier-Stokes equation for incompressible fluid and the advection equation representing the behavior of the free surface. Because the wave generation source is placed within the computational domain, these equations involve the wave generation source.

The developed numerical model is verified by comparing the model generated wave with the wave as per Stokes 3rd order wave theory. The time series water surface profiles, water particle velocity field, VOF function F, pressure around a breakwater of different heights (20 cm, 25 cm, 30 cm, 35 cm and 40cm) are simulated using the numerical model. The experimentally measured data shows good agreement with the water surface profiles and breaking positions simulated by the developed numerical model. This study is expected to serve as a useful model to analyze wave deformation due to submerged breakwater and will be important for designing submerged breakwater as a coastal protection measure.

CHAPTER 1: INTRODUCTION

1.1 General

The coastal zone is a dynamic area comprising the natural boundary between land and ocean. In many countries of the world, the coastal zones have become the subject of major concern due to their multi-functional favorable uses. The intense uses of coastal zones, for building harbors, fisheries and recreational areas, utilizing food and mineral resources, energy procurement, industrial uses, providing water supply and so on, have make them multi-functional regions. However, the use of coastal zones is rather limited because of the existence of the wave actions, severe storm surges and tsunamis etc. Large-scale tsunamis and storm surges have occasionally flooded low-lying coastal areas and tremendous loss of life and property has been reported in various locations throughout the world.

Coastal Zone Policy 2005 defines that the coastal zone of Bangladesh consist of nineteen districts comprising one hundred and forty seven upazilas. Among them a total of forty eight upazilas are the exposed coasts and the remaining ninety-nine upazilas are interior coasts. The three basic natural system processes that govern opportunities and vulnerabilities of the coastal zone of Bangladesh are: tidal fluctuations; salinities (soil, surface water, ground water); cyclone and storm surge risk. From the analysis of 22 year data (1977-1998), sea level rise has been estimated as maximum 7.8 mm/year at Cox's Bazar in Bangladesh which will force the increase in the salinity of the coastal rivers and will make the irrigation fields unfit for cultivation because of salt deposits. The effect of tectonic subsidence may be more pronounced for this rapid rise in sea level. At least one hundred and twenty three polders have been created through construction of 5110 kilometers of embankment providing protection to 1.5 million hector of coastal land in Bangladesh. But the performance of coastal polders mainly depends on the tidal characteristics of the rivers surrounding the polders and the degree of siltation in the rivers. So the exposed coastal areas of Bangladesh needs

appropriate coastal protection works badly to prevent the intrusion of sea water into the main land and to mitigate the shoreline erosion.

The first world-wide attempts to mitigate shoreline erosion problems were by the use of sea walls, revetments and groins. Groins are built approximately perpendicular to the shoreline and serve to trap a portion of the longshore sediment-laden current or the littoral drift. Long stretches of coastline may be protected by constructing a series of groins, known as groin field. Revetments and sea walls are constructed along eroding shorelines, frequently resulting in the disappearance of beach. Additional studies on whether the sea walls and revetments cause beach erosion have been underway, sometimes with conflicting results.

Recent developments in shore protection structures are offshore breakwaters. The primary objectives of an offshore breakwater system are to increase the longevity of a renourished beach, provide a wider beach for recreation and provide protection to upland areas from waves and flooding. Offshore breakwaters, also called bulkheads, reduce the intensity of wave action in inshore waters and thereby reduce coastal erosion. They are constructed some distance away from the coast or built with one end linked to the coast. The breakwaters may be placed one to three hundred feet offshore in relatively shallow water, designed to protect a gently sloping beach.

Breakwaters may be either fixed or floating: the choice depends on normal water depth and tidal range**.** Breakwater construction is usually parallel or perpendicular to the coast to maintain tranquility condition in the important coastal regions like port. Most of breakwater construction depends upon wave approach with consideration of some other environmental parameters. When oncoming waves hit these breakwaters, their erosive power is concentrated on these structures some distance away from the coast. In this way, there is an area of slack water behind the breakwaters. Deposition occurring in these waters and beaches can be built up

or extended in these waters. However, nearby unprotected sections of the beaches do not receive fresh supplies of sediments and may gradually shrink due to erosion, namely longshore drift.

Generally, many offshore breakwaters have been built with their crest above the water surface, that's to say, the emerge structures. Submerged breakwaters are a special type of breakwaters distinguished from other emerged offshore ones. They are built with their crests submerged in the water. With this advantage, they avoid the generation of significant reflected wave that affect the nearby shoreline. Although it might take some disadvantage for navigation, they may be used efficiently as a mean of erosion control as they provide an inexpensive measure of protecting beaches exposed to small or moderate waves and offer fast installation for temporary offshore works.

Fixed submerged breakwaters are more effective in reducing wave heights and are also less susceptible to structural failure during catastrophic storms. This nature-conscious coastal protection work has become increasingly popular due to their multiple functions, which are to protect shoreline or harbor and to prevent beach erosion by providing a safe and agreeable environment in coastal areas. This structure scarcely harms the coastal scenery nor obstructs the utilization of sea area; thus, by creating a calm sea, it facilitates the utilization of the sea for recreational and residential developments.

For safety design, many researchers have investigated the interaction between waves and the fixed submerged breakwater experimentally and numerically. In this study, two-dimensional experimental studies are carried out in the laboratory to investigate the performance of submerged breakwater in wave breaking as well as dissipating the incoming wave energy. The two-dimensional moored floating body–wave interaction model developed by Rahman (2005) is updated to adapt it for simulating wave interaction with submerged breakwater. Also experimentally measured data are used to compare with the numerical simulation, thus to check the validity of the developed numerical model.

1.2 Different types of coastal protection works

Successful long-term coastal protection solutions seek to directly address and work with the natural physical processes responsible for the erosion problems. To select the most appropriate device(s) for a particular site both an understanding of the existing physical environment of the site and an understanding of the function and impact of various coastal protection options are required. This section describes the existing knowledge of the function and impacts of various coastal protection options that are presently used world-wide. The two different types of coastal protection works are the hard structural coastal protection options and the soft structural coastal protection options.

1.2.1 Hard structural/engineering options

Hard structural/engineering options use structures constructed on the beach or further offshore. The examples of onshore hard structures may be seawalls, groins, breakwaters/artificial headlands whereas, offshore breakwaters are the most common examples of offshore coastal protection works. These options influence coastal processes to stop or reduce the rate of coastal erosion.

(a) Groin

Groin is a coastal structure constructed perpendicular to the coastline from the shore into the sea to trap longshore sediment transport or control longshore currents. This type of structure is easy to construct from a variety of materials such as wood, rock or bamboo and is normally used on sandy coasts. They form a cross-shore barrier that traps sand that moves alongshore, thereby increasing the width of the beach on the upstream side. Thus, they function best on beaches with a predominant alongshore transport direction. Some disadvantages of groins are:

- Induces local scour at the toes of the structures.
- Causes erosion downdrift; requires regular maintenance.
- Typically more than one structure is required.

Some photographs of existing groins are shown in Fig. 1.1.

(b) Seawall

A seawall is a structure constructed parallel to the coastline that shelters the shore from wave action. This structure has many different designs; it can be used to protect a cliff from wave attack and improve slope stability and it can also dissipate wave energy on sandy coasts. The disadvantages of this structure are:

- It creates wave reflections and promotes sediment transport offshore.
- Scour occurs at the toes of eroded beaches.
- It does not promote beach stability.
- It should be constructed along the whole coastline; if not, erosion will occur on the adjacent coastline.

Fig. 1.2 shows some photo views of seawalls.

(c) Artificial headland

This structure is constructed to promote natural beaches because it acts as an artificial headland. It is relatively easy to construct and little maintenance is required. The disadvantages of these structures are:

- It is a relatively large structure.
- It can cause erosion downdrift of the protected length of coastline.
- Has poor stability against large waves.

Some artificial headlands are shown in Fig. 1.3.

(d) Offshore Breakwater

The main purpose of installing a breakwater is to reduce the height of incident water waves on the leeward side to a level compatible with the intended use of the site to be protected. Thus offshore breakwaters provide shelter from waves that trap sand by manipulating the littoral transport. Fig. 1.4 shows some photographs of offshore breakwaters. It reduces wave energy in its lee and creates a calm water body behind the structure that influences longshore transport of sediment. More recently, most offshore breakwaters have been of the submerged type; they become multipurpose artificial reefs where fish habitats develop and enhance surf breaking for water sport activities. These structures are appropriate for all

coastlines. There are different types of breakwaters like floating breakwater and submerged breakwater.

Fig.1.1: Groins

Fig.1.2: Sea wall

Fig.1.3: Headland

Fig.1.4: Offshore breakwater

(i) Floating breakwaters

Floating breakwaters (Fig. 1.5) are normally used as piers in marinas, but they are also used as protective structures for marinas in semi-protected areas. They are especially suited for areas where the tidal range is high, as they follow the water-level. Floating breakwaters work by dissipating and reflecting part of the wave energy. No surplus water is brought into the sheltered area in this situation. Floating breakwaters are seldom used as shoreline management structures because they are not suitable for installation in the open sea. Floating breakwaters can only be used in waters of very limited fetch.

Fig. 1.5 : Floating breakwater

Advantages of floating breakwater

- Floating breakwaters are less expensive than fixed structures in deeper water (depths greater than 10 feet).
- Floating breakwaters can effectively attenuate moderate wave heights (less than about 6.5 feet).
- Poor soil conditions may make floating breakwaters more feasible to use than heavy rubble fixed breakwaters.
- Floating breakwaters can be easily moved and rearranged in different layouts or transported to another site.

Disadvantages of floating breakwater

- Floating breakwaters are less effective in reducing wave heights for slow waves than fixed structures are; a practical upper limit for the design wave period is in the range of 4 to 6 seconds.
- Floating breakwaters are susceptible to structural failure during catastrophic storms.
- If the structure fails and is detached from its moorings, the breakwater may become a hazard.
- Relative to common fixed breakwaters, floating breakwaters require a high amount of maintenance.

(ii) Submerged or low-crested breakwater

Submerged or low-crested breakwaters (Fig. 1.6) function by inducing wave-breaking and by allowing some wave transmission so that a milder wave climate is obtained in lee of the submerged structure.

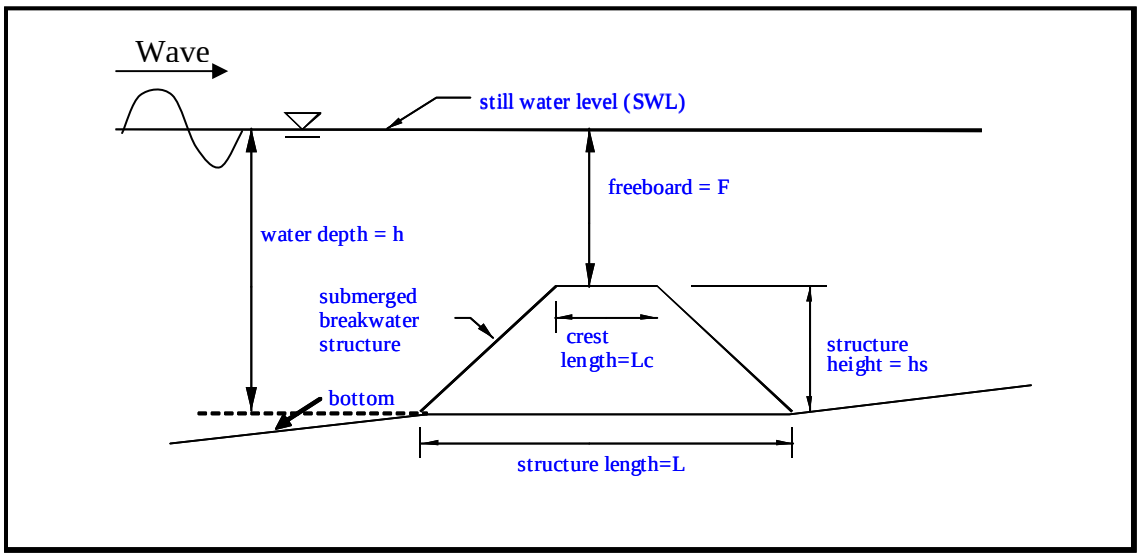

Fig. 1.6 : Definition sketch for submerged breakwater

A submerged breakwater is constructed some distance away from the coast or built with one end linked to the coast. As the sediment transport capacity behind the breakwater is decreased, sand is accumulated in the low energy zone behind the submerged breakwater. This structure is designed to absorb the energy of the

waves that hit it. This is done either by using mass (e.g. with caissons) or by using a revetment slope (e.g. with rock or concrete armour units).Caisson breakwaters (Fig. 1.7 (a)) typically have vertical sides and are usually used where it is desirable to berth one or more vessels on the inner face of the breakwater. They use the mass of the caisson and the fill within it to resist the overturning forces applied by waves hitting them. They are relatively expensive to construct in shallow water, but in deeper sites they can offer a significant saving over revetment breakwaters. Rubble mound breakwaters (Fig. 1.7 (b)) use the voids in the structure to dissipate the wave energy. Rock or concrete armour units on the outside of the structure absorb most of the energy, while gravels or sands are used to prevent the wave energy continuing through the breakwater core. The slopes of the revetment are typically between 1:1 and 1:2, depending upon the materials used. In shallow water revetment breakwaters are usually relatively cheap, but as water depth increases, the material requirements, and hence costs increase significantly.

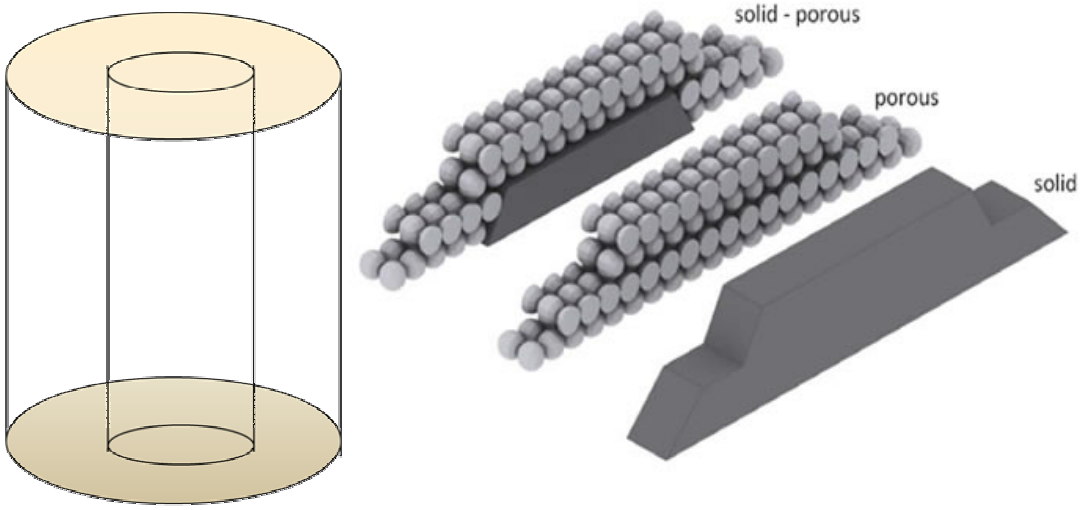

(a) Caisson breakwater (b) Rubble mound breakwaters

Fig. 1.7 : Different types of submerged breakwaters

When oncoming waves hit these breakwaters, their erosive power is concentrated on these structures some distance away from the coast. In this way, there is an

area of slack water behind the breakwaters. Deposition occurring in these waters and beaches can be built up or extended in these waters. This is shown in Fig. 1.8.

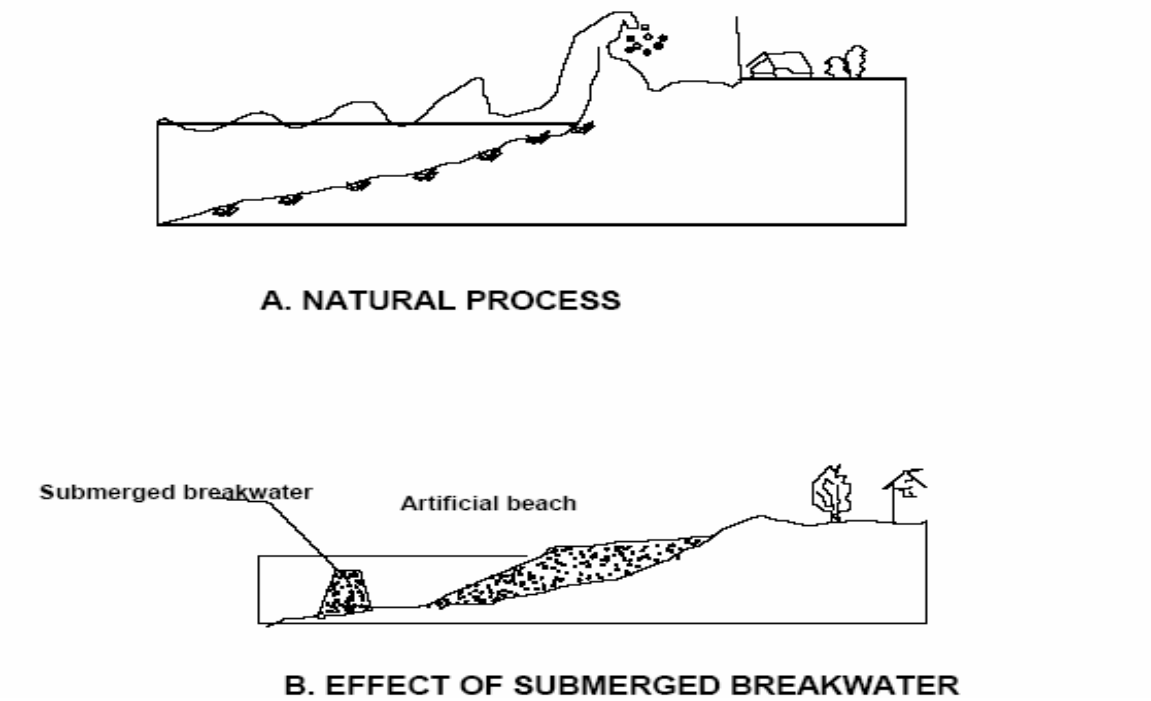

Fig. 1.8 : Role of submerged breakwater to prevent beach erosion

Reasons for selecting a submerged/low breakwater

- The visual impact of a submerged/low structure is less damaging.
- A submerged or low-crested structure is less expensive.
- The impact on the sand accumulation is smoother.
- The overtopping water generates good water circulation behind breakwater.
- Submerged breakwaters are very similar to natural reefs. They attract fish and are therefore economically beneficial.

Disadvantages of submerged/low crested breakwater

- A submerged structure can be dangerous for small craft navigation

- The overtopping water initiates local currents, which can be dangerous for swimmers
- A submerged or low-crested structure provides only partial attenuation of the wave action as well as partial shore protection and coast protection
- The efficiency of a submerged structure with respect to shore protection by the reduction of both waves and littoral transport very much depends on the crest freeboard of the design.
- The design is very difficult and challenging because the proper function of a submerged or low-crested structure depends on both water-level and wave conditions as well as on the specific structure.

1.2.2 Soft structural/engineering options

Soft structural/engineering options aim to dissipate wave energy by mirroring natural forces and maintaining the natural topography of the coast. They include beach nourishment or feeding, dune building, revegetation and other non-structural management options.

(a) Beach nourishment

The aim of beach nourishment is to create a wider beach by artificially increasing the quantity of sediment on a beach experiencing sediment loss, improving the amenity and recreational value of the coast and replicating the way that natural beaches dissipate wave energy. Offshore sediment can be sourced and is typically obtained from dredging operations; landward sources are an alternative, but are not as effective as their marine equivalents because the sediment has not been subject to marine sorting. This method requires regular maintenance with a constant source of sediment and is unlikely to be economical in severe wave climates or where sediment transport is rapid. It has been used in conjunction with hard structural/engineering options, i.e. offshore breakwaters, headlands and groins to improve efficiency. Some photo views of beach nourishment are shown in Fig.1.9.

(b) Dune building/reconstruction

Sand dunes are unique among other coastal landforms as they are formed by wind rather than moving waters; they represent a store of sand above the landward limits of normal high tides where their vegetation is not dependent on the inundation of seawater for stability. They provide an ideal coastal defense system; vegetation is vital for the survival of dunes because their root systems bind sediment and facilitate the build-up of dune sediment via wind baffle. During a storm, waves can reach the dune front and draw the sand onto the beach to form a storm beach profile; in normal seasons the wind blows the sand back to the dunes. In dune building or reconstruction, sand fences and mesh matting in combination with vegetation planting have successfully regenerated dunes via sediment entrapment and vegetation colonization. The vegetation used should be governed by species already present, such as marram, sand couch grass and lyme grass. Fig. 1.10 shows some photos of dune building.

(c) Coastal revegetation

Based on studies and scientific results, the presence of vegetation in coastal areas improves slope stability, consolidates sediment and reduces wave energy moving onshore; therefore, it protects the shoreline from erosion. It may be successful in estuarine conditions with low energy environment if the environmental conditions favour the growth of species at the particular site and there is adequate knowledge on proper way of plantation. Site suitability for vegetation can be extended by other factors such as the beach slope, site elevation, tidal range and salinity of sea water and other existing hydrological parameters. Some photo views of coastal revegetation are shown in Fig.1.11.

1.3 Literature Review

Breakwaters may be either fixed or floating: the choice depends on normal water depth and tidal range. Two types of breakwaters were used during the Normandy invasion of World War II. The first were fixed breakwaters that were barges

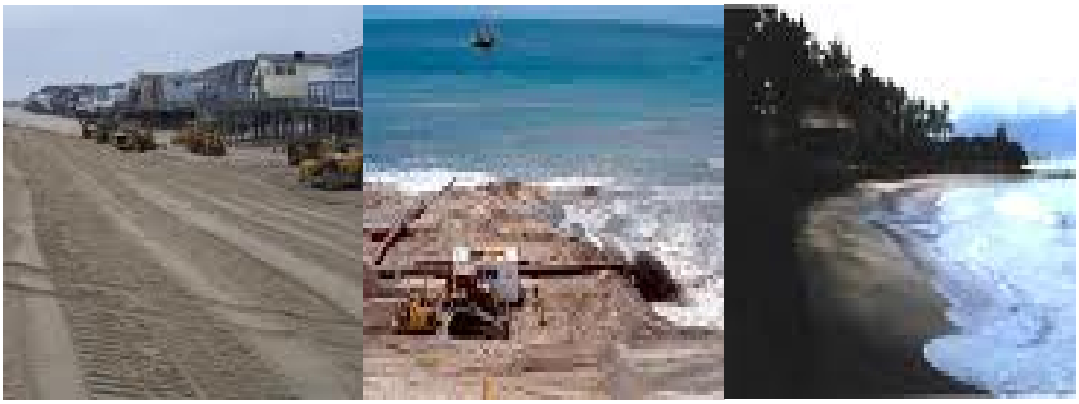

Fig.1.9: Beach Nourishment

Fig. 1.10: Dune building

Fig.1.11: Coastal revegetation

floated from Great Britain positioned just off shore and sunk. The second were actual floating breakwaters. These floating breakwaters were steel structures arranged in two lines along the Normandy coast.

Research engineers and scientists have realized the potential for breakwaters in certain areas, and research interest has been directed towards this subject during the last decades. Among the two types of breakwaters, fixed submerged breakwaters are more effective in reducing wave heights and are also less susceptible to structural failure during catastrophic storms.

The interaction of wave with submerged, bottom founded, or floating surface-piercing structures have been studied experimentally by many investigators and among them some researchers developed or updated numerical model for presenting a systematic solution for their particular problems. Several reports on submerged breakwaters have appeared in the recent past (Rufin, Mizutani, Iwata, 1996; Mizutani, Mostofa, Hur, 1998; Golshani, Mizutani, Hur,2003; Hur. D.S., 2003; Hur, Kawashima and Iwata, 2003), and the state-of-the-art literature review for complete review of the performance characteristics of various types of submerged breakwaters is done (Cheng, S., Liu, S. and Zheng, 2003).

Dong-Soo Hur (2003) investigated the wave deformation of multi-directional random waves passing over an impermeable submerged breakwater installed on the slope. The experiments were carried out in the three-dimensional wave basin which is equipped with a multi-directional random wave generator with a segmented wave-maker installing the wooden submerged breakwater on a sloping bed. To estimate the location and limit of wave breaking Hur, Kawashima and Iwata (2003) conducted experiments in a three-dimensional wave basin a multi-directional random wave generator. This study investigates experimentally the breaking wave height of multi-directional random waves passing over an impermeable submerged breakwater. A special type of wave gauge has been newly devised to record the water surface elevations in the breaker zone as accurately as possible. A study on application analysis of submerged breakwaters

to compare the reflection and transmission characteristics with other kinds of breakwaters were done by Cheng (2003). He studied the performance of different types of submerged breakwaters both experimentally and numerically.

Al-Banna and Liu (2007) conducted a numerical study on the hydraulic performance of submerged porous breakwater under solitary wave attack based on solving the Reynolds-Averaged Navier-Stokes (RANS) equations. Lee et al. (2007) studied the transformation of irregular waves propagating over a submerged breakwater. By providing the incident irregular waves with repeatable amplitude and phase for each wave component, effects of the height and width of the breakwater on the wave transformation were studied systematically. Lau et al. (1990) solved the three-dimensional problem of the dynamics of a moored floating object under the action of regular waves numerically as a boundary value problem by the use of the infinite element method. Sen (1993) developed a numerical method to simulate the motions of two-dimensional floating bodies. Shirakura et al. (2000) developed a 3-D fully nonlinear wave tank to simulate floating bodies interacting with water waves. They used quadratic boundary element method (QBEM) to solve the velocity field and acceleration field taking into account the interaction between the fluid and the floating body motions. Hur and Mizutani (2003) have developed a numerical model, which combine the VOF model and porous body model, to estimate the wave forces acting on a three-dimensional body on a submerged breakwater. They examined wave induced deformation on the permeable submerged structure making use of the porous body model (Sakakiyama and Kajima, 1992) to express the governing equations of fluid motion. Rahman (2005) developed a two-dimensional numerical model combining the SOLA-VOF model and porous body model, to estimate the wave forces acting on a pontoon type submerged floating breakwater.

1.4 Study Objectives

In this research work the interaction between waves and rectangular submerged breakwater has been investigated. To predict the interaction, a two-dimensional

numerical model based on the SOLA-VOF method is proposed here. Also a two-dimensional laboratory experiment has been carried out to investigate the performance of submerged breakwater in wave breaking as well as in dissipating the wave energy in terms of reduction of wave height.

The specific objectives of this study are:

(i) To conduct experimental investigation of wave interaction with submerged breakwater.
(ii) To adapt a two-dimensional numerical model using the Volume Of Fluid (VOF) technique to simulate interaction (wave breaking, deformation, energy dissipation etc) between wave and submerged breakwater.
(iii) To verify the performance of the developed numerical model by comparing the model simulated water surface profiles with the experimentally measured data.

1.5 Study Scope and Contents

The interaction between a rectangular shaped fixed type submerged breakwater and waves is studied in this thesis. Both the numerical and experimental studies are carried out in a two-dimensional field. The numerical studies evaluate water surface profiles along the channel length, distribution of water particle velocity field, the value of VOF function F and pressure around the breakwater, etc. Laboratory experiments are carried out in a two-dimensional wave tank with different wave conditions and different submergence ratios of the breakwater. All the theories, analyses, numerical estimations, experimental investigations are presented in the following chapters.

In Chapter 2, the details of the numerical model are discussed. The key developments of VOF type numerical models are summarized here. Then the modified governing equations and boundary conditions used in the model are described. The elaborated discussions of the computational procedures in

numerical model are also given in this chapter. Then the numerical stability considerations are presented in chapter 2. The detail of Volumes of Fluid method (VOF) in the developed model are described then. The computational procedures using SOLution Algorithm (SOLA) scheme are also presented. Finally the donor-acceptor flux approximation used for improved free water surface shaping are described.

In Chapter 3, the details of the laboratory experiment are described. Two experimental investigations are carried out. Experiments were carried out with three different submergence ratios of the breakwater and five different wave conditions. The details of the experimental setup, submerged body model, experimental conditions, instrumentation and data acquisition system etc are presented in this chapter. The effect of breakwater height and breakwater length on wave height reduction in a given still water depth are investigated. Based on experimentally measured data water surface profiles along the channel length are developed .The wave breaking types and breaking positions are also investigated from the photographs and video clips taken during the laboratory experiments.

The numerical analyses of fixed submerged body under wave action are presented in Chapter 4. At first the verification of the numerical model based on SOLA-VOF scheme are done using the waves generated according to Stokes 3rd order wave theory. The numerical analyses are done for rectangular fixed submerged breakwater of varying heights under different wave conditions. The detail results of the numerical analyses of both wave breaking and non-breaking conditions are presented here. Time series water surface profiles, distribution of water particle velocity, VOF function F and pressure around fixed submerged breakwater of different heights are analyzed under different wave conditions. The comparisons between numerically simulated results with the experimentally measured data are also presented in this chapter.

Finally, an overview of the main conclusions of this study and recommendations for further study are presented in Chapter 5.

CHAPTER 2: LABORATORY EXPERIMENT

2.1 Introduction

To investigate the performance of proposed rectangular type submerged breakwater, experimental studies are carried out in a two-dimensional wave flume at the Hydraulics and River Engineering Laboratory of Bangladesh University of Engineering and Technology. A set of experiments are carried out with fixed submerged breakwaters of different heights for different wave periods in the same wave flume. All about the experiments are presented in the following sections.

2.2 Wave-structure interaction and wave breaking criteria

The waves approaching the shoreline break due to small depths. Because of the breaking process wave energy is dissipated, which energy is converted mainly into turbulence. The wave action causes an increase in the mean water level in the breaker one which is defines as wave set-up. Part of the wave will proceed up the beach, where it rushes up and back along the slope, usually referred to as run-up or run-down. The important wave characteristics are:

- Wave height, H: vertical distance from the top of the crest to the bottom of the trough.
- Wave length, L: horizontal distance between two successive crests.
- Wave period, T: time between two successive crests to pass a certain point.

Usually, the most concentrated change that occurs to waves as they propagate forward takes place when they interact with a variety of structures, including beaches. When wave arrive at a structure, be floating or fixed, they will undergo some degree of reflection and dissipation. Moored floating structures allow a significant portion of the transmitted wave energy to directly pass the structure, but a component of the transmitted energy is produced by wave regeneration by

the moving structures. Wave run-up and overtopping of stone-mound breakwaters will cause wave transmission and regeneration of waves on the lee side and energy may be transmitted through the structure if it is sufficiently permeable. Wave transmission is accomplished by direct transmission of waves over the submerged solid stone mound structures. There is a decrease in the transmitted energy owing to reflection and dissipation of some of the incident wave energy.

A breaking wave is one whose base can no longer support its top, causing it to collapse. A wave breaks when it runs into shallow water, or two wave systems oppose or combine forces. When the slope, or steepness ratio of a wave is too great, breaking is inevitable. Usually an oncoming wave breaks due to any of the following reasons.

- Individual waves in deep water break when the wave steepness H/L_0 (H= wave height, L_0 = wave length) exceeds about 0.17, so for wave height, H> 0.17L.
- In shallow water, with the water depth small compared to the wavelength, the individual waves break when their wave height, H is larger than 0.8 times the water depth, h. That is for H>0.8h.
- Waves can also break if the wind grows strong enough to blow the crest off the base of the wave.

A wave can dissipate its energy in a very short time or gradually. Battjes (1974) shown that the breaker type is closely related to the offshore similarity parameter:

$\xi_0 = \tan\alpha / (H_0 / L_0)^{0.5}$

where,

H_0 = deep water wave height,

L_0 = deep water wave length

$\tan\alpha$ = beach slope

The breaker type can be distinguished based on the value of ξ_0 as follows:

$\xi_0 < 0.5$: spilling

$0.5 < \xi_0 < 3$: plunging

$\xi_0 > 3$: surging or collapsing

Breaker index is another parameter which is defined as $\gamma_b = H_b / d_b$

where,

H_b= breaking wave height

d_b= depth at the point of wave breaking

2.3 Experimental setup

2.3.1 The two-dimensional wave flume

The wave flume is 21.3 meters long, 0.76 meter wide and 0.74 meter deep. The bottom of the wave flume is made of steel, whereas both of its sides are made of glass. In the wave flume artificial regular waves are generated by wave generator. To damp the transmitted wave a wave absorber is installed at the end of the flume. The two-dimensional wave flume is shown in Fig. 2.1.

Fig. 2.1 : Wave flume

2.3.2 The wave generator

The wave generator generates artificial regular waves of controlled wave period (T). The frequency of the wave paddle is set to the desired wave period (T) from a developed relationship between $4\pi^2 h/(gT^2)$ and $(e+f)/f$, where 'h' is the still water depth and 'g' is the gravitational acceleration. For this particular wave generator, 'e' and 'f' are the horizontal movement of the wave paddle at still water level and

at the bed of the flume respectively (Fig. 2.2 (a)). The wave generator is placed at one side of the wave flume which is also 800 cm in front of the rectangular fixed submerged breakwater. Fig. 2.2 shows some photo views of wave generator.

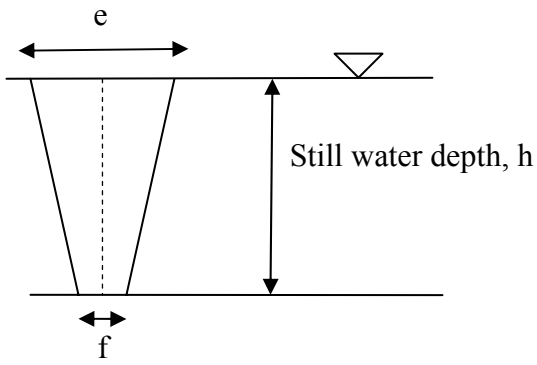

Fig. 2.2a: Wave generator

Fig.2.2b: Photo views of wave generator

After setting the frequency of the wave paddle of the wave generator, it is seen that the wave generator can generate waves with wave periods deviating very negligible amount (maximum ± 0.1%) from the desired wave period, which results slight difference in experimentally generated wavelength than that of actual one.

2.3.3 The submerged breakwater

A rectangular shaped fixed type submerged body is installed at the bottom of the flume. The submerged body is made by compacted sand. The top surface of the sand body is made impermeable by plastering with a mixture of cement and sand

in a ratio of 4:1 with appropriate amount of water. Two wooden plates (1.5 cm thick) are attached to the front and rear surfaces of the body. All the sides of this composite submerged body are tightly sealed with the flume to ensure full restriction to the water movement through the body. The dimensional and photo views of the submerged body are shown in Fig. 2.3.

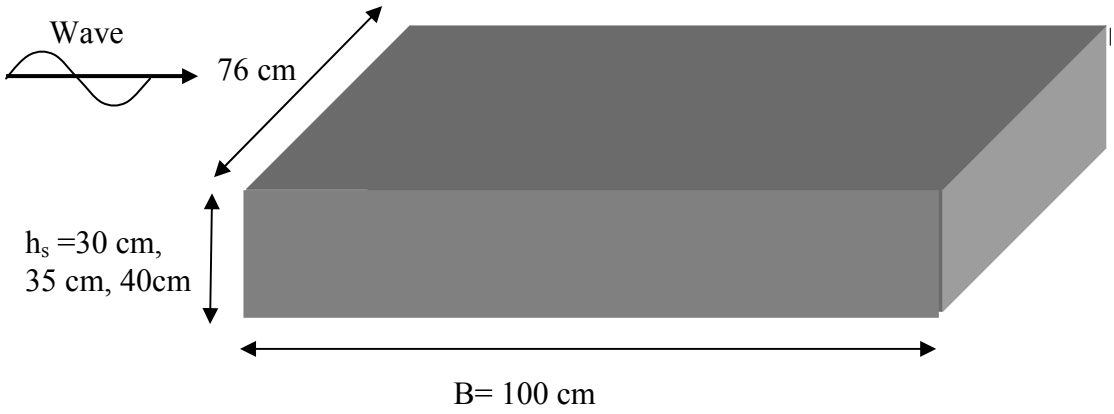

Fig.2.3a: Dimensional view of submerged breakwater

Fig.2.3b: Photo views of submerged breakwater

The width of breakwater along the wave direction is 100 cm and the length of breakwater is kept constant at 76 cm which is same as the width of the wave flume. 30 cm, 35 cm and 40 cm high breakwaters are used.

Basis of breakwater size selection:

Dick, T.M. and Brebner, A. (1968) proved in their study on solid and permeable submerged breakwaters that for optimum reduction in transmitted wave height, breakwater width B should be as large as possible in fact up to 2 wavelengths.

This is unlikely to be an economical proposition, so that some narrower breakwater with greater height was investigated later. Kawasaki, K., Iwata, K. (2001) investigated the breaking limit, the breaker type and the breaking point due to various submerged trapezoidal breakwaters. In their study, they found for relative structure height h_s/h =0.8, usually the waves break when the relative breakwater width B/L is in the range of 0.2 to 0.4.

In this study, the laboratory experiments are conducted for five different wave periods ranging from T= 1.5 sec to 2.0 sec and corresponding wavelengths of 250 cm to 400 cm to investigate the interaction of waves with submerged body of different relative structure heights of 0.6, 0.7 and 0.8 by installing breakwater heights of 30 cm, 35 cm and 40 cm in 50 cm depth of water. For optimum reduction in transmitted wave height, the breakwater width along the wave direction was selected as 100 cm so that the relative structure width B/L ranges from 0.25 to 0.4. Breakwater lengths are usually selected so that they can cover the protection required length of the coastline. In this two-dimensional study, the breakwater length is selected as 76 cm which covers the full width of the two-dimensional wave flume.

2.3.4 The wave absorber

To damp the transmitted wave after passing the breakwater a wave absorber is installed at the end of the wave flume. It is a sloped surface (3.3H : 1V) made of wood. Its total horizontal length is 245 cm. The wave absorber dissipates the

Fig. 2.4: Photo views of wave absorber

energy of the transmitted wave at the end of the flume to reduce the generation of reflecting wave. Fig. 2.4 shows the photo views of wave absorber.

2.3.5 Experimental setup

In 21.3 m long wave flume the wave generator is placed 190 cm downstream from the starting of the flume. The fixed submerged breakwater is installed at a distance of 800 cm from the wave generator. Six different positions are chosen for data collection. Three locations are in front of the fixed submerged breakwater to investigate the incident wave properties. The fourth position of data collection is set over the breakwater. Then the last two positions are chosen behind the breakwater to observe the effect of breakwater installation in reduction of wave height. The first position of data collection is at 400 cm in front of the breakwater. The other positions are at equidistance of 100 cm from each other. Then finally at the end of the flume a wave absorber of 245 cm length is installed. The detail of experimental setup is shown in Fig 2.5.

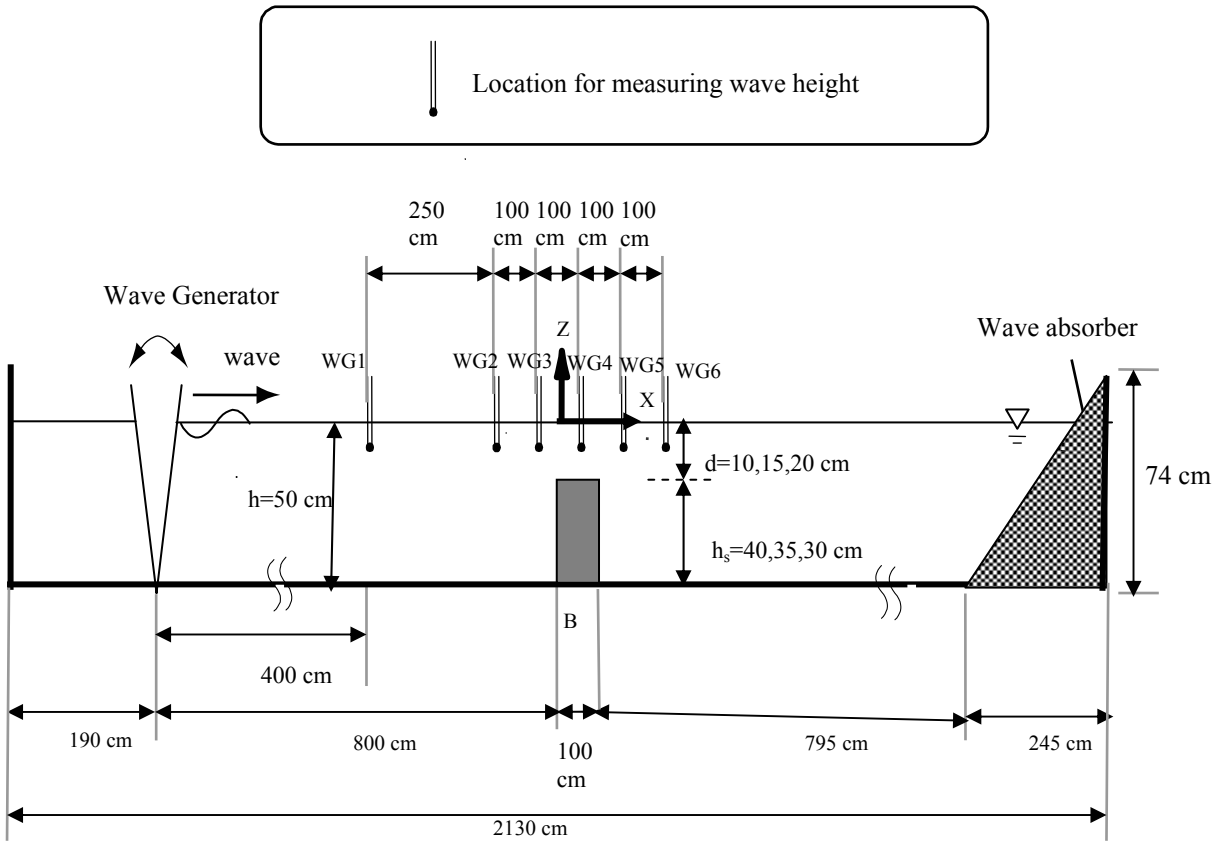

Fig.2.5: Detail of the experimental setup

2.4 Data acquisition

2.4.1 Laboratory experimental run conditions

A set of experiments are conducted by installing rectangular fixed submerged of three different relative structure heights as h_s /h= 0.6, 0.7 and 0.8 in still water depth of 50 cm. Five runs are conducted for five different regular waves with submerged breakwater of a particular height i.e. 30 cm, 35 cm and 40 cm . Five regular waves of wave periods 1.5 sec, 1.6 sec, 1.7 sec, 1.8 sec and 2.0 sec are generated by setting the frequency of the wave paddle of the wave generator. The detail of the experimental run conditions are given in table 2.1.

Table 2.1: Experimental Run Conditions

Run No.	**Still water depth, h cm**	**Incident Wave Property**			**Breakwater Property**			**Relative Structure Height, h_s /h**
		Wave Period, T_i sec	**Wave Height, H_i cm**	**Wave Length, L_i cm**	**Break-water width, B cm**	**Break-water Length, L cm**	**Break-water Height, h_s cm**	
1	50	1.5	10	282	100	76	30	0.6
2	50	1.6	12	307	100	76	30	0.6
3	50	1.7	13	332	100	76	30	0.6
4	50	1.8	14	357	100	76	30	0.6
5	50	2.0	15	406	100	76	30	0.6
6	50	1.5	10	282	100	76	35	0.7
7	50	1.6	12	307	100	76	35	0.7
8	50	1.7	13	332	100	76	35	0.7
9	50	1.8	14	357	100	76	35	0.7
10	50	2.0	15	406	100	76	35	0.7
11	50	1.5	10	282	100	76	40	0.8
12	50	1.6	12	307	100	76	40	0.8
13	50	1.7	13	332	100	76	40	0.8
14	50	1.8	14	357	100	76	40	0.8
15	50	2.0	15	406	100	76	40	0.8

2.4.2 Data collection

To understand the interaction between the wave and the fixed submerged breakwater, data of water elevation has been collected. Data of water surface has been collected manually by providing a vertical scale on the flume side made of glass (Fig. 2.6(a)).

Fig. 2.6 (a): Data collection

Six different locations both in front of and behind the breakwater were selected for data collection. Among these six positions three are in front of the breakwater, one is over the breakwater and the last two positions are behind the breakwater. These positions are chosen in such a way to understand the effect of installing submerged breakwater in reducing wave height. At each position data of water surface have been collected for one minute duration at five seconds interval.

To draw the water surface profile at any particular time, it is necessary to start the collection of data at each position simultaneously. This is done by starting the data acquisition at every position when the incident wave reaches the crest. Also the breaking position of wave in each run is measured.

Still photographs and video recordings are taken during each run. Some photographs taken during the experimental runs are given in Fig. 2.6(b) to Fig. 2.6(f). These are categorized as three different types as the incident waves approaching the breakwater; the breaking of waves over the middle of the breakwater, at the onshore end of the breakwater and just behind the breakwater; and the transmitted wave after passing the breakwater.

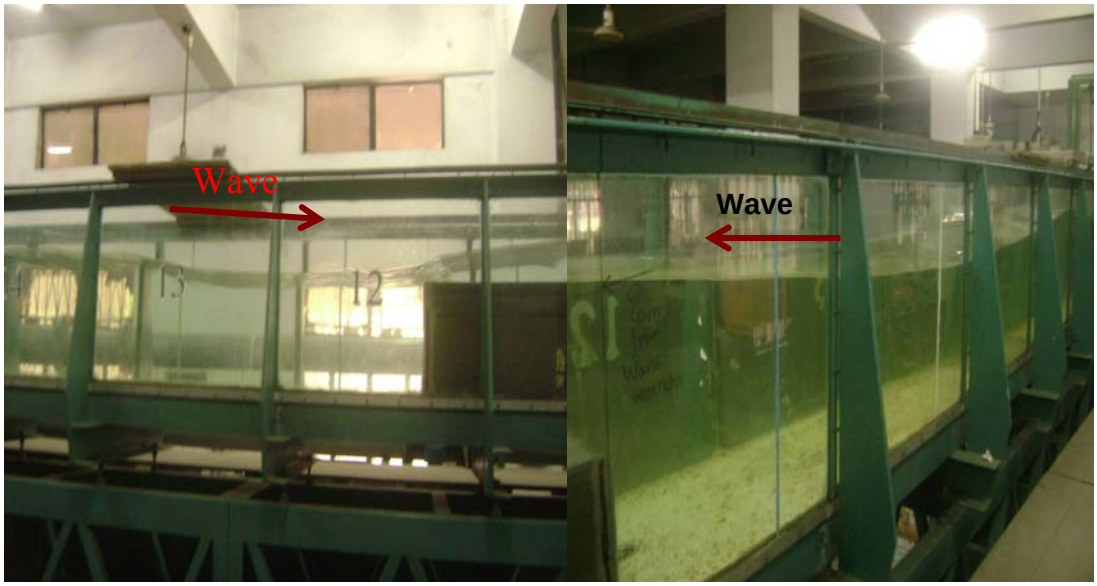

Fig. 2.6 (b): Wave approaching the breakwater

Fig. 2.6 (c): Wave breaking near the middle of the breakwater

Fig. 2.6 (d): Wave breaking at the onshore end of the breakwater

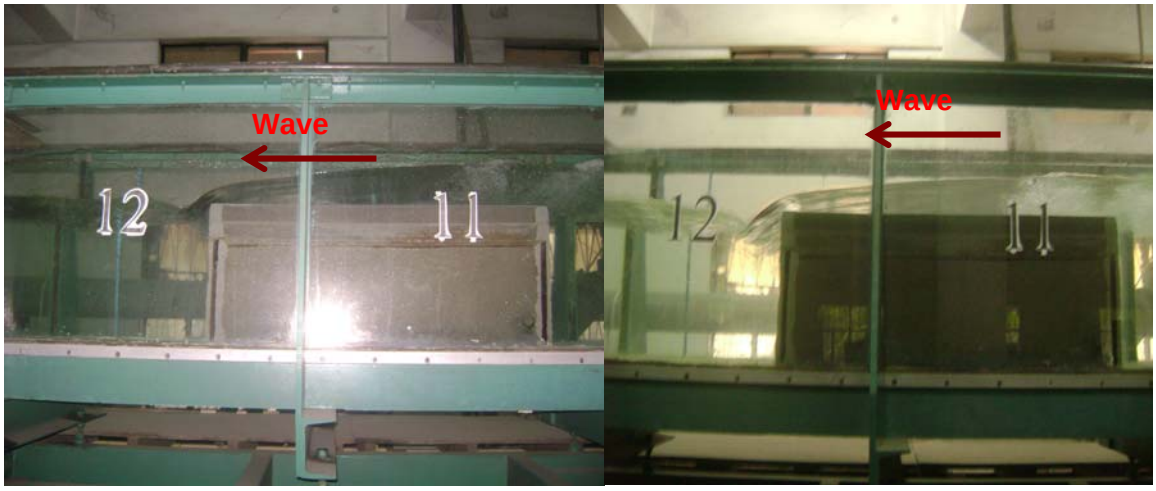

Fig. 2.6 (e): Wave breaking just behind the breakwater

Fig. 2.6 (f): Transmitted wave after passing the breakwater

2.5 Experimental results

2.5.1 Effect of relative structure height on wave height reduction

In Fig. 2.7 the effect of relative structure height, h_s /h (hs is the height of breakwater and h is the still water depth) on wave height reduction, H_b/H_i (H_b is the wave breaking height and H_i is the incident wave height) is shown for five different wave periods. From this figure it is clear that as the relative structure height, h_s /h increases, the breaking wave height, H_b decreases more with respect to the incident wave height, H_i for any particular wave period.

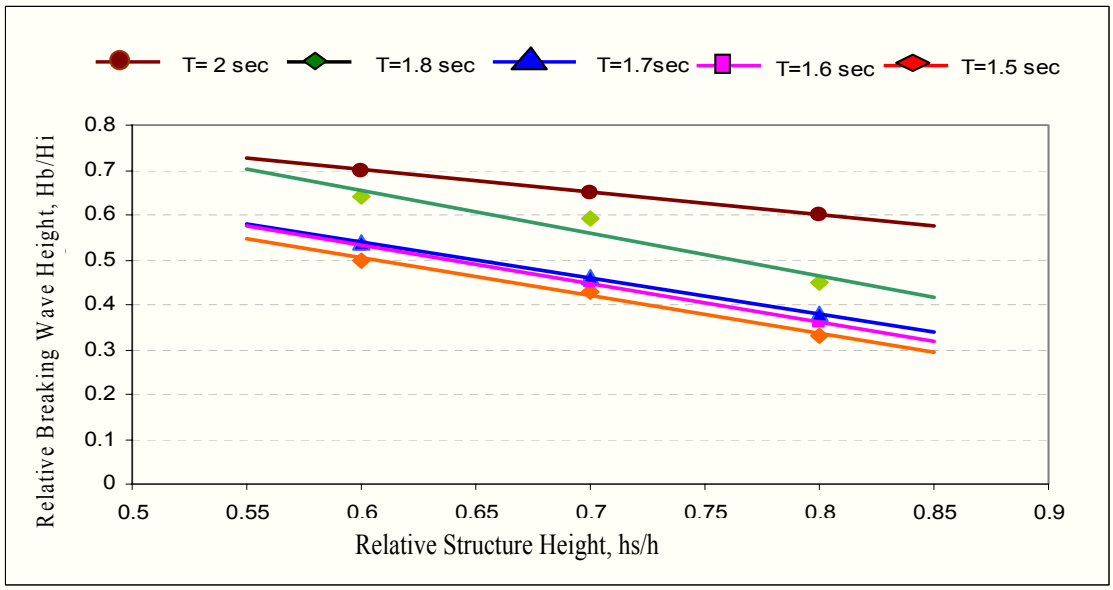

Fig. 2.7 : Effect of relative structure height on wave height reduction

For wave period T=2 sec, wave height after breaking reduce 35% when h_s /h=0.6. For h_s /h=0.7 and 0.8 the wave height reduction occurs up to 35% and 40% respectively. Again for a particular ratio of h_s /h, the reduction of wave height due to breaking occurs more for lower wave periods than for the higher wave periods among the five different waves of wave periods 1.5 sec, 1.6 sec, 1.7 sec, 1.8 sec and 2 sec. When h_s /h=0.8, the wave height reduce 40% and 65% for T= 2.0 sec and 1.5 sec respectively. For h_s /h=0.6 and 0.7, the variation of wave height reduction follow the similar trend.

2.5.2 Effect of relative structure width on wave height reduction

Fig. 2.8 shows the effect of relative structure width, B/L (B is the width of breakwater along the wave direction and L is the wavelength) on wave height reduction, H_b/H_i (H_b is the wave breaking height and H_i is the incident wave height) for three different relative structure heights of h_s/h=0.6, 0.7 and 0.8. For a particular relative structure height, it is seen that as B/L increases, the reduction of wave height due to breaking occurs more.

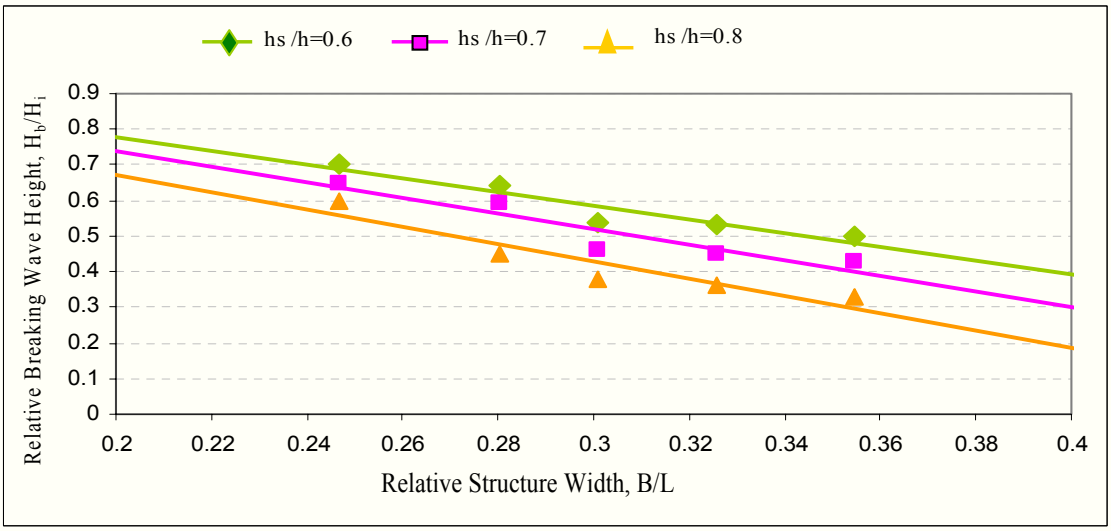

Fig. 2.8: Effect of relative structure width on wave height reduction

For h_s/h =0.6 and B/L= 0.25, reduction of wave height due to breaking is 30%, whereas for the same breakwater wave height reduction becomes 50% as the relative structure width ,B/L becomes 0.4. The scenario is similar for h_s/h= 0.7 and 0.8.Again for any value of B/L, the breaking wave height, H_b decreases more with respect to the incident wave height, H_i for higher value of h_s/h.

When the ratio of relative structure width, B/L is 0.2, wave height is reduced to 32%, 27% and 22% for h_s/h= 0.6, 0.7 and 0.8 respectively. For any ratio of B/L the trend is almost similar. But as discussed previously, as breakwater width increases, the reduction of wave height occurs more for any value of h_s/h.

2.5.3 Effect of wave steepness on wave height reduction

Fig. 2.9 shows the effect of wave steepness, H_i/L_i on wave height reduction, H_b/H_i for different relative structure heights. As the wave becomes steeper, the breaking wave height, H_b becomes greater i.e. for steeper waves the reduction of wave height due to breaking decreases. This trend remains same for different relative structure heights. Here also for any wave steepness, the reduction of wave height due to breaking occurs more for higher relative structure heights.

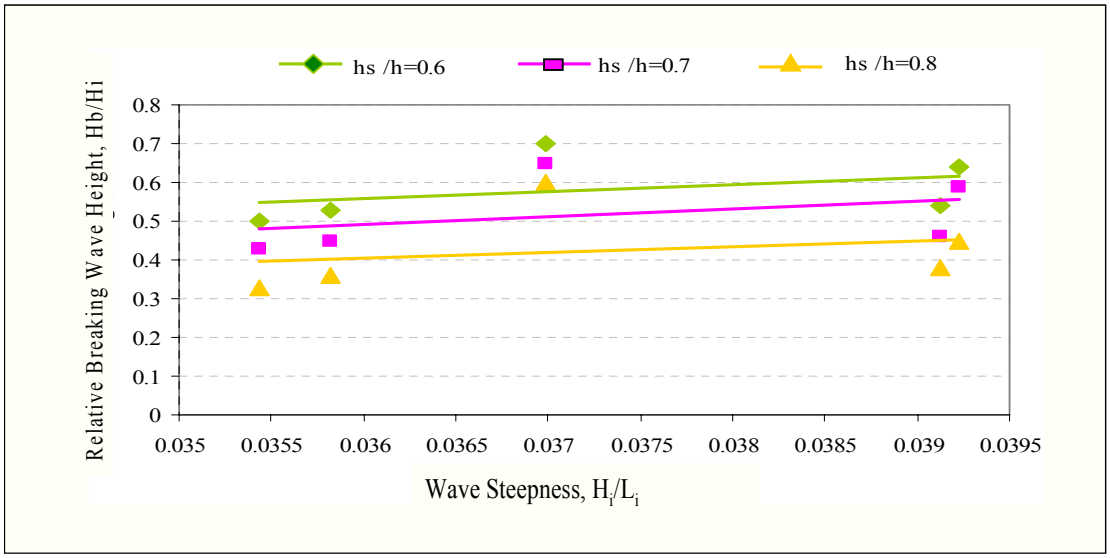

Fig. 2.9: Effect of wave steepness on wave height reduction

For wave steepness 0.0355, the wave height reduces by 45%, 50% and 60% for the ratio of h_s/h= 0.6, 0.7 and 0.8 respectively. For wave steepness 0.039, the reduction of wave height is 40%, 45% and 55% as h_s/h becomes 0.6, 0.7 and 0.8 respectively.

2.5.4 Water surface profile

Fig. 2.10 shows the variation of water surface with time. The high energy of incident wave is reduced drastically because of installing breakwater. This is evident in all the figures from 2.10 (i) to 2.10 (xv) as the incident wave height reduces after passing the breakwater.

Among the three different ratios of h_s/h for which the experiments are conducted, maximum reduction of wave height occurs for maximum value of h_s/h for the same wave period i.e. for ratio of h_s/h =0.8. When h_s/h becomes 0.8 by installing fixed submerged breakwater of 40 cm height, the incident wave height of 10 cm for T=1.5 sec reduces to 4 cm after breaking over the breakwater. With fixed submerged breakwater of 35 cm height in 50 cm still water depth as the ratio of h_s/h becomes 0.7 for the same wave period, incident wave height 10 cm is reduced to 5 cm. Installation of 30 cm breakwater in the same depth of still water (h_s/h=0.6) reduce 10 cm incident wave height to 6 cm. Thus for T=1.5 sec, breakwater having h_s/h=0.6 reduces 40% of incident wave height, whereas breakwater having h_s/h=0.7 and 0.8 decreases incident wave height up to 50% and 60% respectively.

For T= 1.6 sec, 30 cm breakwater covering 60% of still water depth as h_s/h=0.6 reduce 39% of incident wave height, whereas 35 cm breakwater with h_s/h=0.7 decrease incident wave height up to 45% and maximum reduction of wave height (59%) is caused by 40 cm breakwater having h_s/h=0.8 for the same wave period.

For T= 1.7 sec, maximum reduction of wave height is up to 60% which is caused by breakwater of 40 cm height (h_s/h=0.8). For the same wave period, 35 cm high breakwater having h_s/h=0.7 decreases incident wave height up to 45%, whereas 30 cm high breakwater reduces 37% of incident wave height. So for T= 1.7 sec, 40 cm high breakwater is most effective in reduction of wave height among the breakwaters of three different heights in 50 cm deep water.

For T= 1.8 sec, breakwater covering 60% of still water depth as h_s/h=0.6 reduce 35% of incident wave height and breakwater having h_s/h=0.7 decrease incident wave height up to 43%. But for this wave period the maximum reduction (58%) of wave height is caused by breaking of incident wave over 40 cm breakwater.

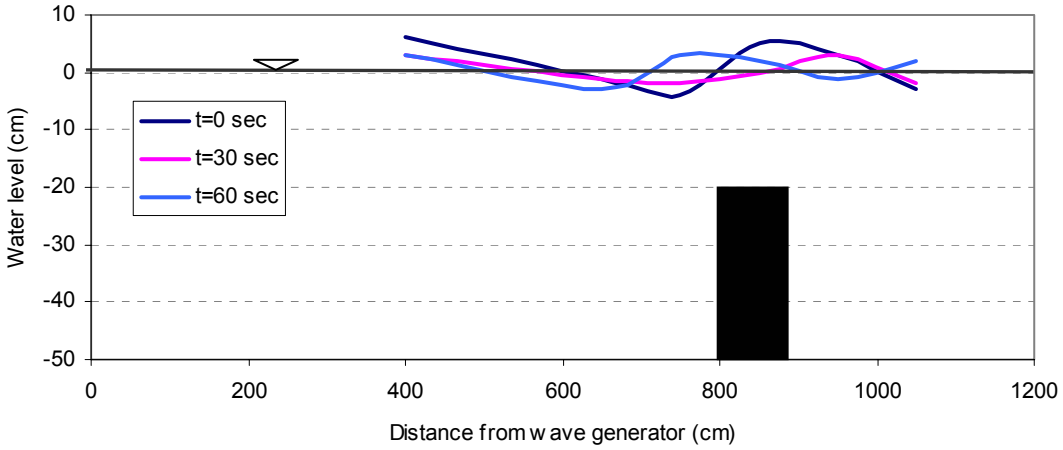

Fig.2.10(i): Water surface profile for T= 1.5 sec, H_i= 10cm, h_s/h=0.6

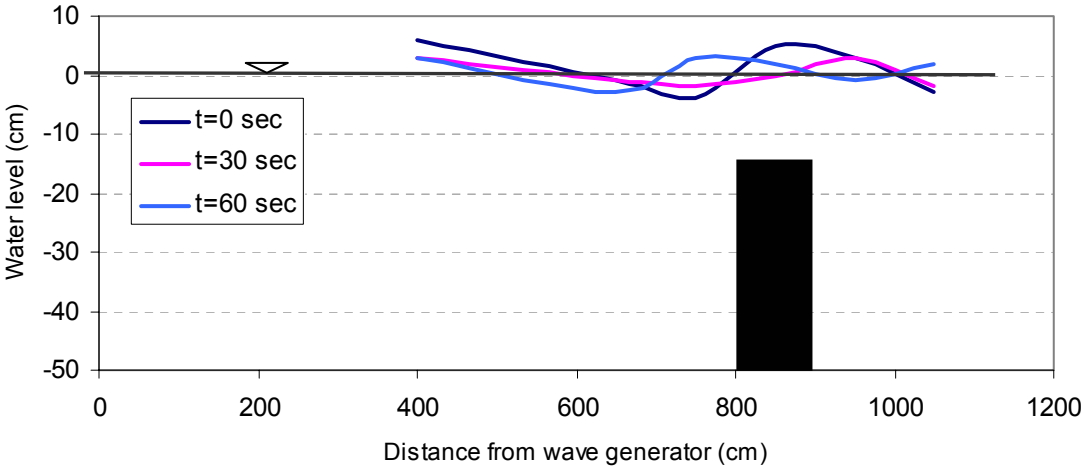

Fig.2.10(ii): Water surface profile for T= 1.5 sec, H_i= 10cm, h_s/h=0.7

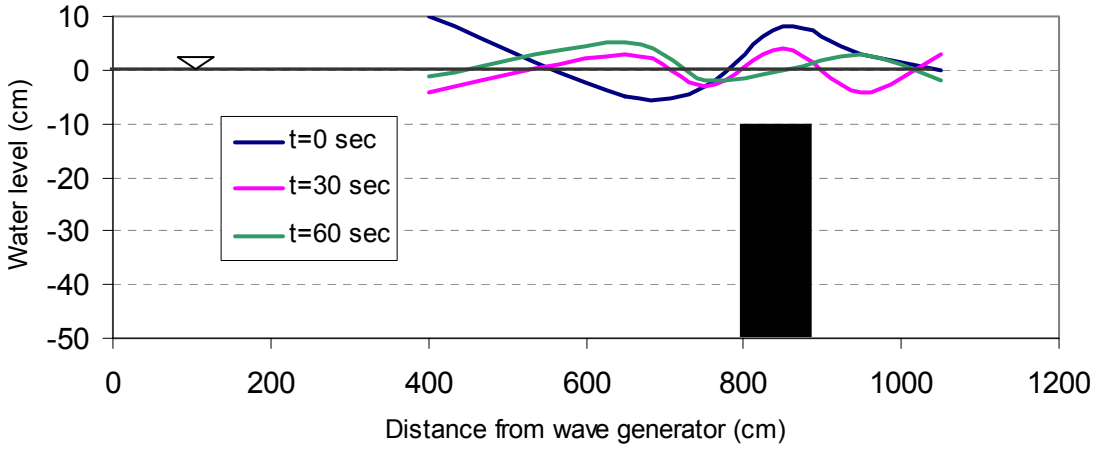

Fig.2.10(iii): Water surface profile for T= 1.5 sec, H_i= 10cm, h_s/h=0.8

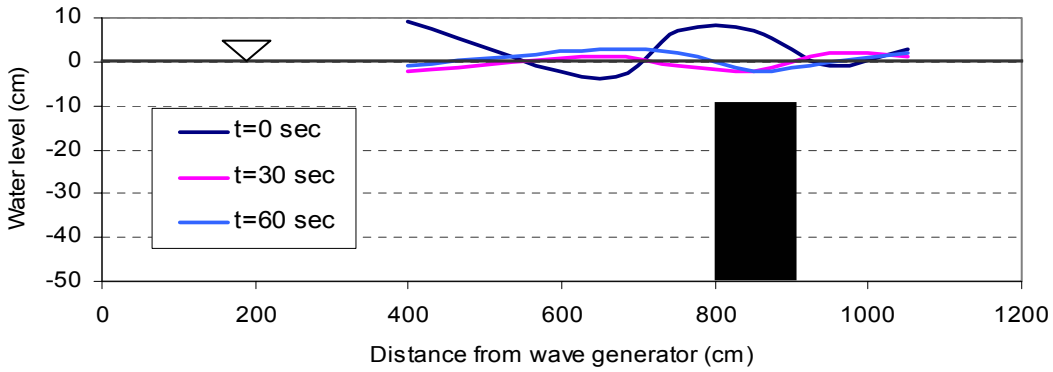

Fig.2.10 (iv): Water surface profile for T= 1.6 sec, H_i= 12cm, h_s/h=0.6

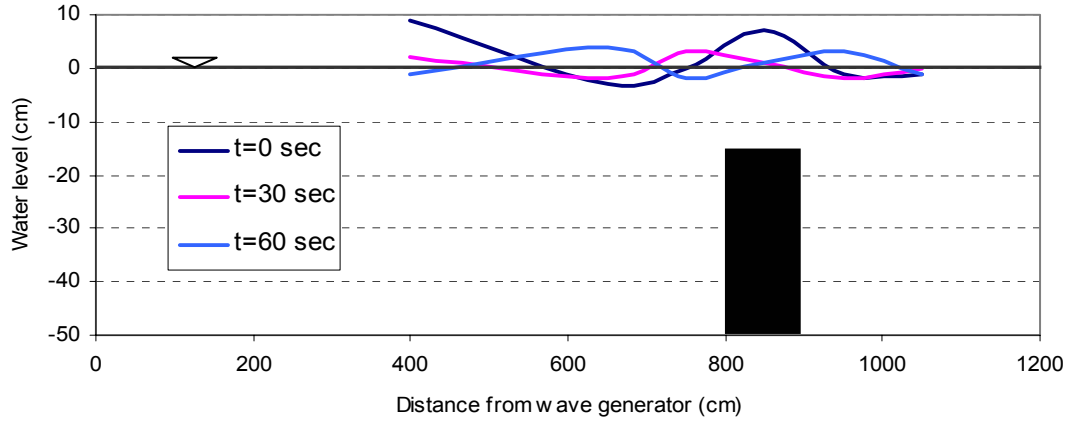

Fig.2.10 (v): Water surface profile for T= 1.6 sec, H_i= 12cm, h_s/h=0.7

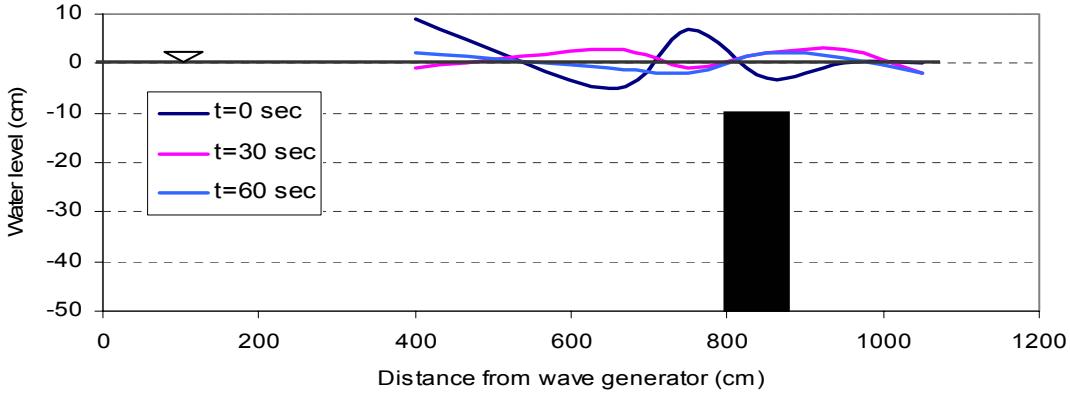

Fig.2.10 (vi): Water surface profile for T= 1.6 sec, H_i= 12cm, h_s/h=0.8

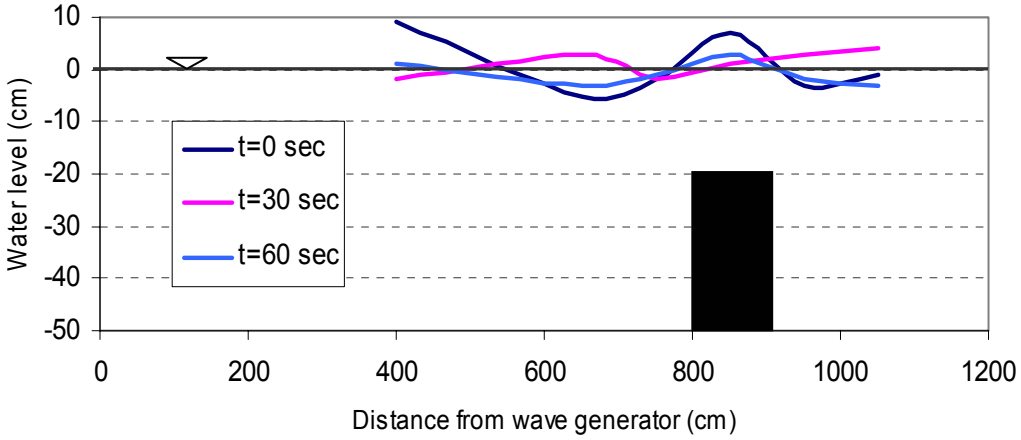

Fig.2.10(vii): Water surface profile for T= 1.7 sec, H_i= 13cm, h_s/h=0.6

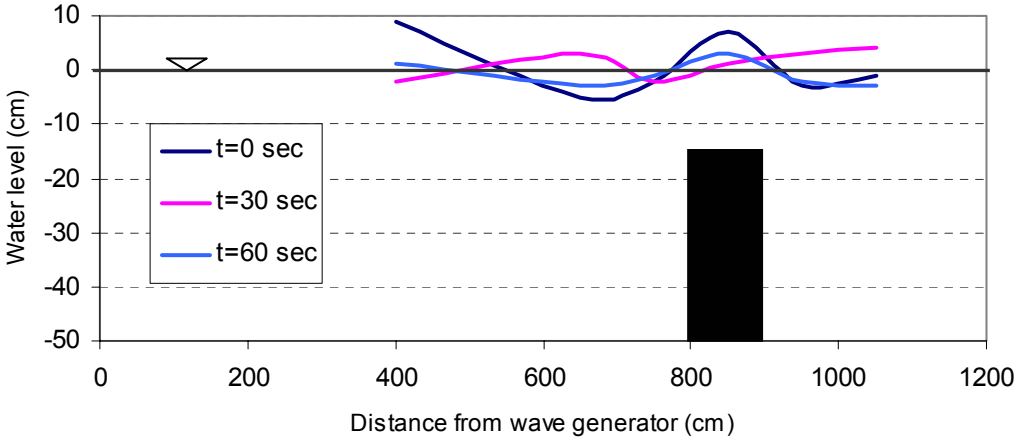

Fig.2.10(viii): Water surface profile for T= 1.7 sec, H_i= 13cm, h_s/h=0.7

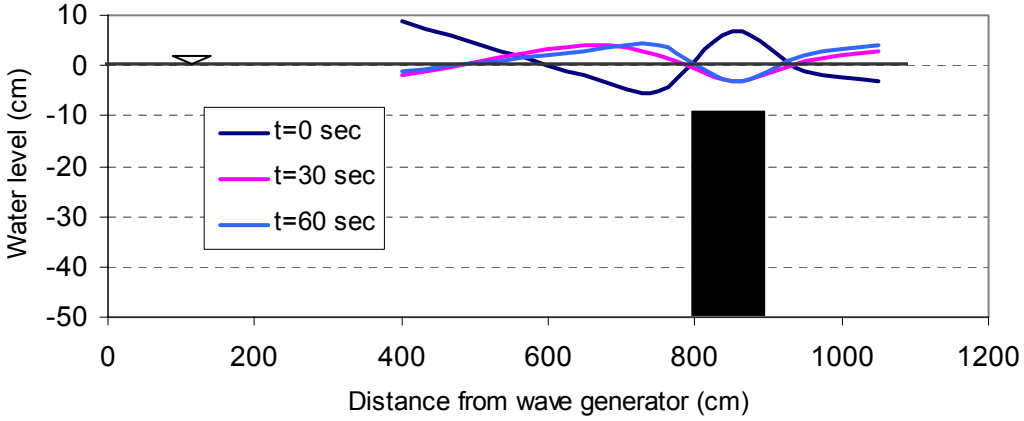

Fig.2.10(ix): Water surface profile for T= 1.7 sec, H_i= 13cm, h_s/h=0.8

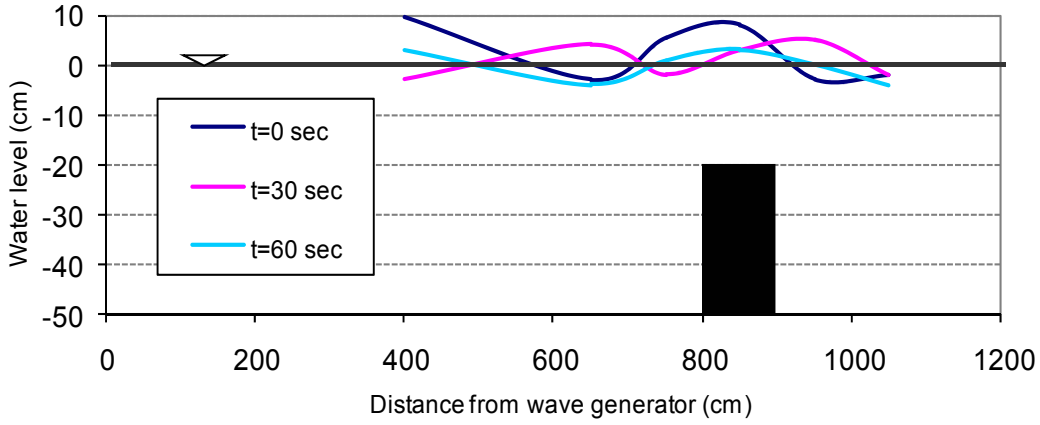

Fig.2.10(x): Water surface profile for T= 1.8 sec, H_i= 14cm, h_s/h=0.6

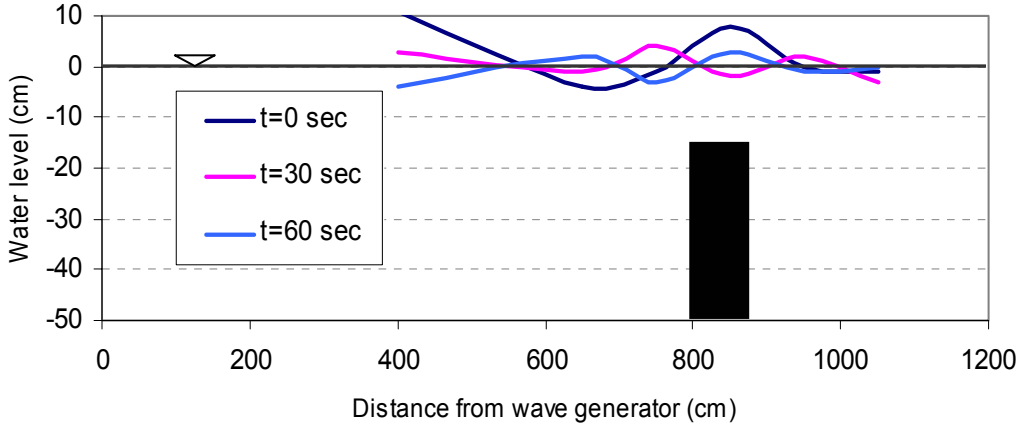

Fig.2.10 (xi): Water surface profile for T= 1.8 sec, H_i= 14cm, h_s/h=0.7

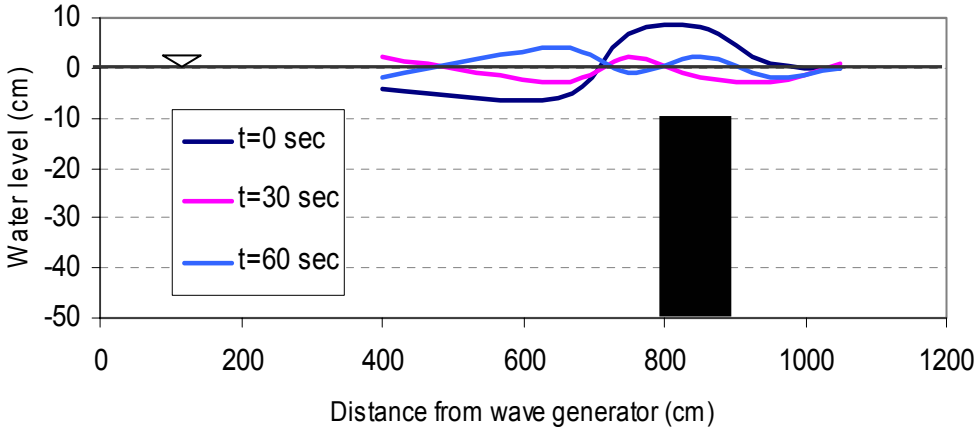

Fig.2.10 (xii): Water surface profile for T= 1.6 sec, H_i= 12cm, h_s/h=0.7

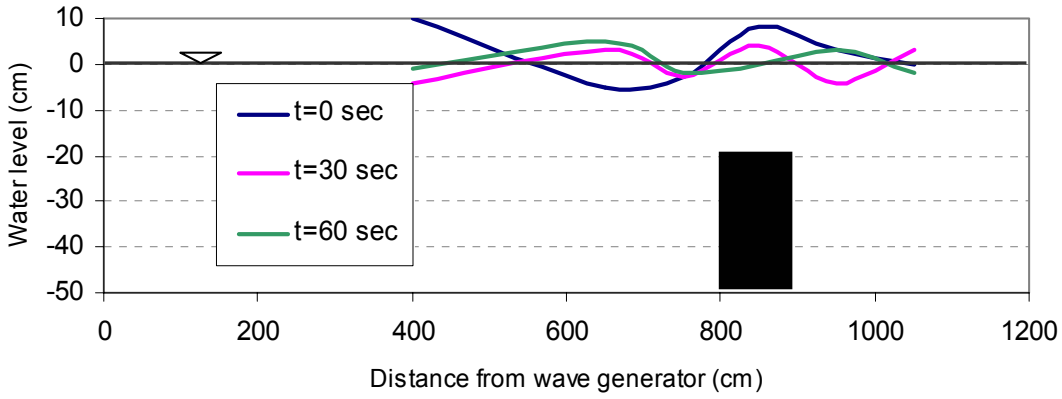

Fig.2.10(x iii): Water surface profile for T= 2.0 sec, H_i= 15cm, h_s/h=0.6

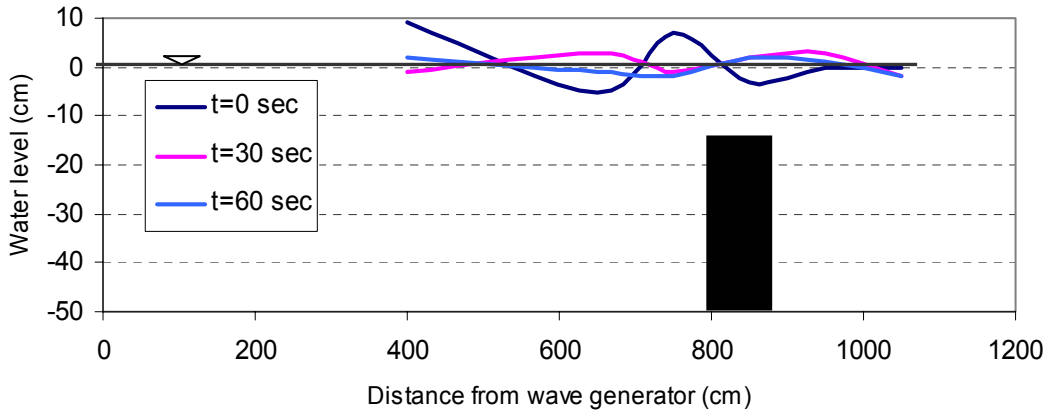

Fig.2.10 (xiv): Water surface profile for T= 2.0 sec, H_i= 15cm, h_s/h=0.7

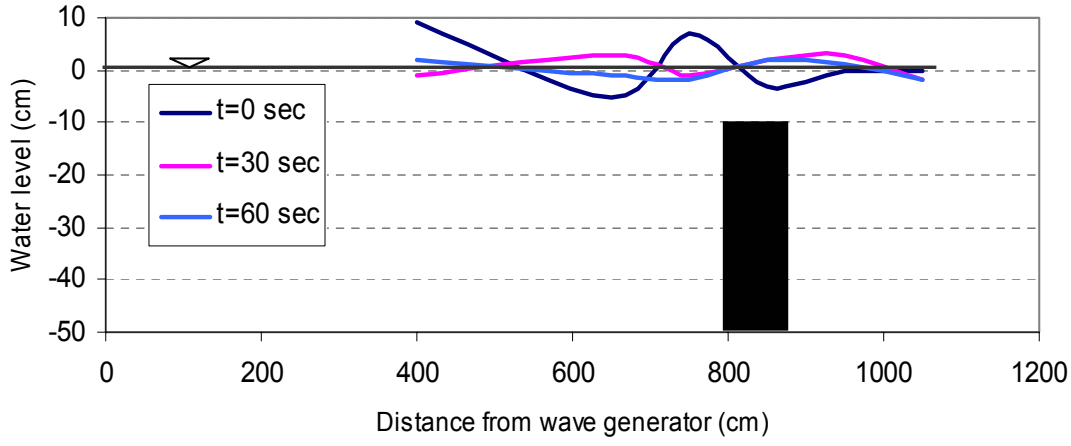

Fig.2.10 (xv): Water surface profile for T= 2.0 sec, H_i= 15cm, h_s/h=0.8

For T= 2 sec, again the 40 cm breakwater causes the maximum reduction of incident wave height as 55%, whereas 35 cm breakwater can reduce 45% and 30 cm breakwater causes 35% reduction of incident wave height when installed in a still water depth of 50 cm.

So it is clear from Fig. 2.10 that for any wave periods among 1.5 sec, 1.6 sec, 1.7 sec, 1.8 sec and 2 sec, maximum reduction of incident wave height is caused by wave breaking over or behind 40 cm breakwater in a still water depth of 50 cm i.e. when the ratio of h_s/h=0.8, installation of rectangular fixed submerged breakwater shows maximum efficiency by reducing incident wave height about 60%. At the same depth of water for the same wave period, 35 cm breakwater and 30 cm breakwater can decrease the incident wave height up to 45% and 40% respectively.

2.5.5 Position of wave breaking over or behind the breakwater

Fig. 2.11 shows the position of wave breaking over or behind the breakwater for three different heights in same still water depth. For breakwater height h_s = 30 cm, 35 cm and 40 cm, the breaking positions are seen just behind, at the onshore and at the middle position over the breakwater respectively. For a particular height of breakwater, as the wave height increases, the breaking position comes toward the offshore side. For setting breakwater of h_s/h=0.6 in 50 cm depth of water, the variation of wave breaking positions are within 20 cm behind the breakwater for T=1.5 sec, 1.6 sec, 1.7 sec, 1.8 sec and 2 sec respectively. For the same wave periods, breakwater having h_s/h= 0.7 and 0.8 wave breaks with 25 cm and 15 cm variation in length over the breakwater respectively.

Again when the breakwater height increases in the same depth of water, the waves tend to break more quickly than that for lower height of breakwater. Hence for the same wave, the wave breaking position comes closer to the breakwater for higher ratio of h_s/h.

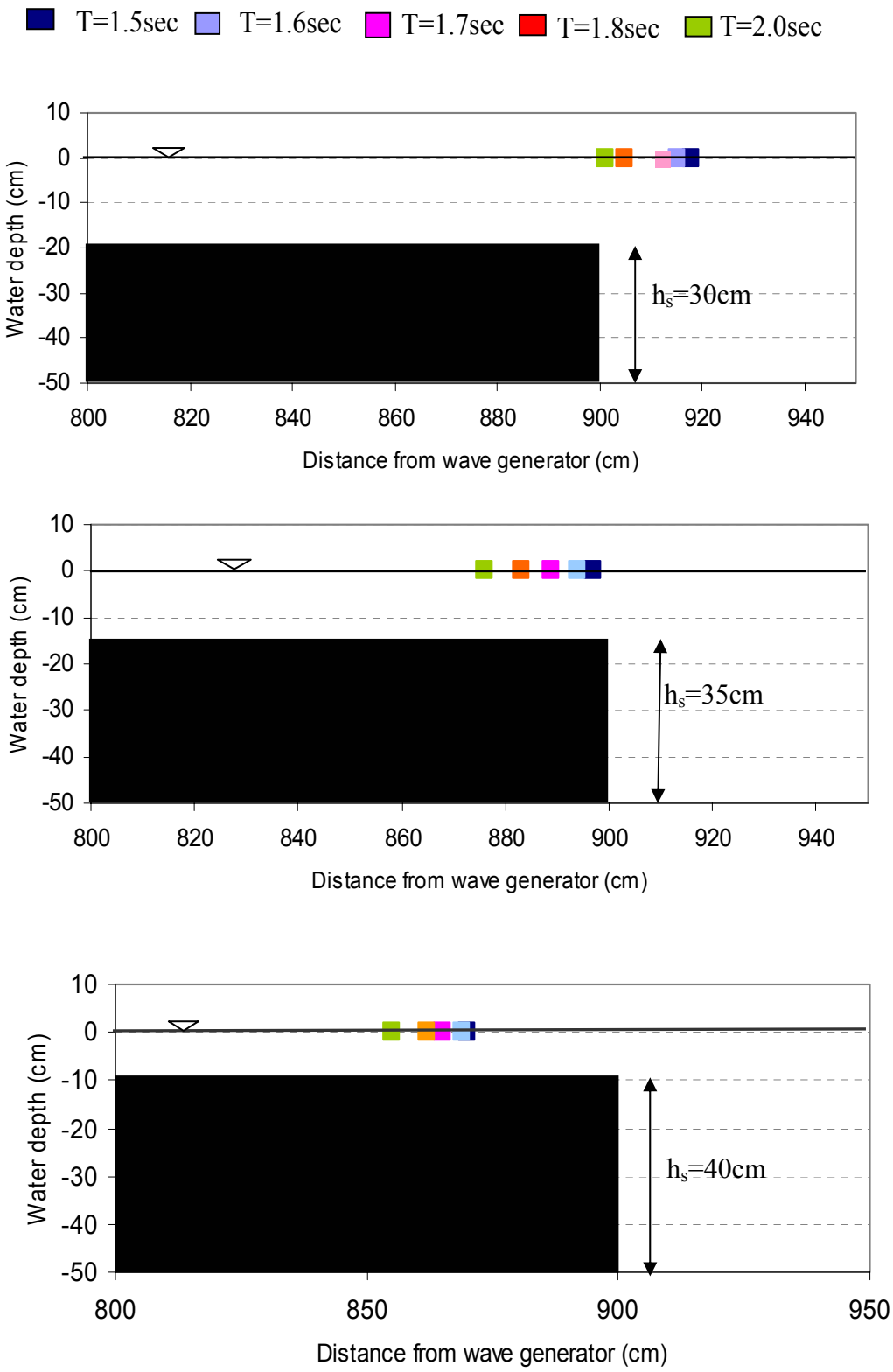

Fig. 2.11: Position of wave breaking over or behind the breakwater

2.5.6 Variation of η/H_i with t/T

Variation of water surface (η) with time (t) is shown in the non-dimensional form as variation of η/H_i with t/T in Fig. 2.12. In Fig. 2.12(i). for wave period 1.5 sec, the incident wave height 10 cm is reduced after breaking due to breakwater installation. When the breakwater height is 60% of the still water depth, the incident wave height is 40% reduced. For installation of breakwater with 70% submergence of the still water, the wave height due to breaking is reduced to 50% of the incident wave height. When the breakwater submerges 80% of the still water depth, 60% wave height is reduced due to wave breaking.

In Fig. 2.12(ii), for wave period of 1.6 sec, the maximum reduction of incident wave height is 59% for 40 cm breakwater. For 35 cm breakwater, the reduction of incident wave height is 55% and for 30 cm breakwater it is up to 39%.

In Fig. 2.12(iii), for T=1.7 sec, 40 cm breakwater reduces incident wave height upto 60%, whereas 35 cm breakwater reduces wave height upto 45% and 30 cm breakwater causes 37% reduction of incident wave height.

In Fig. 2.12(iv), for wave period 1.8 sec, reduction of incident wave height is 58% for breaking by 40 cm breakwater, by 35 cm breakwater it is 43% and by 30 cm breakwater the reduction is 35%.

Again in Fig. 2.12(v) it is seen that for wave period of 2 sec, reduction of incident wave height because of breaking by 40 cm breakwater is 55%, by 35 cm breakwater it is 45% and by 30 cm breakwater reduction of incident wave height occurs upto 35%. So here again installation of 40 cm breakwater in 50 cm still water depth is seen as most effective(maximum 60% reduction) for reduction of incident wave height followed by providing 35 cm breakwater (maximum 45% reduction) and 30 cm breakwater (maximum 35% reduction) in the same still water depth of 50 cm.

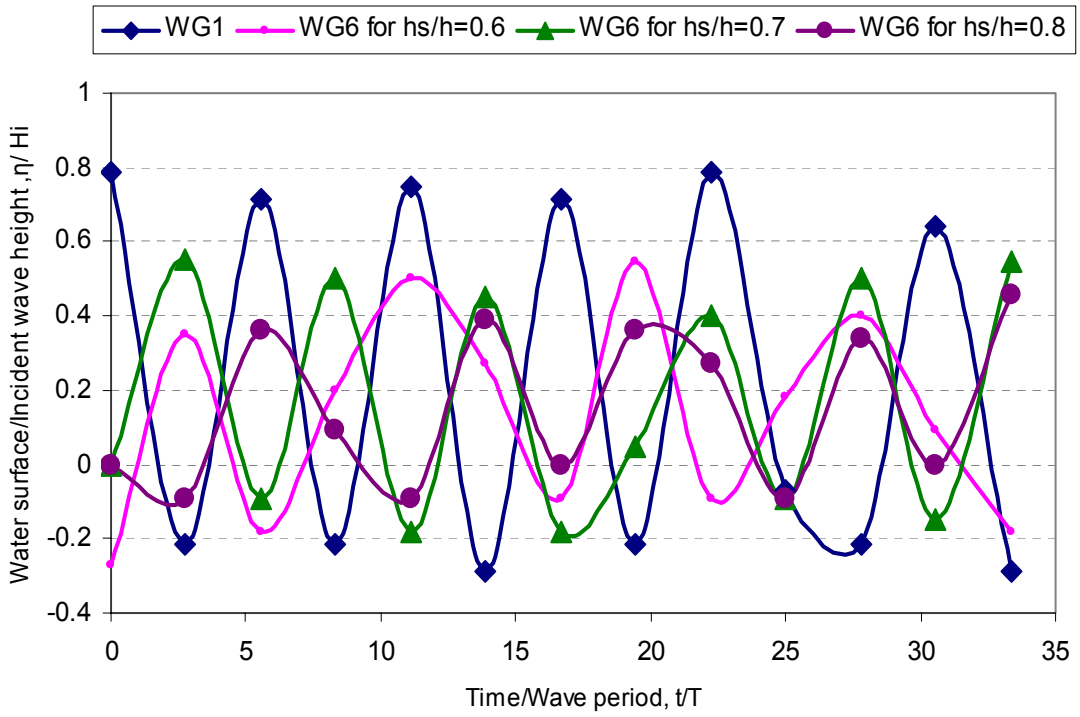

Fig.2.12 (i): Variation of η/H_i with t/T for T= 1.5 sec, H_i= 10cm

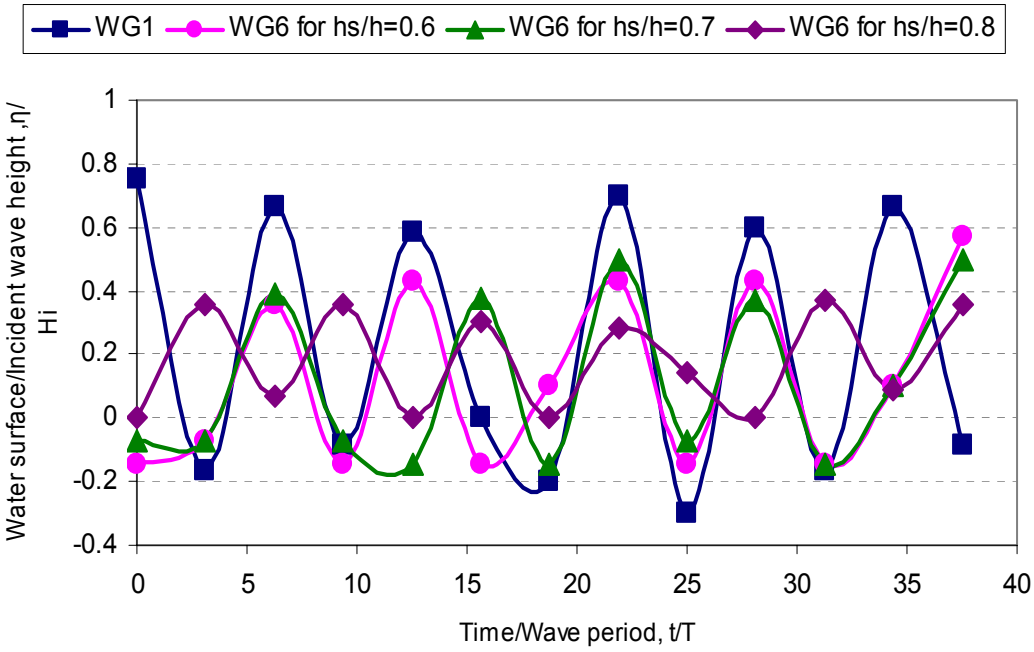

Fig.2.12 (ii): Variation of η/H_i with t/T for T= 1.6 sec, H_i= 12cm

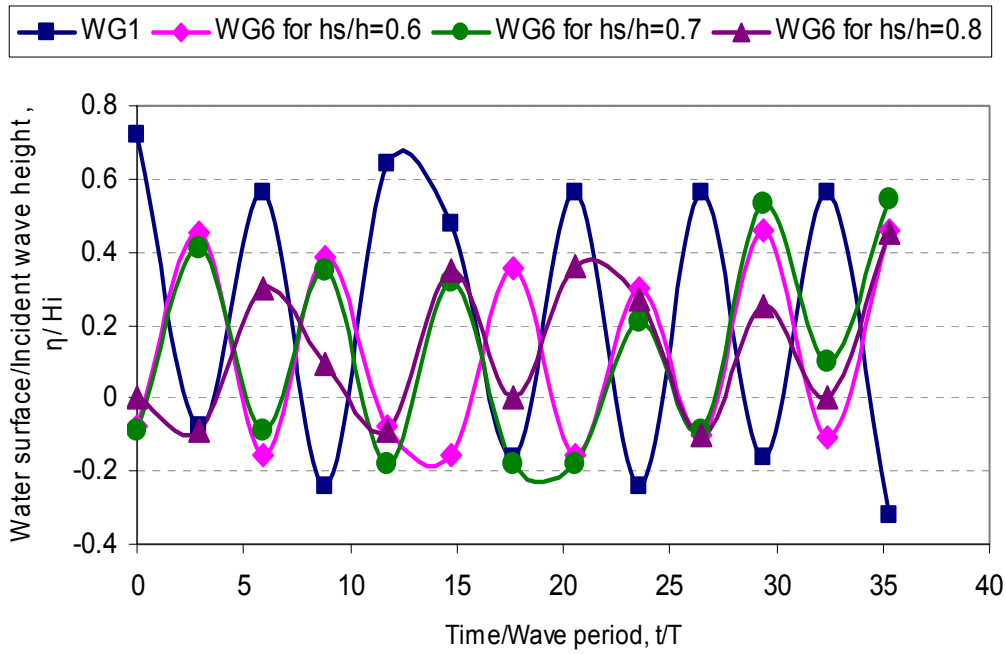

Fig.2.12(iii): Variation of η/H_i with t/T for T= 1.7 sec, H_i= 13cm

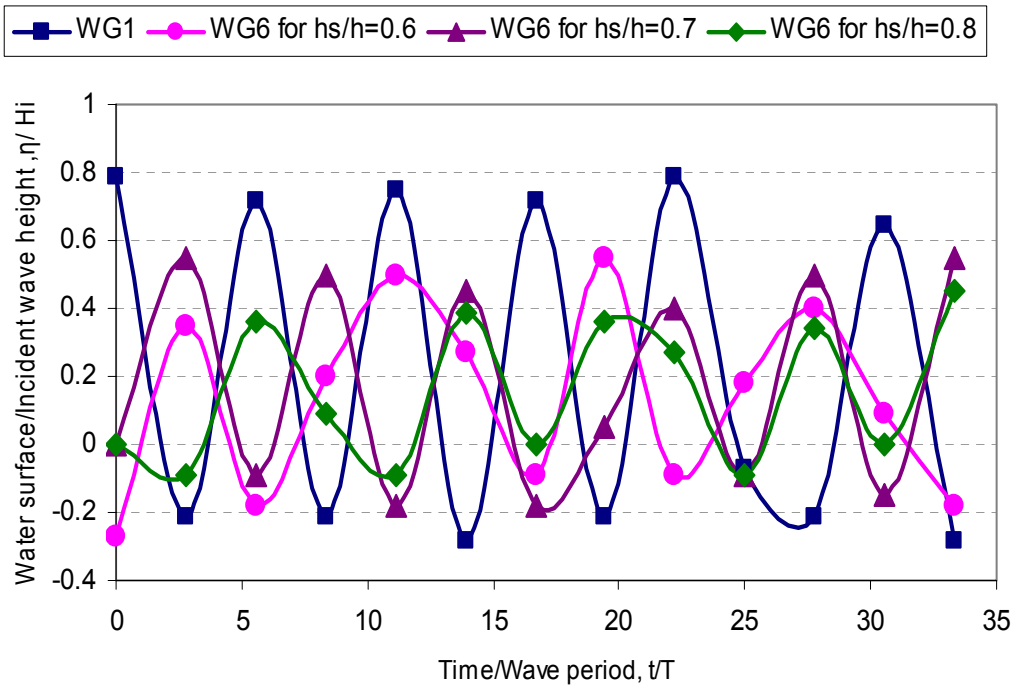

Fig.2.12 (iv): Variation of η/H_i with t/T for T= 1.8 sec, H_i= 14cm

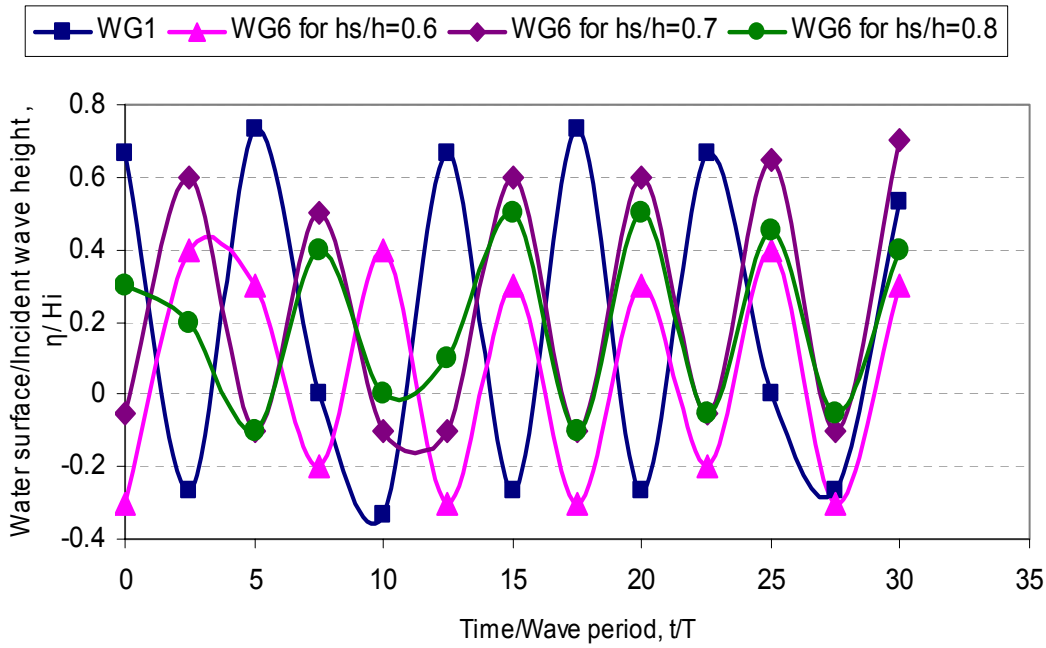

Fig.2.12 (v): Variation of η/H_i with t/T for T= 2.0 sec, H_i= 15cm

2.5.7 Variation of η/H_i with x/L

The curves of Fig. 2.13 show the variation of water surface/ incident wave height (η/H_i) with respect to distance from breakwater/ wave length (x/L). These

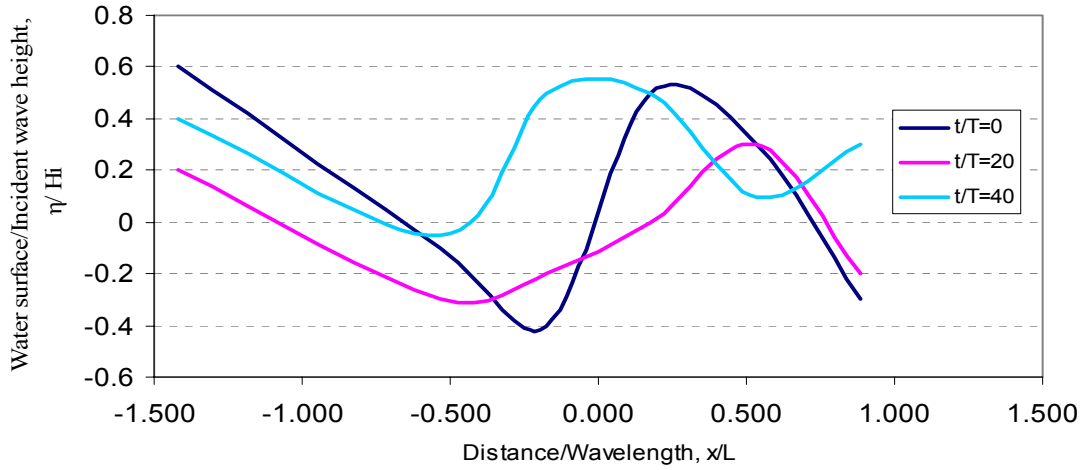

Fig.2.13(i): Variation of η/H_i with x/L for T= 1.5 sec, H_i= 10cm, h_s/h=0.6

represent the non-dimensional water surface profiles for installing breakwater of three different heights of 30cm, 35cm and 40 cm in a still water depth of 50 cm at five different wave periods of 1.5sec, 1.6sec, 1.7sec, 1.8sec and 2.0 sec respectively .

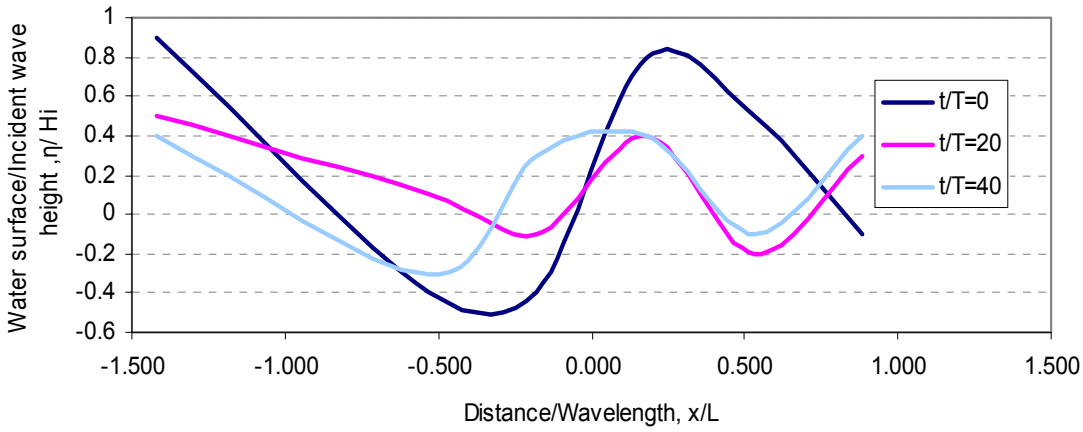

Fig. 2.13(ii): Variation of η/H_i with x/L for T= 1.5 sec, H_i= 10cm, h_s/h=0.7

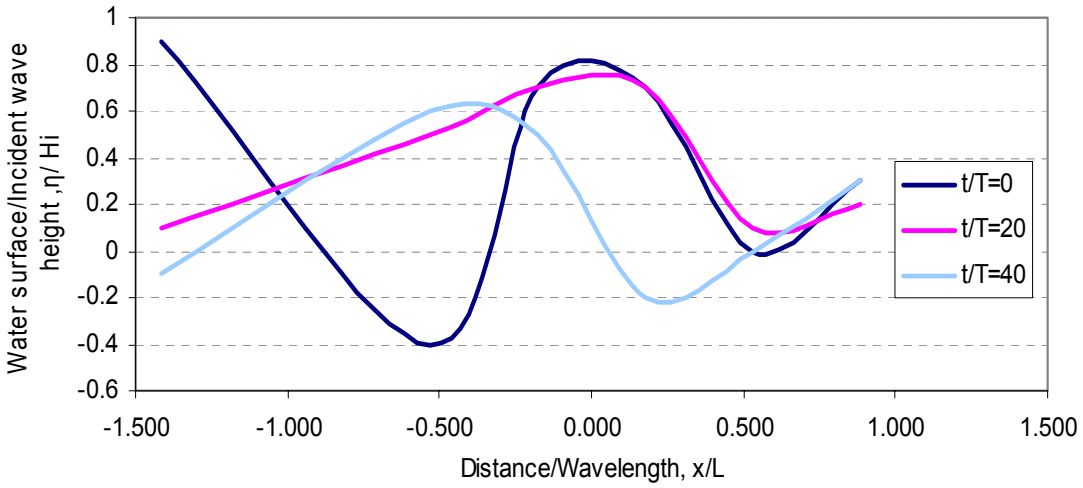

Fig. 2.13 (iii): Variation of η/H_i with x/L for T= 1.5 sec, H_i= 10cm, h_s/h=0.8

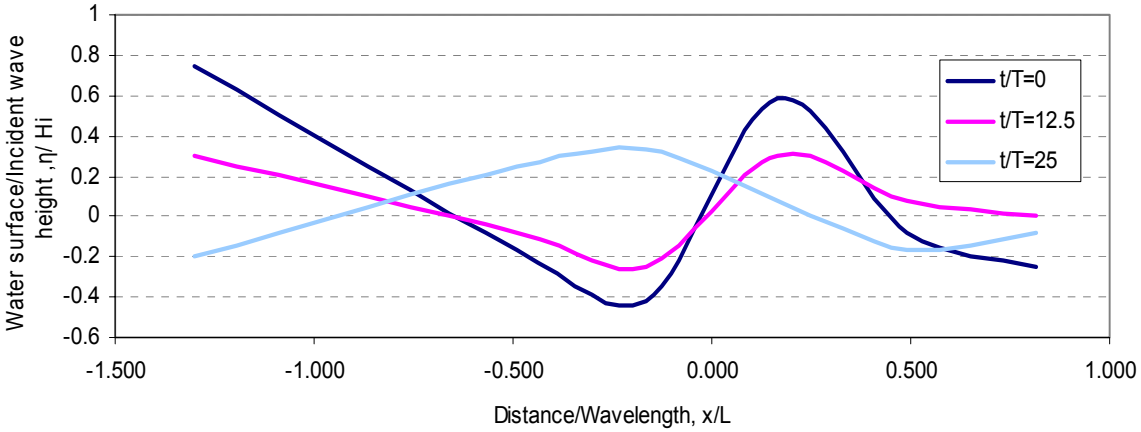

Fig. 2.13 (iv): Variation of η/H_i with x/L for T= 1.6 sec, H_i= 12cm, h_s/h=0.6

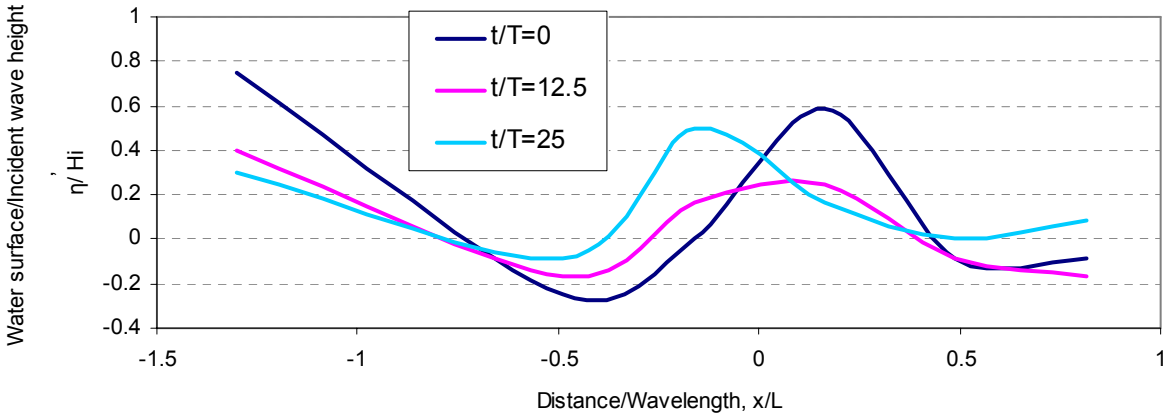

Fig. 2.13 (v): Variation of η/H_i with x/L for T= 1.6 sec, H_i= 12cm, h_s/h=0.7

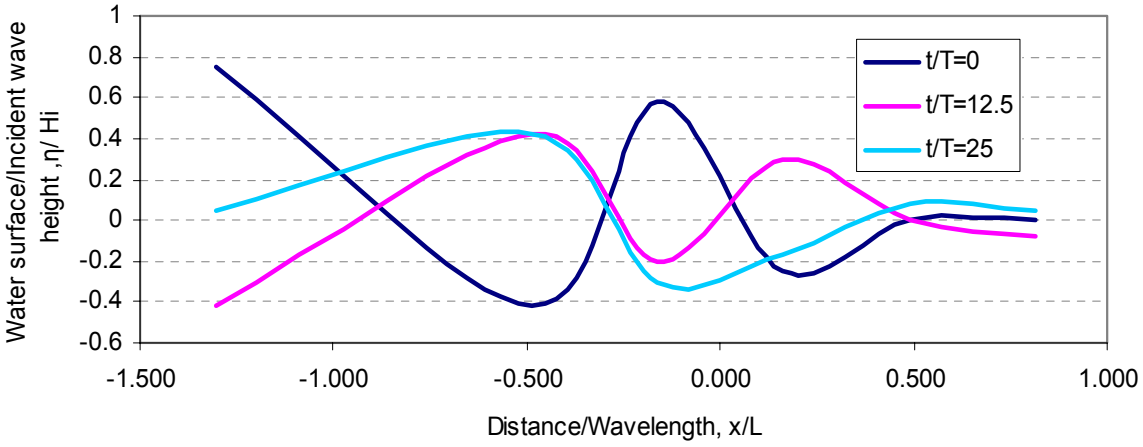

Fig.2.13 (vi): Variation of η/H_i with x/L for T= 1.6 sec, H_i= 12cm, h_s/h=0.8

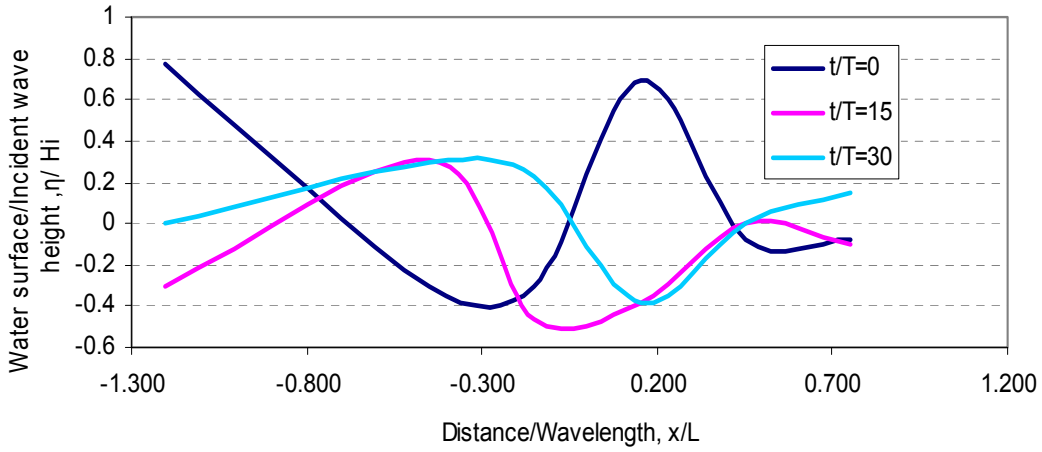

Fig.2.13(vii): Variation of η/H_i with x/L for T= 1.7 sec, H_i= 13cm, h_s/h=0.6

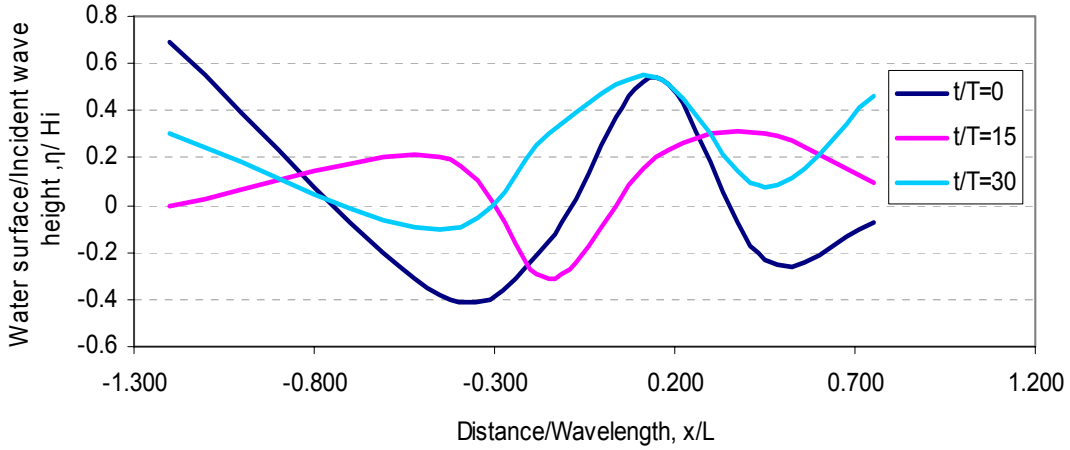

Fig.2.13(viii): Variation of η/H_i with x/L for T= 1.7 sec, H_i= 13cm, h_s/h=0.7

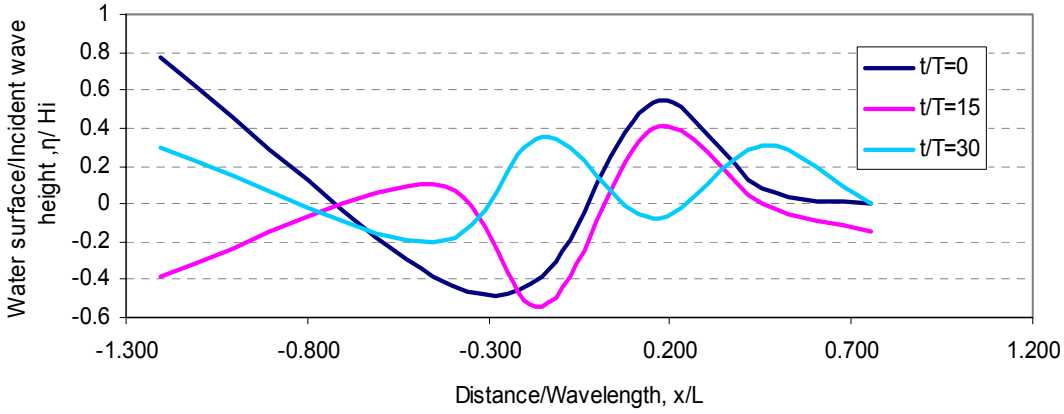

Fig.2.13 (ix): Variation of η/H_i with x/L for T= 1.7 sec, H_i= 14cm, h_s/h=0.8

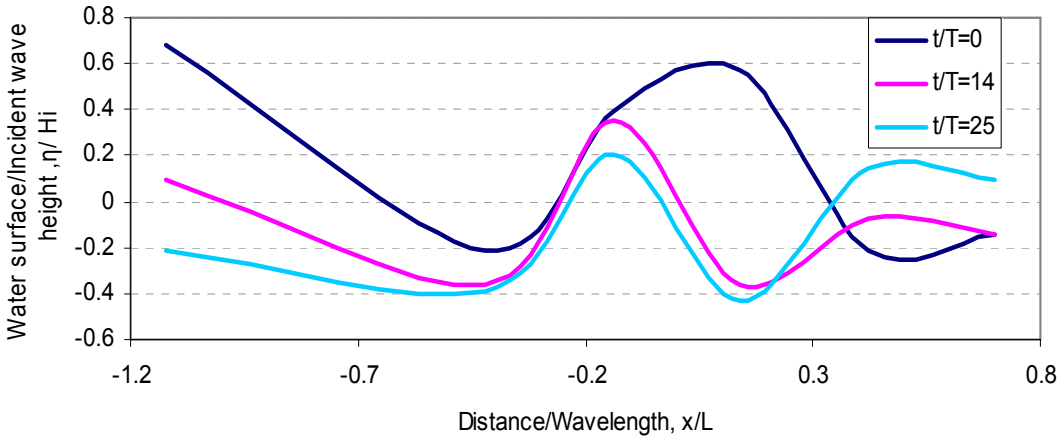

Fig. 2.13(x): Variation of/H_i with x/L for T= 1.8 sec, H_i= 14cm, h_s/h=0.6

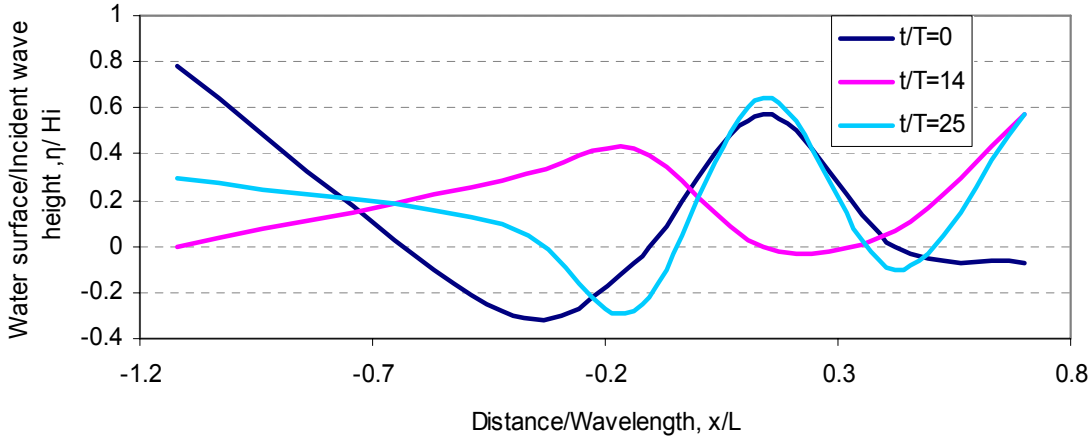

Fig. 2.13(xi): Variation of η/H_i with x/L for T= 1.8 sec, H_i= 14cm, , h_s/h=0.7

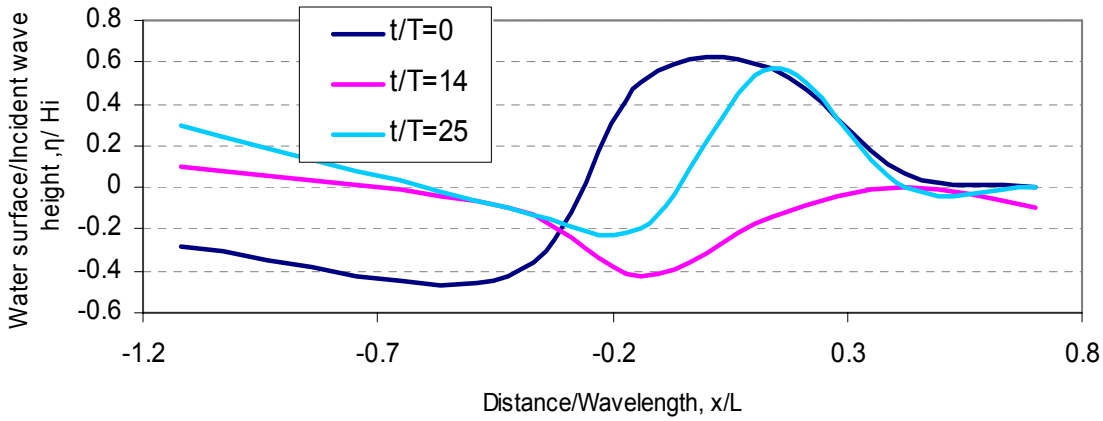

Fig. 2.13(xii): Variation of η/H_i with x/L for T= 1.8 sec, H_i= 14cm, , h_s/h=0.8

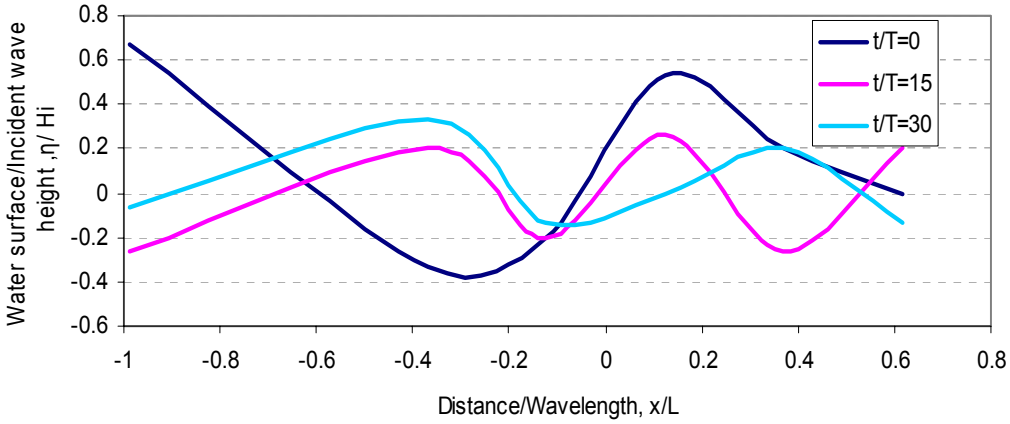

Fig. 2.13 (xiii): Variation of η/H_i with x/L for T= 2.0 sec, H_i= 15cm, h_s/h=0.6

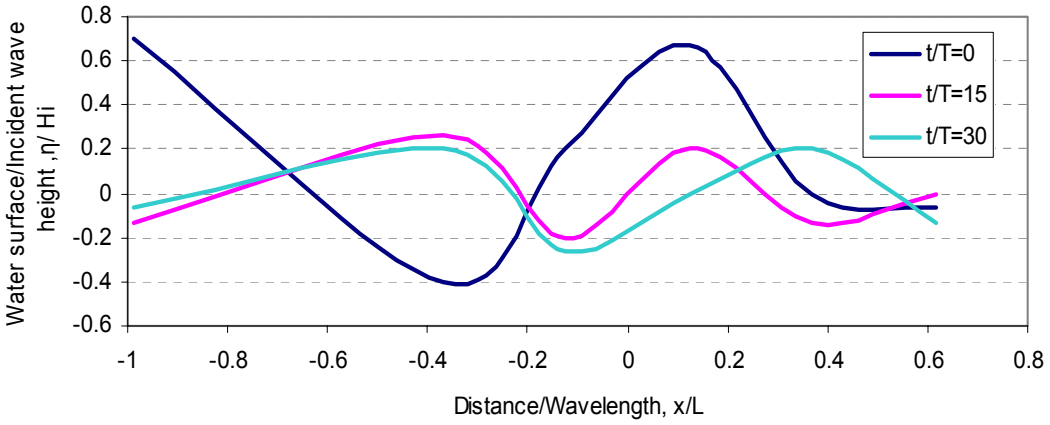

Fig. 2.13 (xiv): Variation of η/H_i with x/L for T= 2.0 sec, H_i= 15cm, h_s/h=0.7

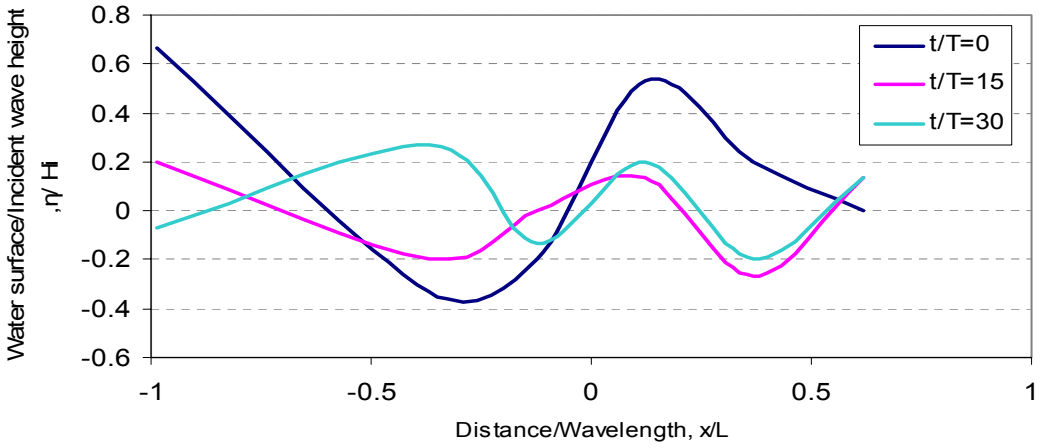

Fig. 2.13 (xv): Variation of η/H_i with x/L for T= 2.0 sec, H_i= 15cm, h_s/h=0.8

2.5.8 Wave breaking type

Breaking waves are classified into four different types as spilling, plunging, collapsing and surging based on the physical changes of surface profile during the breaking process. For given water depth and wave period, a wave breaks when the wave height grows to reach a certain limiting height. In these experimental runs fixed submerged body of rectangular shape are used as breaker. The incident waves of wave period ranging from 1.5 sec to 2.0 sec break in different patterns as they are passing over the breakwaters of depth 30 cm, 35 cm and 40 cm creating 60%, 70% and 80% submergence in 50 cm depth of water.

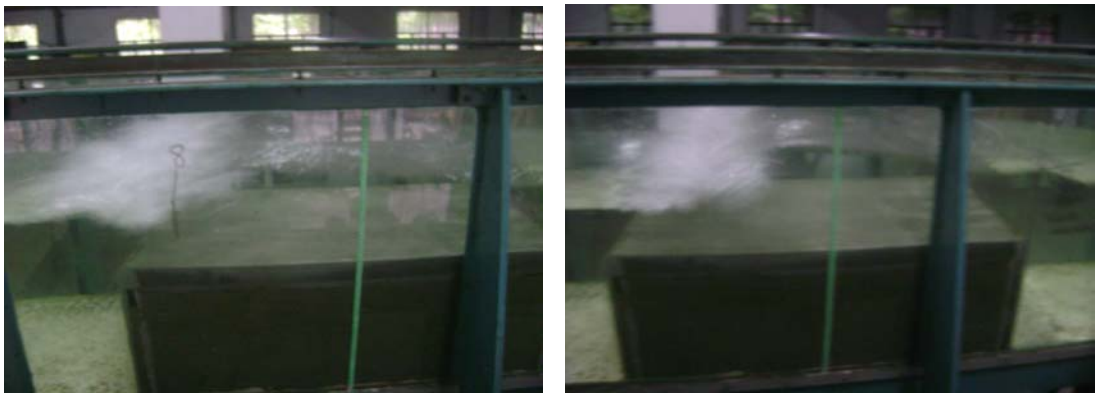

Fig. 2.14 (i): Spilling type wave breaking

Spilling appears as the wave is plowing the foam with its movement. In this case turbulence and foam first appear at the wave crest and spread down the front face as the wave propagates forward. In this study, spilling type breaking occurs as the incident waves are passing over the breakwater of 70% submergence for five different waves of wave periods 1.5 sec, 1.6 sec, 1.7 sec, 1.8 sec and 2 sec.

In plunging type wave breaking, the wave crest sharpens and then curls forward over the front face to plunge at the base of the front face of the wave. In this study plunging wave breaking occurs rarely only when the incident wave is passing over the breakwater of 30 cm height in 50 cm still water depth for wave periods of 1.5 sec and 1.7 sec only.

Fig. 2.14 (ii): Plunging type wave breaking

As the front face of the wave steepens at incipient wave breaking, the lower portion of the face plunges forward and the wave collapses. Collapsing type wave breakings of incident waves are common in this study when the waves are passing over the breakwater of , h_s/h =0.8 for five different wave periods of 1.5 sec, 1.6 sec, 1.7 sec, 1.8 sec and 2.0 sec. Again as the waves of wave period 1.8 sec to 2.0 sec move over the breakwater of 35 cm height, they also collapse.

Fig. 2.14 (iii): Collapsing type wave breaking

The crest and front face of the wave retain a fairly stable shape as they surge up the beach slope and return. Usually the waves surge in a beach of large slope. In this study, all the experiments are done on horizontal bed and no surging has been observed.

CHAPTER 3: NUMERICAL MODEL BASED ON SOLA-VOF

3.1 Introduction

Accurate prediction and evaluation of the interaction between waves and the submerged breakwater are important for multi-purpose utilization of coastal areas and design of coastal structures. The Volume of Fluid (VOF) method has become powerful numerical computation technique for evaluating the free surface due to wave-structure interaction. The developed numerical model outputs water surface profile, velocity distribution, pressure distribution along both axes of two-dimensional grid and also the value of fraction of volume occupied by fluid at any time. In this chapter, the developments of VOF type numerical models are discussed in section 3.2, the governing equations and boundary conditions of two-dimensional moored floating body-wave interaction model by Ataur (2005) are given in section 3.3, the governing equations, computational procedures and boundary conditions for adapting the model with VOF method are described in section 3.4 and then finally SOLA-VOF scheme for modeling of submerged body against wave action is described in section 3.5. A typical numerical model run is described in section 3.6.

3.2 Development of VOF type numerical model

This section summarizes the key developments of the VOF type models, and relates the progress in the field of coastal engineering. Fig. 3.1 shows the 'family tree' of VOF type models. The thick solid line connects the evolution stages of the original VOF models by the inventors of the VOF technique. The branches identify the major models developed mainly for coastal engineering applications. The MAC method (Welch et al., 1966) was developed for the solution of viscous, incompressible and transient fluid flow problems involving free surfaces. This method used for the first time velocity and pressure directly as the dependent variables. The fluid configuration is defined using a set of marker particles

moving with the fluid. These massless particles are used to determine the status of the computational cells as "full", "empty" or "surface", but do not influence the

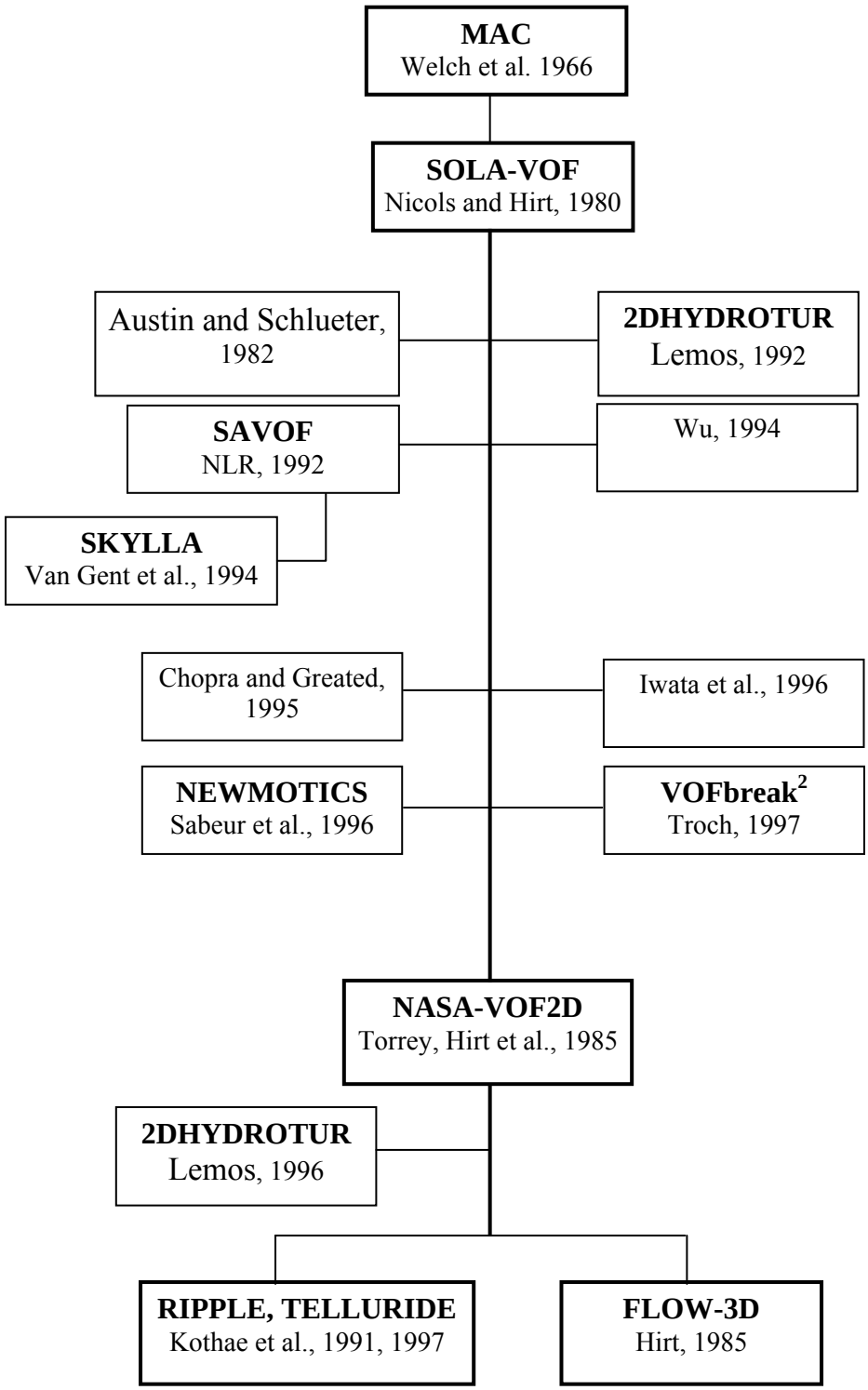

Fig. 3.1: Overview of key developments of VOF type numerical models with special emphasis on the progress in the field of Coastal Engineering.

dynamics of the fluid flow. It was the first method to successfully treat problems involving complicated free surface motions. However, an accurate approximation of the free surface required a huge number of marker particles, and is computationally inefficient. Also, the numerical scheme was prone to instability. Several researchers subsequently improved the original MAC method. The SOLA-VOF algorithm is a highly optimized variant of the MAC method, in which the free surfaces are treated by means of a single mesh-wide array. The continuity equation is satisfied using a pressure–velocity relaxation that is particularly simple to program in a staggered mesh. This method has been applied in the SOLA-VOF model (Hirt and Nichols, 1981). The main advantages are that the pressure solution does not require pressure boundary conditions, and that the SOLA-VOF model allows a more efficient tracking of the free surface. It is based on the concept of a fractional VOF for tracking free surface boundaries using the donor–acceptor approximation algorithm. The treatment of the free surface configuration using a single function F is computationally very efficient. This general-purpose code has very promising features and is generally acknowledged as the basis for all subsequent developments in the VOF-field.

Its successor code NASA-VOF2D (Torrey et al., 1985) contains several improvements. A partial-cell treatment (FAVOR) allows for curved or sloping boundaries. Fixes have been made in the donor–acceptor algorithm, and an optional conjugate gradient solver is used rather than the original successive over-relaxation method for solving the pressure equation. Both SOLA-VOF and NASA-VOF2D codes have been developed at Los Alamos National Laboratory (LANL), NM, USA.

From 1985 on, Hirt continued developments on the VOF model in the commercial CFD code FLOW-3D. It is regarded as a state-of-the-art CFD code for general applicability. At LANL, other successor codes have been developed since then: RIPPLE (Kothe et al., 1991) for 2D and TELLURIDE (Kothe et al., 1997) for 3D simulations. In RIPPLE and TELLURIDE, a projection method is used to solve for the incompressible flow. The pressure Poisson equation is solved via

conjugates gradient technique. Particularly, the modeling of surface tension problems and the modeling of the filling, cooling and solidification processes of castings have been enhanced. These models incorporate the latest advances in numerical algorithms and parallel processing.

These VOF codes have been applied in the fields of casting, coating, dynamics of drops, ship hydrodynamics, etc. In the field of coastal engineering, VOF-type models are not yet very well known or widely used. Nevertheless, during the last few years, there has been significant advance towards the implementation of numerical "wave flumes" using the VOF concept because of increasing speed and storage memory of modern computers that become available.

Austin and Schlueter (1982) presented the first rough application of the SOLA-VOF model in the field of coastal engineering. The model predicted the flow field in a porous amour layer of a breakwater schematized as a rectangular block system. Although in a relatively crude form, these calculations were the start of the simulation of wave propagation and interaction with structures in coastal engineering.

Lemos (1992) incorporated a $k-\varepsilon$ turbulence model in a SOLA-VOF based code 2DHYDROTUR that allowed a limited description of the turbulence field. Lemos (1992) also implemented higher order finite difference schemes in a VOF-based code for improving stability and accuracy of the numerical solutions. These improved schemes were applied to simulations of wave impact on structures, and included the computation of the wave impact forces. No wave absorption boundaries or open sea boundaries have been implemented.

The SKYLLA model (Van der Meer et al., 1992) presently being developed at Delft Hydraulics is based on SAVOF, a stripped version of SOLA-VOF obtained from the National Aerospace Laboratory (NLR) in the Netherlands. The first computations showed that it is possible to simulate breaking waves on a slope. Several extensions have been added since then. The most important are the

inclusion of a conjugate gradient solver for the pressure Poisson equation (Van der Meer et al., 1992), another algorithm (FLAIR; Ashgriz and Poo, 1991) for the calculation of the *F* flux between adjacent cells and the subsequent free surface calculation (Petit and van den Bosch, 1992), simulation of porous flow inside permeable coastal structures, implementation of a 'weakly reflective boundary' (i.e., a Sommerfeld radiation boundary) (Van Gent et al., 1994). The model has been validated using both analytical and experimental data (Van Gent, 1995). The SKYLLA code is currently one of the most versatile and powerful numerical models today for applications in the field of coastal engineering.

Wu (1994) applied a VOF model based on the SOLA-VOF model for the simulation of breaking and non-breaking wave kinematics for vertical structures with various impermeable foreshore geometries. He simulated the complete impact pressure and the resulting loading when entrapped air is neglected. A poorly reflecting boundary condition similar to the SKYLLA model has been implemented.

Chopra and Greated (1995) used a SOLA-VOF model and that was an improvement over VOF model by Wu. It included a basic model for air pocket entrapment.

Iwata et al. (1996) used a modified SOLA-VOF model for numerical comparison with experimental data from breaking and post-breaking wave deformation due to submerged impermeable structures. Waves are generated internally in the computational domain using the source generation technique (Brorsen and Larsen, 1987). Absorption of the waves is done using the Sommerfeld radiation boundary condition.

Sabeur et al. (1996) presented a modified SOLA-VOF model called NEWMOTICS. Special attention is paid to improve the free surface boundary conditions. At the wave-generating boundary, a weakly reflecting boundary condition is used. A conjugate gradient solver is implemented for use in parallel

processing. More recent validation of the model is described in Waller et al. (1998). The code has been validated using theoretical and experimental data in the context of a solitary wave propagating into water of varying depth with impermeable bottom.

Troch (1997) presented the numerical model VOFbreak^2 based on the SOLA-VOF code. Several modifications are implemented to refine the numerical model for wave motion on and in coastal structures. Special attention is paid to applications involving rubble mound breakwaters. Wave boundary conditions are added, where any wave theory can be applied to provide the surface elevation and the velocity components in horizontal and vertical direction. The governing equations are extended, to include the simulation of porous flow inside the permeable coastal structure, by adding the Forchheimer resistance terms. The numerical model is being verified with both physical model data and prototype data. Some selected improvements from NASA-VOF2D have been implemented into VOFbreak^2, such as a numerical defoamer technique, and fixes on the donor–acceptor algorithm.

There is no general model presented including most of the physical processes involved, but researchers add only selected physical processes for their particular applications. It is clear that all codes still are research codes that need very careful validation before these become (coastal) engineering tools for daily use in the design process.

3.3 Two-dimensional moored-floating body-wave interaction model developed by Rahman (2005)

Rahman (2005) developed a two-dimensional numerical model combining the SOLA-VOF model and porous body model, to estimate the wave forces acting on a pontoon type submerged floating breakwater. As the floating body oscillates due to the wave action, the position of the floating body as well as the obstacle cell positions always changes. In Fig. 3.2, the treatment of the cells during the

oscillation of the floating body due to wave action is shown. Partially obstacle cells are obtained due to cutting the fluid or empty or surface cells by the surfaces of the floating body. These cells are partially filled by floating body material and partially by fluid and /or air. From the concept of porosity of the cell, this kind cell is treated by the concept of porous cell.

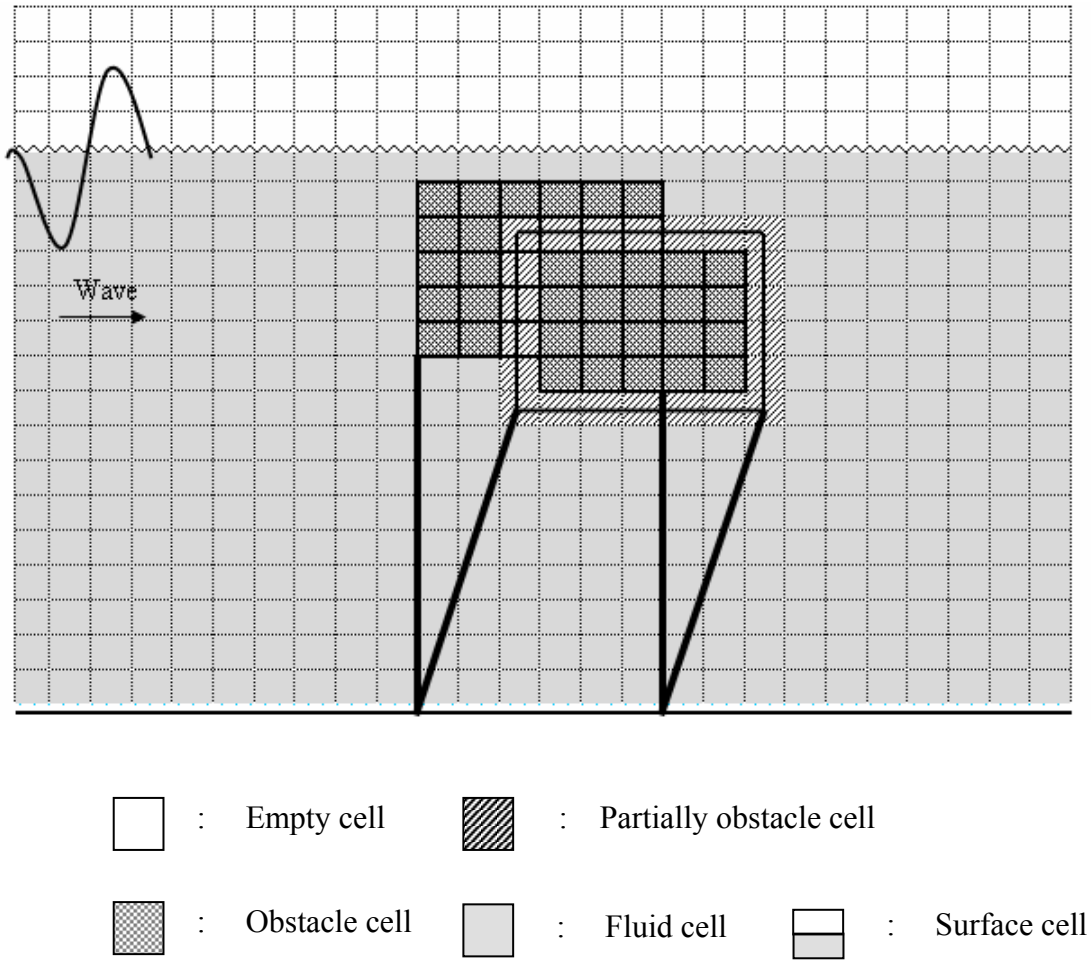

Fig. 3.2: Treatment of the cells during the oscillation of the floating body

The governing equations used in the model include added terms of γ_x, γ_z and γ_v. Here, γ_x and γ_z represent the ratio of the permeable length to the cell length in vertical and horizontal directions respectively and γ_v represents the ratio of the permeability volume in a cell.

So the continuity equation, Navier Stokes equations and the VOF function equation should be modified as below considering the effects of γ_x, γ_z and γ_v:

The modified continuity equation is,

$$\frac{\partial(\gamma_x u)}{\partial x}+\frac{\partial(\gamma_z w)}{\partial z}=q(x,z,t) \tag{3.1}$$

$$q(x,z,t)=\begin{cases} q^*(z,t) & : \ x=x_S \\ 0 & : \ x\neq x_S \end{cases} \tag{3.2}$$

where u and w are the flow velocity of x and z direction respectively, q is the wave generation source with q^* as the source strength which is only located at $x=x_S$ and t is the time.

The modified Navier-Stokes equations are as follows,

$$\gamma_v\frac{\partial u}{\partial t}+\gamma_x u\frac{\partial u}{\partial x}+\gamma_z w\frac{\partial u}{\partial z}=-\frac{\gamma_v}{\rho}\frac{\partial p}{\partial x}+\upsilon\left[\frac{\partial}{\partial x}\left\{\gamma_x\left(2\frac{\partial u}{\partial x}\right)\right\}+\frac{\partial}{\partial z}\left\{\gamma_z\left(\frac{\partial u}{\partial z}+\frac{\partial w}{\partial x}\right)\right\}\right] \tag{3.3}$$

$$\gamma_v\frac{\partial w}{\partial t}+\gamma_x u\frac{\partial w}{\partial x}+\gamma_z w\frac{\partial w}{\partial z}=-\frac{\gamma_v}{\rho}\frac{\partial p}{\partial z}+\upsilon\left[\frac{\partial}{\partial x}\left\{\gamma_x\left(\frac{\partial u}{\partial z}+\frac{\partial w}{\partial x}\right)\right\}+\frac{\partial}{\partial z}\left\{\gamma_z\left(2\frac{\partial w}{\partial z}\right)\right\}\right] +\frac{1}{3}\upsilon\frac{\partial q}{\partial z}-\gamma_v g-\beta w \tag{3.4}$$

where, p is the pressure, υ is the kinematic viscosity, ρ is the fluid density, g is the gravitational acceleration and β is wave dissipation factor which equals 0 except for the added dissipation zone. The modified advection equation of VOF function F is,

$$\gamma_v\frac{\partial F}{\partial t}+\frac{\partial(\gamma_x uF)}{\partial x}+\frac{\partial(\gamma_z wF)}{\partial z}=Fq \tag{3.5}$$

In case of oscillating floating body, special boundary condition is applied to the cells adjacent to the obstacle faces. That is, the water particle velocities at obstacle

face cells are set to equal as the velocities of the moving breakwater in respective directions of x and z axis.

3.4 Numerical wave model with VOF method

3.4.1 Governing equations

The basic equations used for VOF method are the continuity equation, the Navier-Stokes equation for incompressible fluid and the advection equation that represents the behavior of the free surface. Because the wave generation source is placed within the computational domain, these equations involve the wave generation source. The continuity equation is,

$$\frac{\partial u}{\partial x}+\frac{\partial w}{\partial z}=q(x,z,t) \tag{3.6}$$

$$q(x,z,t)=\begin{cases} q^*(z,t) & : \quad x=x_S \\ 0 & : \quad x\neq x_S \end{cases} \tag{3.7}$$

where u and w are the flow velocity of x and z direction respectively, q is the wave generation source with q^* as the source strength which is only located at $x =$ (3.8) and t is the time. The wave generation source q^* is defined as follows so that the vertically integrated quantity of q^* is equal to that in the non-reflection case (Ohyama and Nadaoka, 1991). q^* is also gradually intensified for the three wave periods (Fig. 3.3) from the start of wave generation in order to guarantee a stable regular wave train, as mentioned by Brorsen and Larsen (1987), shown in Eq. (3.8).

$$q^*=\begin{cases} \left\{1-\exp\left(-\frac{2t}{T_i}\right)\right\}2U_0\frac{\eta_0+h}{\eta_0+h}/\Delta x_S & : t/T_i\leq 3 \\ 2U_0\frac{\eta_0+h}{\eta_0+h}/\Delta x_S & : t/T_i>3 \end{cases} \tag{2.22}$$

where t is the time from the start of wave generation, T_i is the incident wave period, h is the still water depth, and η_s is the water surface elevation at the source line ($x = x_s = 0$). Δx_s is the mesh size in the x-direction at $x = x_s$, and is required in

order to apply the non-reflective wave generator to the finite difference method. U_0 and η_0 are the time variation of horizontal velocity and water surface based on third-order Stokes wave theory, respectively. The coefficient "2" of U_0 in the right hand side of Eq. (3.8) corresponds to two propagating waves toward both the left and right sides of the wave generation source.

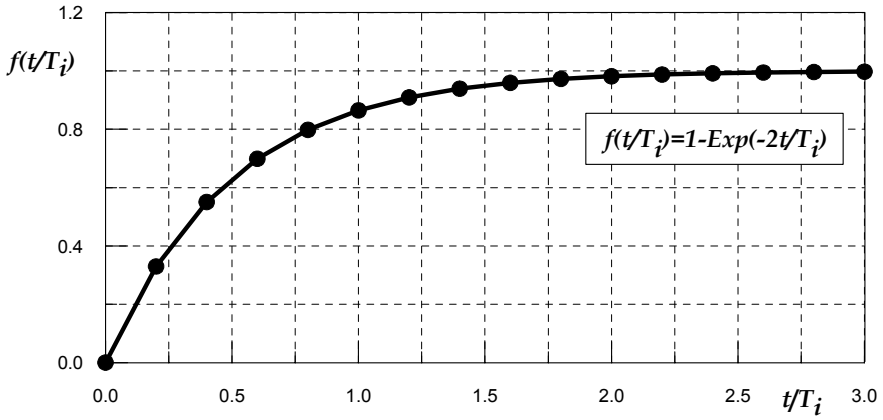

Fig. 3.3: Intensification factor of wave generation source function q for $t/T_i \leq 3$.*

The Navier-Stokes equation,

$$\frac{\partial u}{\partial t} + u\frac{\partial u}{\partial x} + w\frac{\partial u}{\partial z} = -\frac{1}{\rho}\frac{\partial p}{\partial x} + \upsilon\left(\frac{\partial^2 u}{\partial x^2} + \frac{\partial^2 u}{\partial z^2}\right) + uq \tag{3.9}$$

$$\frac{\partial w}{\partial t} + u\frac{\partial w}{\partial x} + w\frac{\partial w}{\partial z} = -\frac{1}{\rho}\frac{\partial p}{\partial z} + \upsilon\left(\frac{\partial^2 w}{\partial x^2} + \frac{\partial^2 w}{\partial z^2}\right) + wq + \frac{1}{3}\upsilon\frac{\partial q}{\partial z} - g - \beta w \tag{3.10}$$

where p is the pressure, υ is the kinematic viscosity, ρ is the fluid density, g is the gravitational acceleration and β is the wave dissipation factor which equals 0 except for the added dissipation zone.

The advection equation of VOF function F is derived by considering conservation of mass of the fluid in each cell. The advection equation of VOF function F,

$$\frac{\partial F}{\partial t} + \frac{\partial uF}{\partial x} + \frac{\partial wF}{\partial z} = Fq \tag{3.11}$$

The equations include the added terms different from the well-known continuity and Navier-Stokes equations because the wave generation source and the added dissipation zone exist within the computational domain.

List of parameters used in the 2-D numerical model based on SOLA-VOF is given in Table 3.1:

Table 3.1: List of parameters

Symbol	Name of the parameter	Value used in the 2-D numerical model
α	Numerical stability factor	0.5
β	Wave dissipation factor	1.03(for added dissipation zone)
		0 (otherwise)
ζ	Tolerance value for divergence term	$1X\ 10^{-3}$
υ	Co-efficient of viscosity	0.0101 cm^2/sec
ω	Acceleration factor	1.7 $rad/\ sec^2$
ρ	Fluid density	1 $gm/\ cm^3$
g	Gravitational acceleration	980 $cm/\ sec^2$

It should be noted that the effect of surface tension and breaking-wave induced air bubbles are ignored in this study on the assumption that they do not have much impact on the wave breaking process. Also, a turbulence model should generally be incorporated into wave breaking simulations. However, the conventional turbulence models have been chiefly developed for unidirectional internal turbulent flows, while the breaking wave-induced turbulence is introduced from the free surface boundary in an oscillatory flow field. Therefore, it is difficult to find a turbulence model that can appropriately reproduce the energy dissipation in the wave breaking process and to give proper boundary conditions for it.

3.4.2 Computational procedure

The equations (3.6) to (3.11) are calculated by a finite difference method using a staggered mesh. The free surface geometric model of VOF method is shown in Fig. 3.4.

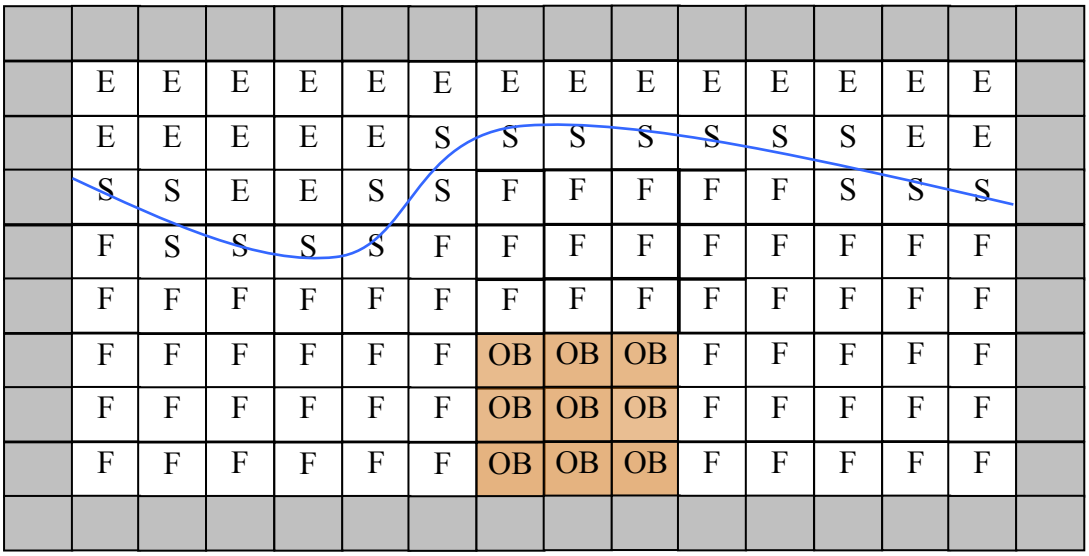

E = Empty cell, S = Surface cell, F = Fluid cell, OB= Obstacle cell

Fig. 3.4: Free surface geometric model of VOF method

On the staggered mesh, the flow velocities u and w are put on the cell boundary, and the pressure p, wave generation source q and VOF function F are set on the center of each cell as shown in Fig 3.5(a). Here Δx and Δz, in Fig. 3.5(a), are the cell lengths in the respective directions of x and z, and each cell is identified by sub suffix (i, k). The cell is classified into four types; a full cell filled with fluid, an empty cell occupied by air, a surface cell containing both fluid and air and an obstacle cell that represents the structure.

The SOLA scheme is employed to calculate the pressure and flow velocity in each time step. And a type of donor-acceptor flux approximation is used to calculate the advection of the VOF function F computing the free surface. The advections are calculated by velocities of the adjoining cell by using a donor cell which transports a fluid and an acceptor cell which receives a advect fluid. The physical characteristics of the cell are defined by the values of VOF function F. The cell in air, in the surface and in the water are denoted with F=0, $0<F<1$, and F=1 respectively, Fig. 3.5 (b).

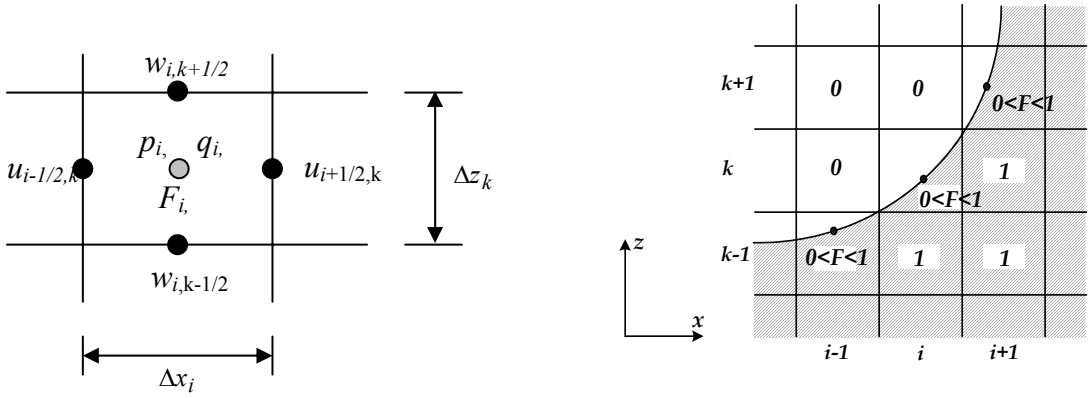

(a) Staggered mesh (b) Value of VOF function *F*

Fig. 3.5: *Staggered mesh and classification of cells*

To determine accurately the location of the free surface at the next time step, it is therefore necessary to know the orientation of the free surface within the surface cell. Table 3.2 shows the classified orientation of the free surface.

Table 3.2 Classification of surface cell (i,k)

RF	Contents
1	Surface normal to the x-axis and full cell at (i-1,k)
2	Surface normal to the x-axis and full cell at (i+1,k)
3	Surface normal to the z-axis and full cell at (i,k-1)
4	Surface normal to the z-axis and full cell at (i,k+1)

As the VOF technique assumes that the free surface is approximated by a straight line cutting through the orientation of the free surface within the surface cell is determined so as to agree with the direction of the maximum fluid amount among the $FX_{i-1,k}, FX_{i+1,k}, FZ_{i,k-1}$ and $FZ_{i,k+1}$ which are calculated from the surrounding cells by Eqs. (3.12) and (3.13).

$$FX_{i,k} = F_{i-1,k} + F_{i,k} + F_{i+1,k} \tag{3.12}$$

$$FZ_{i,k} = F_{i,k-1} + F_{i,k} + F_{i,k+1} \tag{3.13}$$

The basic procedure for the modified SOLA scheme is as follows:

(i) Explicit scheme of the momentum equations (Eqs. (3.9) and (3.10)) is employed to calculate the first approximation of the velocity at the next time step using the velocity, pressure and the wave generation source at the present time step. The calculated velocities do not satisfy the continuity equation in general.

(ii) To satisfy completely the continuity equation Eq.(3.6), the pressure and velocities are iteratively adjusted in the cell occupied by the fluid.

Stable numerical results can be obtained by repeating the above mentioned procedures under suitable boundary conditions at each time step. It should be noticed that the cell which can satisfy the continuity equation by means of the modified SOLA scheme is only the full one. The surface cell, however, can satisfy the continuity equation by employing the velocity boundary condition. The momentum equations are only used to calculate the velocity on the surface of full cell. Since the velocity on the interface between surface cells or between the surface cell and empty cell can not be calculated with the momentum equations only, the boundary conditions are necessary to calculate the velocities. Fig. 3.6 shows the Flow Chart of the two-dimensional numerical model based on SOLA-VOF Scheme.

3.4.3 Boundary conditions

3.4.3.1 Free-surface boundary conditions

Boundary conditions for velocity:

There are two boundary conditions for water particle velocity, that is, (1) a boundary condition for the velocity parallel to the free-surface and (2) a boundary condition for the velocity normal to the free-surface.

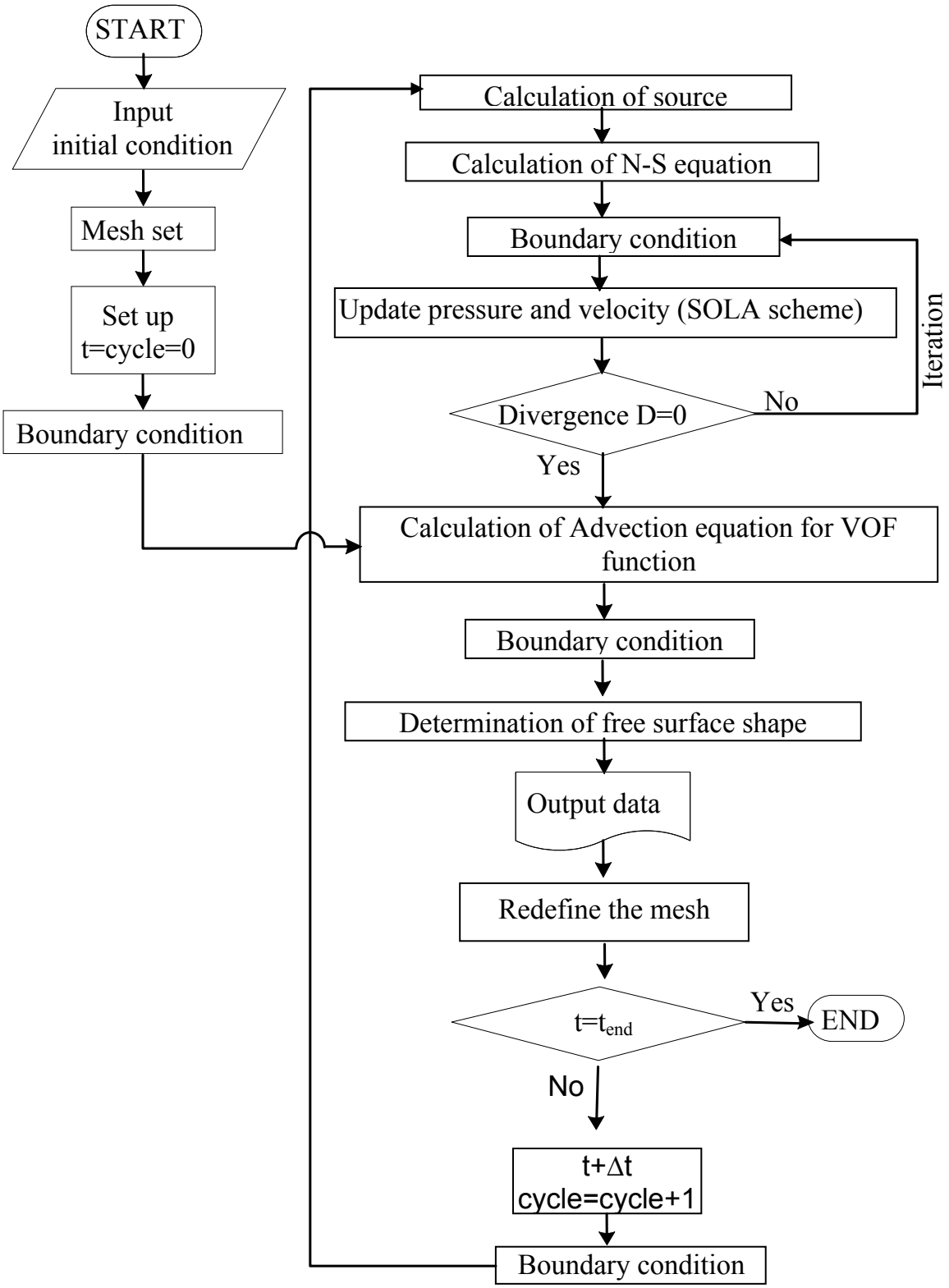

Fig. 3.6: *Flow chart of computational procedures*

In the first boundary condition, since an adjacent full cell exists in the direction indicated be the flag RF, the velocity on the surface cell is set equal to the velocity on the interface in contact with the adjacent full cell, which can be calculated by the governing equations. In the 2nd boundary condition, the velocity is determined so that the continuity equation is satisfied in surface cells. Even if a surface cell may change to a full cell at the next time step, the full cell is still able to satisfy the continuity equation (Fig. 3.7 (a)).

Boundary conditions for pressure:

As mentioned before, the pressure in the full cell can be calculated by means of the SOLA scheme. However, in surface cells, different procedures are required because the locations of the pressure points in the staggered mesh generally differ from the actual locations on the free surface. Therefore, the linear interpolation or extrapolation between the pressure on the free surface (atmospheric pressure) and the pressure of the adjacent full cell in the direction indicated by flag *RF* is used to calculate the pressure of the surface cell (Fig. 3.7 (b)).

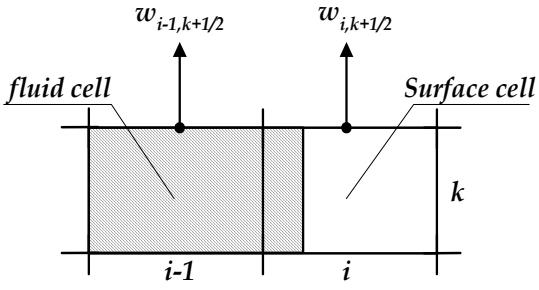

Fig. 3.7(a): Boundary condition of velocity

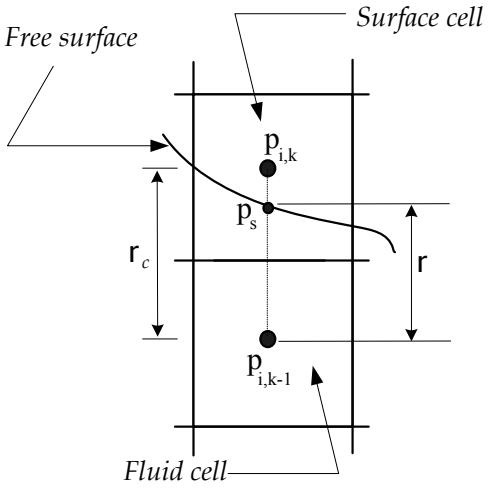

Fig. 3.7(b): Boundary condition of pressure

3.4.3.2 Open boundary condition

An added dissipation zone method (Hinatsu, 1992) is used to treat the open boundaries. As shown in Fig. 3.8, the waves are damped by numerical dissipation effects due to the coarse grids and the fictitious damping forces based on the Stokes damping law. The damping force in the *x*-direction is not taken into account to avoid the velocity damping in the uniform horizontal flow.

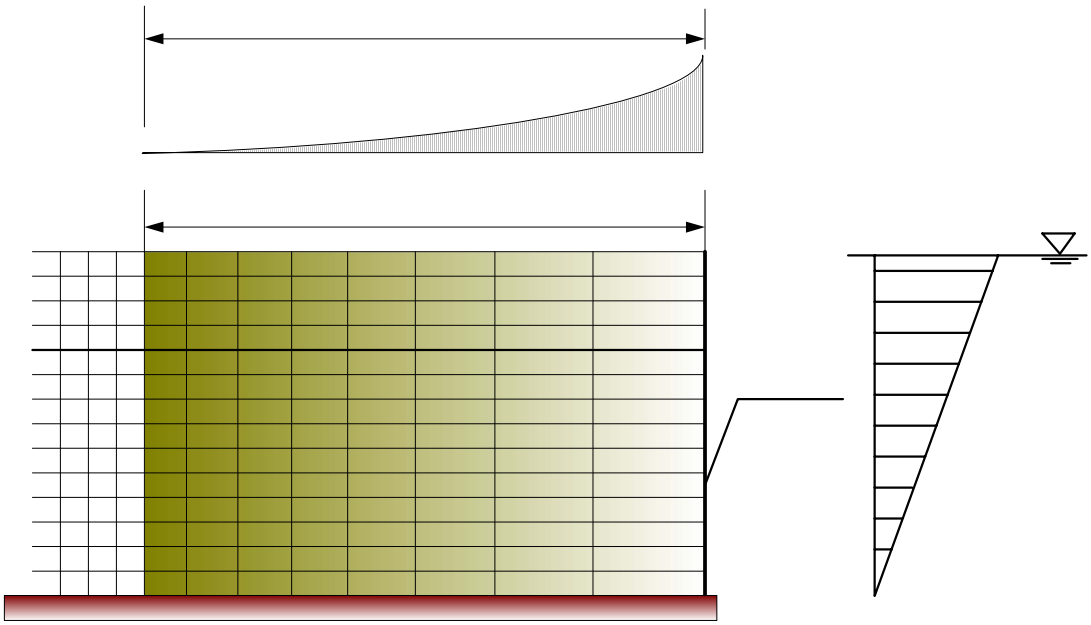

Fig. 3.8: *Open boundary treatment due to added dissipation zone*

3.4.3.3 Other boundary conditions

Sommerfeld radiation condition Eq.(3.14) is applied for the open boundaries. And, non-slip condition is applied on the sea bed.

$$\frac{\partial Q}{\partial t} \pm C \frac{\partial Q}{\partial x} = 0 \tag{3.14}$$

where Q is the quantity representing the velocities u and w, and so on, and C is the wave celerity. The value of water particle velocity tends to 0 at the sea bed because of non-slip condition. So the roughness parameter of the sea bed material has no influence in this model.

3.4.4 Numerical stability considerations

Numerical calculations often have computed quantities that develop large, high frequency oscillations in space, time, or both. This behavior is usually referred to as a numerical instability, especially if the physical problem being studied is known not to have unstable solutions. When the physical problem does have unstable solutions and if the calculated results exhibit significant variations over distances comparable to a cell width or over times comparable to the time increment, the accuracy of the results cannot be relied on. To prevent this type of numerical instability or inaccuracy certain restrictions must be observed in defining the mesh increments Δx_i and $\Delta z_{k,}$ the time increment Δt, and the upstream differencing parameter α.

For accuracy, the mesh increments must be chosen small enough to resolve the expected spatial variations in all dependent variables. When this is impossible because of limitations imposed by computing time or memory requirements, special care must be exercised in interpreting calculation results. For example, in computing the flow in a large chamber it is usually impossible to resolve thin boundary layers along the confining walls. In many applications, however the presence of thin boundary layers is unimportant and free-slip boundary conditions can be justified as a good approximation.

Once a mesh has been chosen, the choice of the time increment necessary for stability is governed by two restrictions. First, material cannot move through more than one cell in one time step because the difference equations assume fluxes only adjacent cells. Therefore, the time increment must satisfy the inequality

$$\Delta t < \min\left\{\frac{\Delta x_i}{|u_{i,k}|}, \frac{\Delta z_k}{|w_{i,k}|}\right\} \tag{3.15}$$

where the minimum is with respect to every cell in the mesh. Typically, Δt is chosen equal to one-fourth to one-third of the minimum cell transit time. Second, when a nonzero value of kinematic viscosity is used, momentum must not diffuse

more than approximately one cell in one time step. A linear stability analysis shows that this limitation implies

$$\nu\Delta t < \frac{1}{2}\left\{\frac{\Delta x_i^{\,2}\Delta z_k^{\,2}}{\Delta x_i^{\,2}+\Delta z_k^{\,2}}\right\} \tag{3.16}$$

With Δt chosen to satisfy the above two inequalities, the last parameter need to ensure numerical stability is α. The proper choice for α is

$$1 \geq \alpha > \max\left\{\left|\frac{u_{i,k}\Delta t}{\Delta x_i}\right|, \left|\frac{w_{i,k}\Delta t}{\Delta z_k}\right|\right\} \tag{3.17}$$

As a rule of thumb, an α approximately 1.2 to 1.5 times larger than the right-hand inequality is a good choice. If α is too large an unnecessary smoothing (diffusion-like truncation errors) may be introduced.

3.5 SOLA-VOF Scheme for Modeling of Fixed Submerged Body

3.5.1 The Volume of Fluid (VOF) Method

Several methods have been previously used to approximate free boundaries in finite-difference numerical simulations. A simple but powerful, method is described that is based on the concept of a fractional volume of fluid (VOF). This method is shown to be more flexible and efficient than other methods for treating complicated free boundary configurations. A free surface is an interface between a liquid and a gas in which the gas can only apply a pressure on the liquid. The free surfaces are modeled with the Volume of Fluid (VOF) technique, which was first reported in Nichols and Hirt (1975), and more completely in Hirt and Nichols (1981). The VOF method consists of three ingredients: a scheme to locate the surface, an algorithm to track the surface as a sharp interface moving through a computational grid, and a means of applying boundary conditions at the surface.

In VOF method, a function F is defined whose value is unity at any point occupied by fluid and zero otherwise. The average value of F in a cell would then

represent the fractional volume of the cell occupied by fluid. In particular, a unit value of F would correspond to a cell full of fluid, while a zero value would indicate that the cell contained no fluid. Cells with F values between zero and one must then contain a free surface. In addition to defining which cells contain a boundary, the information can be obtained in the VOF method. The normal direction to the boundary lies in the direction in which the value of F changes most rapidly. Because F is a step function, however, its derivatives must be computed in a special way, as described below. When properly computed, the derivatives can then be used to determine the boundary normal. Finally, when both the normal direction and the value of F in a boundary cell are known, a line cutting the cell can be constructed that approximates the interface there. This boundary location can then be used in the setting of boundary conditions.

Although the VOF technique can locate free boundaries and with a minimum of stored information, the method is worthless unless an algorithm can be devised for accurately computing the evolution of the F field. The time dependence of F is governed by the equation,

$$\frac{\partial F}{\partial t}+u\frac{\partial F}{\partial x}+v\frac{\partial F}{\partial y}=0 \qquad (3.18)$$

This equation states that F moves with the fluid. However, the flux of F through each cell face of Eulerian grid will be required. Standard finite-difference approximations would lead to a smearing of the F function and interfaces would lose their definition. Fortunately, the fact F is a step function with values of zero or one permits the use of a flux approximation that preserves its discontinuous nature. This approximation, referred to as a donor-acceptor method, is described below in more detail.

In summary, with minimum storage requirements the VOF method follows regions rather than surfaces. So all logic problems associated with intersecting surfaces are avoided with the VOF technique. The method is also applicable to 3-D computations, where, its conservative use of stored information is highly advantageous. Thus the VOF method provides a simple and economical way to

track free boundaries in 2- or 3-D meshes. In principle the method could be used to track surfaces of discontinuity in material properties, in tangential velocity, or any other property. The particular case being represented determines the specific boundary condition that must be applied at the location of the boundary.

3.5.2 SOLA Scheme

SOLA is the numerical SOLution Algorithm for transient fluid flows. It solves the time-dependent incompressible Navier-Stokes equations on a 2-D rectangular domain. In the 2-D computation, the velocity components *u* and *w*, and the pressure *p* at the next time step are calculated using the SOLA scheme. Then, using the new calculated velocity components, the new free surface configuration is computed with the advection equation of VOF function *F,* which is solved by using the donor–acceptor method (Hirt and Nichols, 1981). Using 2nd order central difference approximation, the equation of continuity (Eq. 3.6) at the center of the cell can be written as,

$$\frac{u_{i+1/2,k}^{n+1} - u_{i-1/2,k}^{n+1}}{\Delta x_i} + \frac{w_{i,k+1/2}^{n+1} - w_{i,k-1/2}^{n+1}}{\Delta z_k} = q_{i,k}^{n+1} \tag{3.19}$$

where, the superscripts represent the number of time step and the subscripts represent the position of the cell.

The time derivative is discretized by the forward time difference method. The central difference method is used to discretize the pressure gradient terms and stress gradient terms. The combination of 2nd order central difference method and 1st order upwind method is employed to discretize the convection terms.

So the Navier Stokes equations (Eq. 3.8 and Eq. 3.9) can be written as

$$u_{i+1/2,k}^{n+1} = u_{i+1/2,k}^{n} + \Delta t\left[-\frac{p_{i+1,k}^{n} - p_{i,k}^{n}}{\rho \Delta x_{i+1/2}} - ADVX^{n} + VISX^{n} \right] \tag{3.20}$$

$$w_{i,k+1/2}^{n+1} = w_{i,k+1/2}^{n} + \Delta t\left[-g - \frac{p_{i,k+1}^{n} - p_{i,k}^{n}}{\rho \Delta z_{k+1/2}} - ADVZ^{n} + VISZ^{n} + SWZ^{n} \right] \tag{3.21}$$

where,

$$\begin{aligned} ADVX^{n} &= (u\frac{\partial u}{\partial x} + w\frac{\partial u}{\partial z})_{i+1/2,k} \\ &= \frac{u_{i+1/2,k}^{n}}{\Delta x_{\alpha 1}}\left[\Delta x_i \frac{u_{i+3/2,k}^{n} - u_{i+1/2,k}^{n}}{\Delta x_{i+1}} + \Delta x_{i+1} \frac{u_{i+1/2,k}^{n} - u_{i-1/2,k}^{n}}{\Delta x_i} \right. \\ &\quad \left. + \alpha sign(u_{i+1/2,k}^{n})\left(\Delta x_{i+1} \frac{u_{i+1/2,k}^{n} - u_{i-1/2,k}^{n}}{\Delta x_i} - \Delta x_i \frac{u_{i+3/2,k}^{n} - u_{i+1/2,k}^{n}}{\Delta x_{i+1}} \right) \right] \\ &\quad + \frac{w_{i+1/2}^{n}}{\Delta z_{\alpha 1}}\left[\Delta z_{k-1/2} \frac{u_{i+1/2,k+1}^{n} - u_{i+1/2,k}^{n}}{\Delta z_{k+1/2}} + \Delta z_{k+1/2} \frac{u_{i+1/2,k}^{n} - u_{i+1/2,k-1}^{n}}{\Delta z_{k-1/2}} \right. \\ &\quad \left. + \alpha sign(w_{i+1/2,k}^{n})\left(\Delta z_{k+1/2} \frac{u_{i+1/2,k}^{n} - u_{i+1/2,k-1}^{n}}{\Delta z_{k-1/2}} \right.\right. \\ &\quad \left.\left. - \Delta z_{k-1/2} \frac{u_{i+1/2,k+1}^{n} - u_{i+1/2,k}^{n}}{\Delta z_{k+1/2}} \right) \right] \end{aligned} \tag{3.22}$$

$$\begin{aligned} ADVZ^{n} &= (u\frac{\partial w}{\partial x} + w\frac{\partial w}{\partial z})_{i,k+1/2} \\ &= \frac{u_{i,k+1/2}^{n}}{\Delta x_{\alpha 12}}\left[\Delta x_{i-1/2} \frac{w_{i+1,k+1/2}^{n} - w_{i,k+1/2}^{n}}{\Delta x_{i+1/2}} + \Delta x_{i+1/2} \frac{w_{i+1/2,k}^{n} - w_{i-1,k+1/2}^{n}}{\Delta x_{i-1/2}} \right. \\ &\quad \left. + \alpha sign(u_{i,k+1/2}^{n})\left(\Delta x_{i+1/2} \frac{w_{i,k+1/2}^{n} - w_{i-1,k+1/2}^{n}}{\Delta x_{i-1/2}} \right.\right. \\ &\quad \left.\left. - \Delta x_{i-1/2} \frac{w_{i+1,k+1/2}^{n} - w_{i,k+1/2}^{n}}{\Delta x_{i+1/2}} \right) \right] \\ &\quad + \frac{w_{i}^{n}}{\Delta z_{\alpha 2}}\left[\Delta z_k \frac{w_{i,k+3/2}^{n} - w_{i,k+1/2}^{n}}{\Delta z_{k+1}} + \Delta z_{k+1} \frac{w_{i,k+1/2}^{n} - w_{i,k-1/2}^{n}}{\Delta z_k} + \alpha sign(w_{i,k+1/2}^{n}) \right. \\ &\quad \left. \left(\Delta z_{k+1} \frac{w_{i,k+1/2}^{n} - w_{i,k-1/2}^{n}}{\Delta z_k} - \Delta z_k \frac{w_{i,k+3/2}^{n} - w_{i,k+1/2}^{n}}{\Delta z_{k+1}} \right) \right] \end{aligned} \tag{3.23}$$

$$VISX^n = \left\{ \nu \left(\frac{\partial^2 u}{\partial x^2} + \frac{\partial^2 u}{\partial z^2} \right) \right\}_{i+1/2,k}$$

$$= \left(\nu + (1-\alpha)\frac{\Delta t}{2}(u^n_{i+1/2,k})^2 \right) \left\{ \frac{1}{\Delta x_{i+1/2}} \left(\frac{u^n_{i+3/2,k} - u^n_{i+1/2,k}}{\Delta x_{i+1}} - \frac{u^n_{i+1/2,k} - u^n_{i-1/2,k}}{\Delta x_i} \right) \right\}$$

$$+ \left(\nu + (1-\alpha)\frac{\Delta t}{2}(w^n_{i+1/2,k})^2 \right) \left\{ \frac{1}{\Delta z_k} \left(\frac{u^n_{i+1/2,k+1} - u^n_{i+1/2,k}}{\Delta z_{k+1/2}} - \frac{u^n_{i+1/2,k} - u^n_{i+1,k-1}}{\Delta z_{k-1/2}} \right) \right\} \quad (3.24)$$

$$VISZ^n = \left\{ \nu \left(\frac{\partial^2 w}{\partial x^2} + \frac{\partial^2 w}{\partial z^2} \right) \right\}_{i,k+1/2}$$

$$= \left(\nu + (1-\alpha)\frac{\Delta t}{2}(u^n_{i,k+1/2})^2 \right) \left\{ \frac{1}{\Delta x_i} \left(\frac{w^n_{i+1,k+1/2} - w^n_{i,k+1/2}}{\Delta x_{i+1/2}} - \frac{w^n_{i,k+1/2} - w^n_{i-1,k+1/2}}{\Delta x_{i-1/2}} \right) \right\}$$

$$+ \left(\nu + (1-\alpha)\frac{\Delta t}{2}(w^n_{i,k+1/2})^2 \right) \left\{ \frac{1}{\Delta z_{k+1/2}} \left(\frac{w^n_{i,k+3/2} - w^n_{i,k+1/2}}{\Delta z_{k+1}} - \frac{w^n_{i,k+1/2} - w^n_{i,k-1/2}}{\Delta z_k} \right) \right\} \quad (3.25)$$

$$SWZ^n = \left(\frac{\nu}{3}\frac{\partial q}{\partial z} - \beta w \right)_{i,k+1/2} = \frac{\nu}{3}\frac{q^n_{i,k+1} - q^n_{i,k}}{\Delta z_{k+1/2}} - \beta_{i,k+1/2} w^n_{i,k+1/2} \quad (3.26)$$

Here,

$$\Delta x_{i-1/2} = \frac{1}{2}(\Delta x_{i-1} + \Delta x_i)$$

$$\Delta x_{i+1/2} = \frac{1}{2}(\Delta x_i + \Delta x_{i+1})$$

$$\Delta z_{k-1/2} = \frac{1}{2}(\Delta z_{k-1} + \Delta z_k)$$

$$\Delta z_{k+1/2} = \frac{1}{2}(\Delta z_k + \Delta z_{k+1})$$

$$\Delta x_{\alpha 1} = \Delta x_i + \Delta x_{i+1} + \alpha sign(u^n_{i+1/2,k})(\Delta x_{i+1} - \Delta x_i)$$

$$\Delta z_{\alpha 1} = \Delta z_{k-1/2} + \Delta z_{k+1/2} + \alpha sign\,(w^n_{i+1/2,k})(\Delta z_{k+1/2} - \Delta z_{k-1/2})$$

$$\Delta x_{\alpha 2} = \Delta x_{i-1/2} + \Delta x_{i+1/2} + \alpha sign\,(u^n_{i,k+1/2})(\Delta x_{i+1/2} - \Delta x_{i-1/2})$$

$$\Delta z_{\alpha 2} = \Delta z_k + \Delta z_{k+1} + \alpha sign\,(w^n_{i,k+1/2})(\Delta z_{k+1} - \Delta z_k)$$

$$u^n_{i,k+1/2} = \frac{1}{4}\left(\frac{\Delta z_k u^n_{i+1/2,k+1} + \Delta z_{k+1} u^n_{i+1/2,k} + \Delta z_k u^n_{i-1/2,k+1} + \Delta z_{k+1} u^n_{i-1/2,k}}{\Delta z_{k+1/2}}\right)$$

$$w^n_{i+1/2,k} = \frac{1}{4}\left(\frac{\Delta x_i w^n_{i+1,k+1/2} + \Delta x_{i+1} w^n_{i,k+1/2} + \Delta x_i w^n_{i+1,k-1/2} + \Delta x_{i+1} w^n_{i,k-1/2}}{\Delta z_{k+1/2}}\right)$$

where Δt is time step, $ADVX^n$, $ADVZ^n$ *are* convective terms, $VISX^n$, $VISZ^n$ are viscosity terms, α is the donor-cell fraction, β is the wave dissipation factor which equals 0 except for the added dissipation zone. When α=0, this formulation reduces to a 2nd order accurate, central difference approximation. When α=1, the 1st order donor cell form is recovered. This particular form is then at least 1st order accurate for any α between this limit. In order to obtain stability while maximizing accuracy, experience indicates that 0.25< α <0.5 may be utilized. In this computation, both 2nd order central difference approximation and 1st order upwind method is used considering α=0.5. In order to prevent numerical diffusion, the artificial viscosity term $+(1-\alpha)\frac{\Delta t}{2}(u^n_{i+1/2,k})^2$ is applied instead of dynamic viscosity, υ, in the viscosity terms equations.

3.5.3 Donor-Acceptor Flux Approximation

The method employed in SOLA-VOF uses a type of donor-acceptor flux approximation. The essential idea is to use information about *F* downstream as well as upstream of a flux boundary to establish a crude interface shape, add then to use this shape in computing the flux. Several researchers have previously used variations of this approach for tracking material interfaces. The VOF method differs somewhat from its predecessors in two respects. First, it uses information

about the slope of the surface to improve the fluxing algorithm. Second, the F function is used to define a surface location and orientation for the application of various kinds of boundary conditions, including surface tension forces.

The basic advection method as developed for use in the VOF technique may be understood by considering the amount of F to be fluxed through the right-hand face of a cell during a time step of duration Δt. Fluxes across other cell faces are completely analogous. The total flux of fluid volume and void volume crossing the right cell face per unit cross sectional area is $V = u.\Delta t$, where u is the normal velocity at the face. The sign of u determines the donor and acceptor cells, i.e., the cells losing and gaining fluid volume, respectively. For example, if u is positive the upstream or left cell is the donor and the downstream or right cell the acceptor. The amount of F fluxed across the cell face in one time step is δF times the face cross-sectional area, where

$$\delta F = \text{MIN}\{F_{AD}\,|V| + CF,\, F_D\,(\Delta x_D)\}$$

and where

$$CF = \text{MAX}\{(1 - F_{AD})\,|V| - (1 - F_D)\,\Delta x_D,\, 0\} \tag{3.27}$$

Single subscripts denote the acceptor (A) and donor (D) cells. The double subscript, AD, refers to either A or D, depending on the orientation of the interface relative to the direction of flow as explained below.

Briefly, the MIN feature in Eq. (3.27) prevents the fluxing of more fluid from the donor cell than it has to give, while the MAX feature accounts for an additional fluid flux, CF, if the amount of void to be fluxed exceeds the amount available. Fig. 3.9 provides a pictorial explanation of Eq. (3.27). The donor and acceptor cells are defined in Fig. 3.9(a) for fluxing across a vertical cell face.

When AD = D, the flux is an ordinary donor-cell value,

$$F = F_D\,|V|$$

in which the F value in the donor cell is used to define the fractional area of the

cell face fluxing fluid as shown in Fig. 3.9(b). As discussed later, numerical stability requires that $|V|$ be less than Δx, so that it is not possible to empty the donor cell in this case.

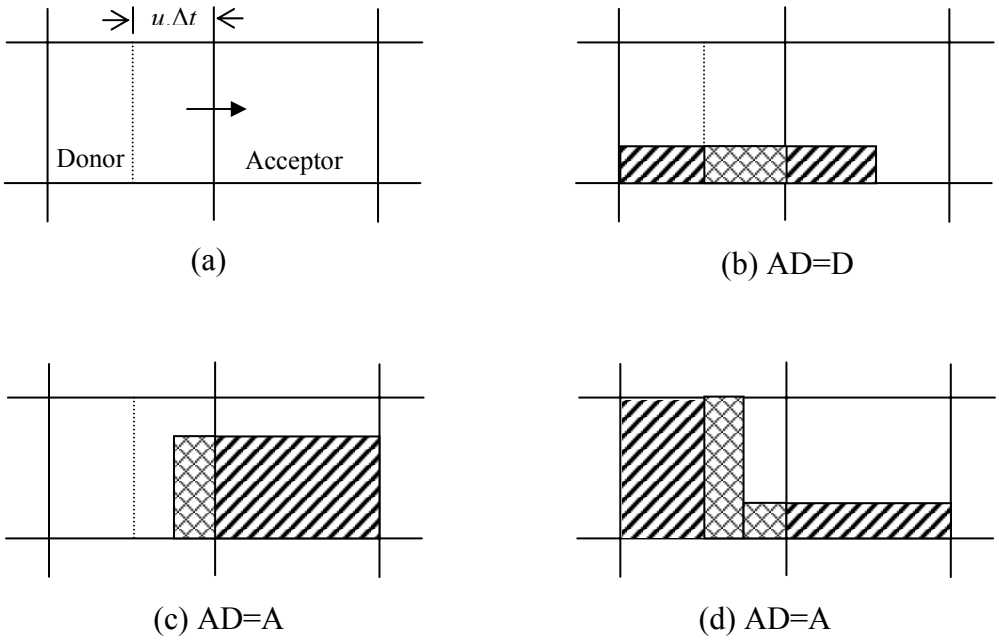

Fig. 3.9: *Examples of free surface shapes used in the advection of F. The donor-acceptor arrangement is shown in (a), where the dashed line indicates the left boundary of the total volume being advected. The cross-hatched regions shown in (b-d) are the actual amounts of F fluxed.*

When AD = A, the value of F in the acceptor cell is used to define the fractional area of the cell face across which fluid is flowing. In case (c) of Fig. 3.9, all the fluid in the donor cell is fluxed because everything lying between the dashed line and the flux boundary moves into the acceptor cell. This is an example exercising the MIN test in Eq. (3.27). In case (d) of Fig. 3.9, more fluid than the amount F_A $|V|$, must be fluxed, so this is an example exercising the MAX test. In particular, the extra fluid between the dashed line and the flux boundary is equal to the CF value in Eq. (3.27).

3.6 Numerical model run conditions

At first, the developed numerical model is run for incident wave period, T= 0.8 sec, incident wave height, H_i= 4 cm and h= 40 cm without any breakwater in the

computational domain. The model simulated water surface profiles are compared with the waves generated from Stokes 3rd order wave theory. Then the model is run for different wave periods ranging from 1.5 sec to 2.0 sec for breakwaters of five different heights as 20 cm, 25 cm, 30 cm, 35 cm and 40 cm to simulate water surface profile, velocity profile, VOF function F and pressure along the computational domain. Table 3.3 shows typical inputs in the numerical model:

Table3.3: Typical inputs in the numerical model

X axis length		1600 cm
Z axis length		74 cm
Structure position		550 cm
Still water depth		50 cm
Incident wave property	Wave height	10 cm
	Wave period	1.5 sec
Structure dimension	Width along wave direction	100 cm
	Length normal to wave direction	76 cm
	Height	30 cm

The typical orientation of the cells in the two-dimensional grid of the numerical model is shown in Fig.3.10.

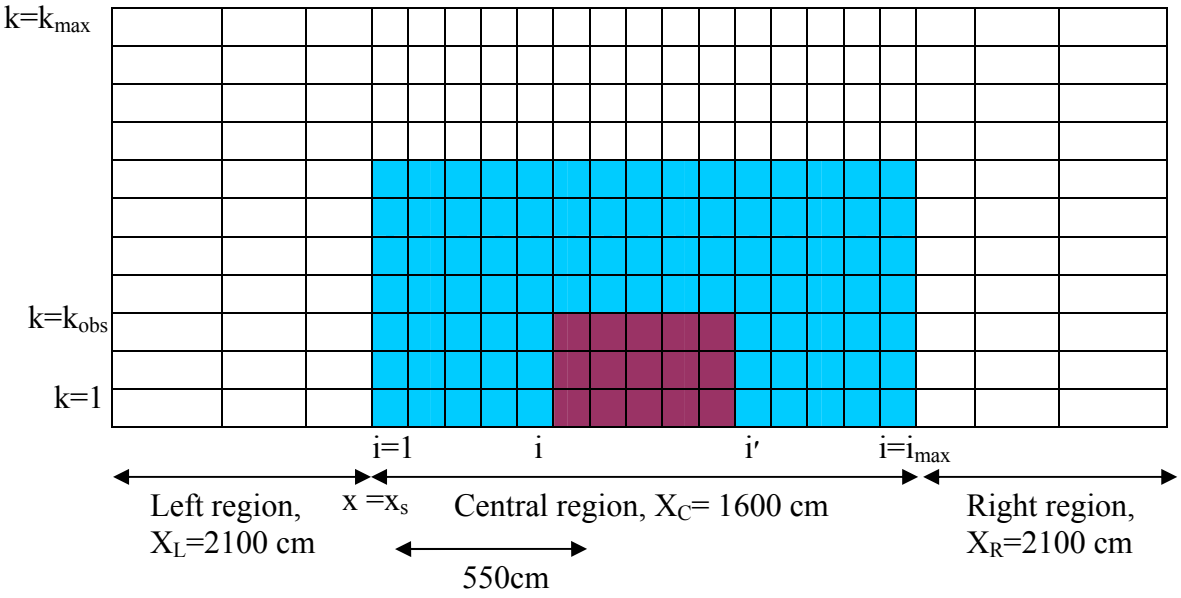

Fig. 3.10: Typical orientation of cells set in numerical model

- Left region: Open boundary of added dissipation zone; Changeable Ratio of Δx =1.03; Number of Cell, IMAXL= 120

- Central region: Main computational grid; Fixed cell width Δx= 2 cm; Number of Cell, IMAXC= 800.
- Right region: Open boundary of added dissipation zone; Changeable Ratio of Δx =1.03; Number of Cell, IMAXR = 120
- Z axis: Constant cell width, Δz = 1 cm. Number of Cell, KMAX= 74

Referring to the Fig. 3.10, Table 3.4 shows input boundary conditions of the velocity as below.

Table 3.4: Input boundary conditions for velocity

Position	Velocity
Boundary cell faces	$u(1,k)=u(2,k)$ $w(1,k)=w(2,k)$ $u(i_{max}, k)= u(i_{max}-1,k)$ $w(i, k_{max})= w(i, k_{max}-1)$
Obstacle cell faces	$u(i-1,k)=0$ $[k= 1, k_{obs}]$ $w(i-1,k)=0$ $[k= 1, k_{obs}]$ $u(i',k)=0$ $[k= 1, k_{obs}]$ $w(i',k)=0$ $[k= 1, k_{obs}]$

The analyses of the numerical model simulated outputs are presented in Chapter 4.

CHAPTER 4: NUMERICAL ANALYSIS

4.1 Introduction

The numerical analysis of submerged structures plays an obvious role in the fields of ocean engineering. This chapter contains discussion about the numerical analysis of the wave interaction with the submerged body. From the developed two-dimensional numerical model based on SOLA-VOF scheme water surface profile, velocity components and magnitude of pressure along the computational domain can be obtained. Additionally a special outcome of the model is the value of F (VOF function) that represents fraction of volume occupied by fluid at any time. The detail results of numerical analyses are presented here. The results of numerical simulation are also verified by the experimentally measured values.

4.2 Verification of the developed numerical model

The developed numerical model is based on SOLA-VOF scheme. The method used for calculating water surface using SOLA-VOF scheme is represented in chapter 2 (article 3.4 and 3.5). Stokes 3rd order wave theory uses the following equation for water surface calculation.

$$\eta^{(3)} = -\frac{3}{8}(\alpha^4 - 3\alpha^2 + 3)a^3k^2\cos\theta + \frac{3}{64}(8\alpha^6 + (\alpha^2 - 1)^2)a^3k^2\cos 3\theta$$

where,

$\alpha = \coth kh,\ k = \dfrac{2\pi}{L}$

h = still water depth

and L = wave length

Fig. 4.1 shows that the waves generated by the developed model show very good agreement with the waves generated by Stokes 3rd order wave theory.

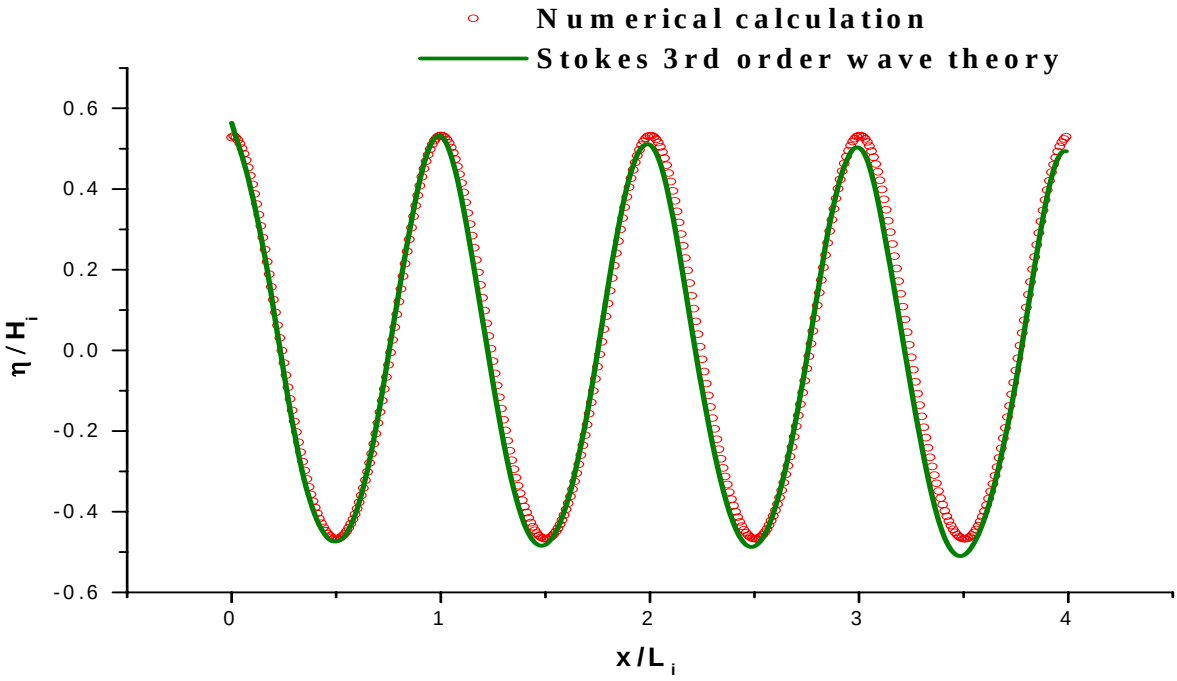

Fig. 4.1:Comparison of numerical and 3rd-order Stokes wave theory results of dimensionless water surface profiles(H_i=4cm, T=0.8 sec, h=40 cm)

4.3 Numerical model simulation for both breaking and non-breaking condition

The numerical model is developed considering that the rectangular submerged body is fixed against the wave action. Fig. 4.2 shows the numerical simulation of water surface profiles along the channel length and the water particle velocity field around the breakwater. The wave height, the wave period and the water depth are considered as 15 cm, 2.0 seconds and 50 cm respectively. Rectangular fixed submerged breakwater of three different heights as 20 cm, 25 cm and 30 cm are considered here for the numerical model simulation.

For installing 20 cm and 25 cm breakwater in 50 cm still water depth no wave breaking occurs. As a result, in the first two figures no disturbance has been seen in the water surface profiles as well as in velocity distribution for these two breakwaters. When 40 cm breakwater is installed in 50 cm depth of water, the wave breaks over the breakwater and water particle velocity abruptly changes due to breaking.

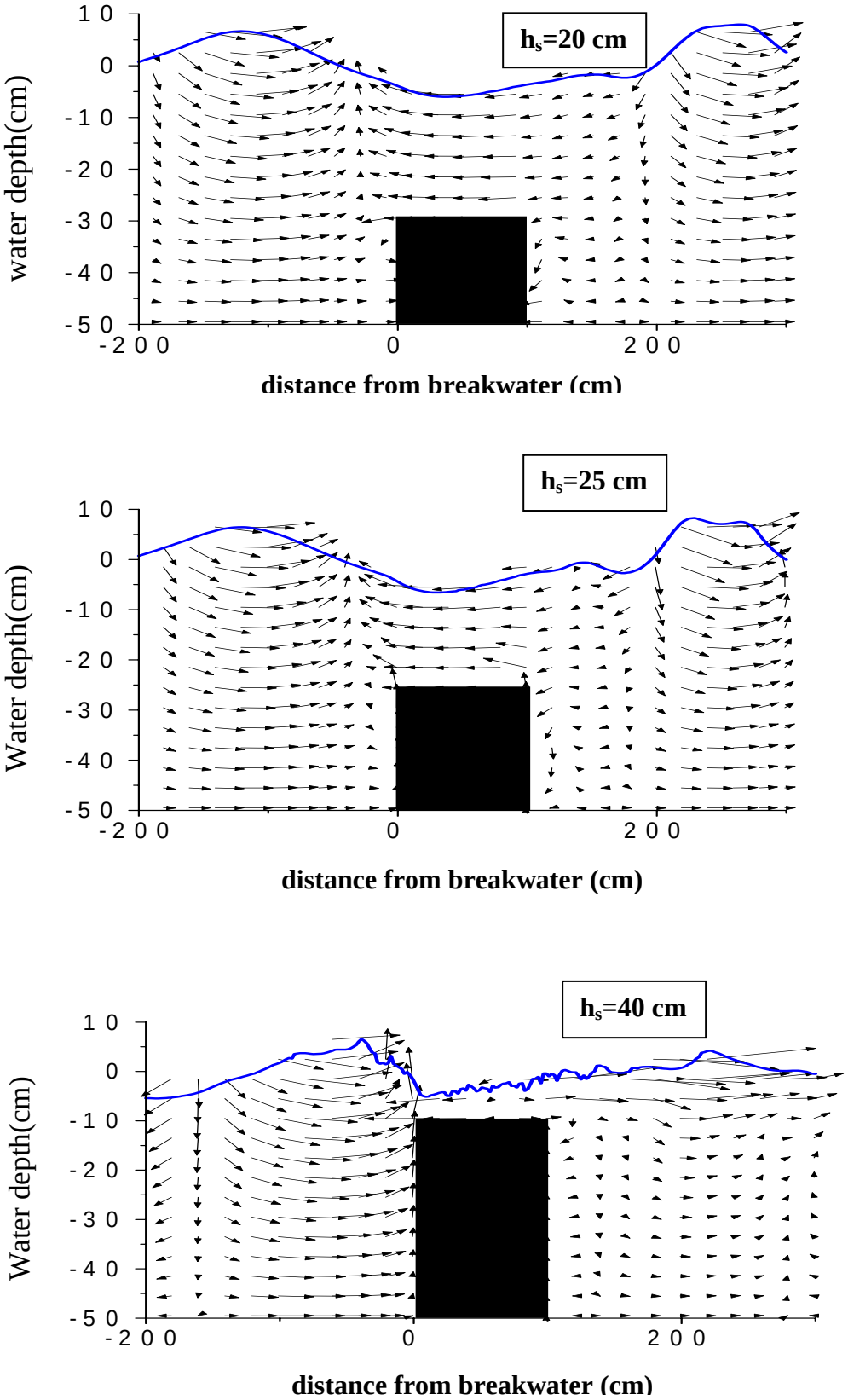

Fig. 4.2 : Numerical model simulation of water surface profile and velocity profile for both breaking and non-breaking condition (H_i=15 cm, T=1.5 sec, h=50 cm)

4.4 Numerical model simulation of time series water surface profiles

Fig. 4.3 shows the numerical simulation of water surface profiles along the channel length for different stages of a wave cycle. The wave height, the wave period and the water depth are considered as 15 cm, 2.0 seconds and 50 cm respectively. The depth and width of the submerged body are 30 cm and 100 cm respectively. The water surface profiles at different moments of a full wave period (T) are shown in the figure. The overtopping of the water surface over the submerged body is seen in the figure. The irregular water surface profiles just behind the breakwater indicate the wave breaking and after breaking it is seen that the wave height reduces the incident wave height. Since the model is able to express the overtopping, the model can calculate the wave deformation around the structure with the nonlinear effects.

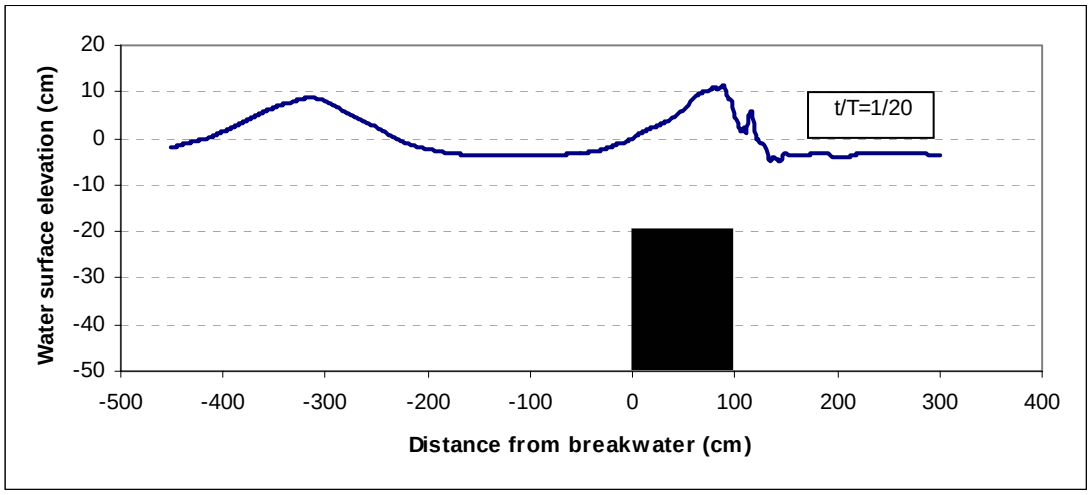

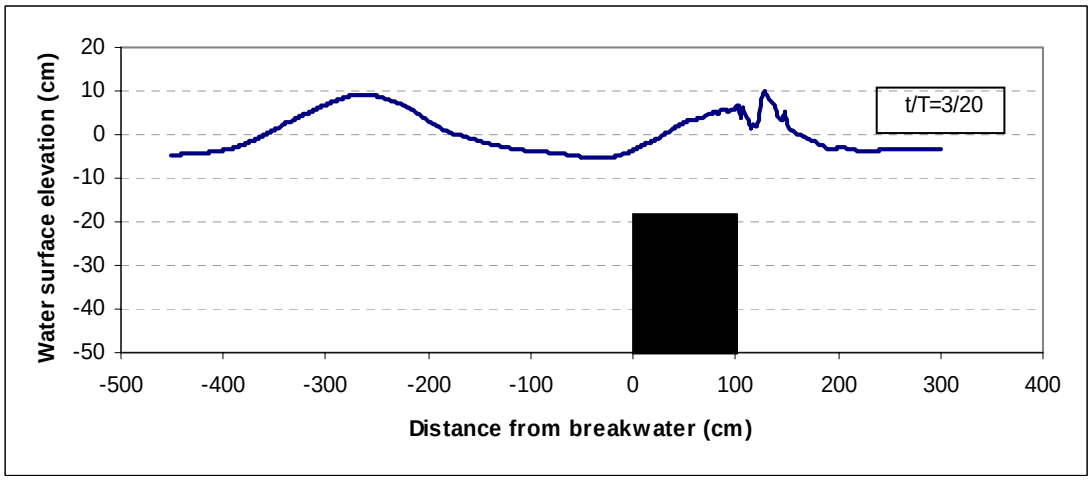

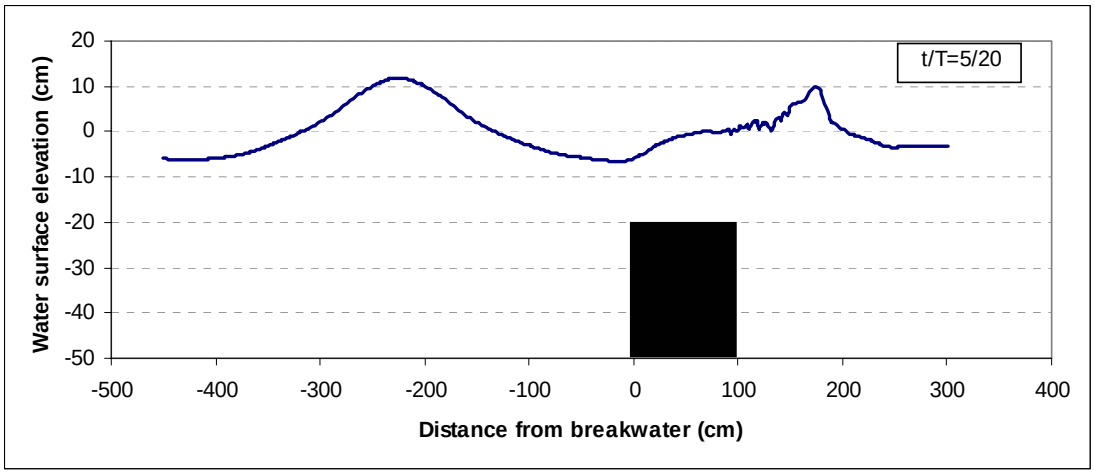
t/T=5/20
Water surface elevation (cm)
20
10
0
-10
-20
-30
-40
-50
-500
-400
-300
-200
-100
0
100
200
300
400
Distance from breakwater (cm)

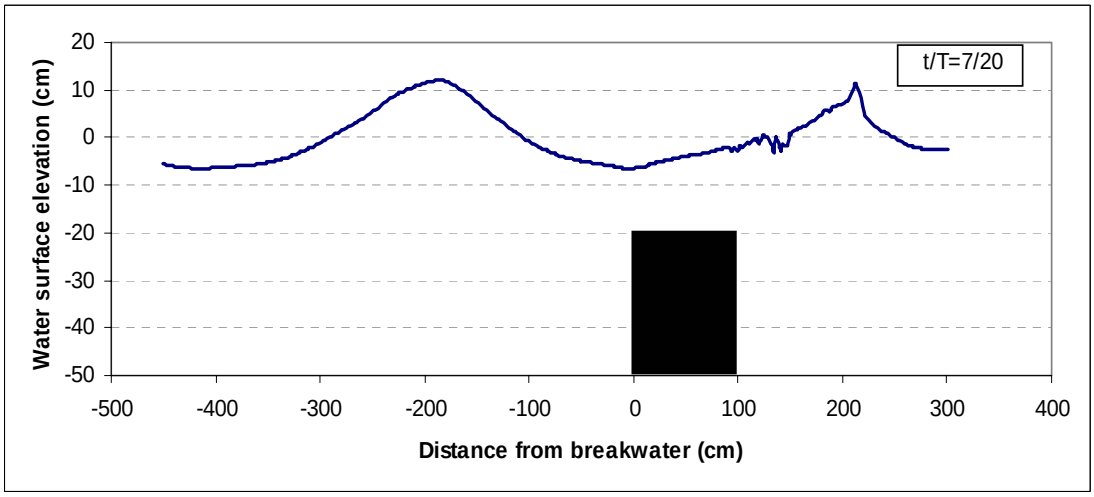
t/T=7/20
Water surface elevation (cm)
20
10
0
-10
-20
-30
-40
-50
-500
-400
-300
-200
-100
0
100
200
300
400
Distance from breakwater (cm)

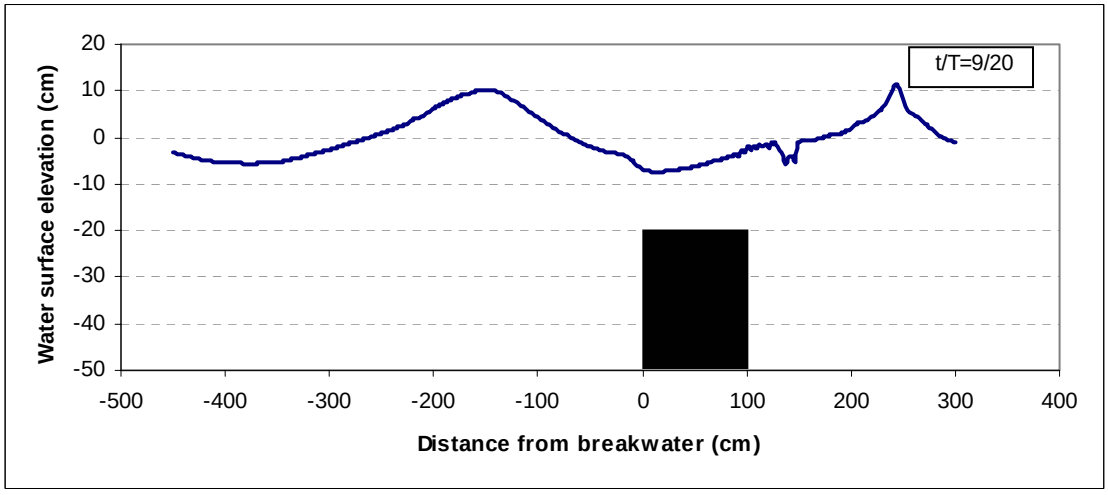
t/T=9/20
Water surface elevation (cm)
20
10
0
-10
-20
-30
-40
-50
-500
-400
-300
-200
-100
0
100
200
300
400
Distance from breakwater (cm)

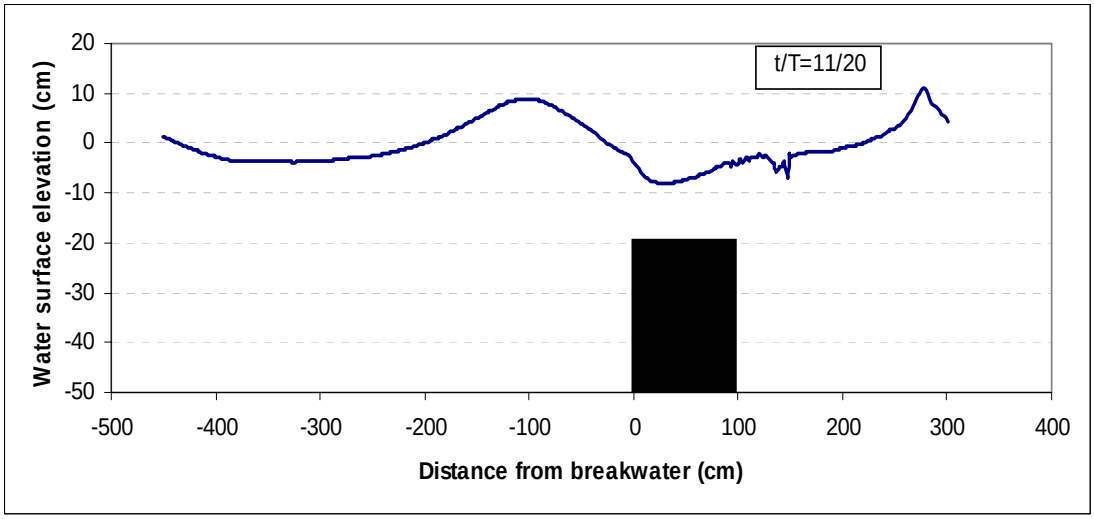
t/T=11/20
Water surface elevation (cm)
20
10
0
-10
-20
-30
-40
-50
-500
-400
-300
-200
-100
0
100
200
300
400
Distance from breakwater (cm)

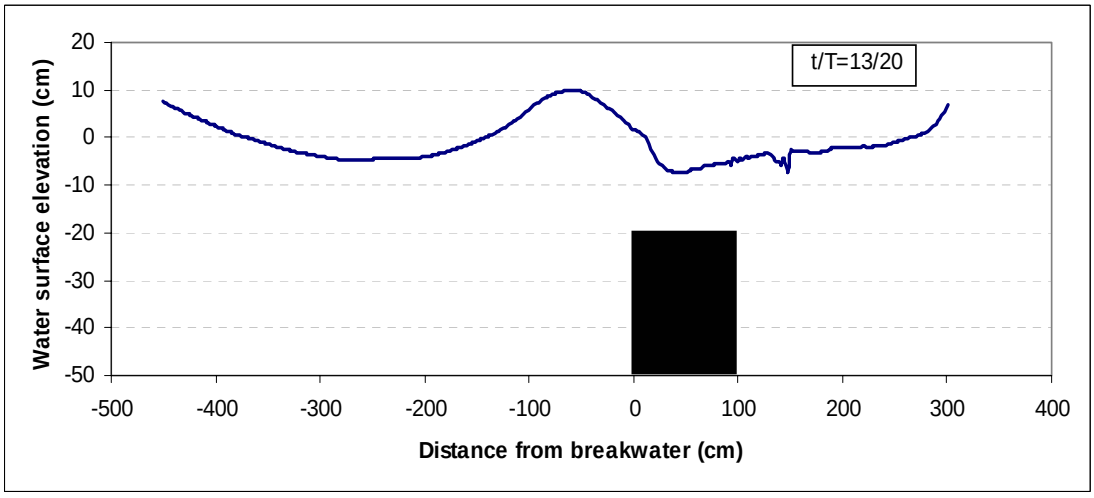
t/T=13/20
Water surface elevation (cm)
20
10
0
-10
-20
-30
-40
-50
-500
-400
-300
-200
-100
0
100
200
300
400
Distance from breakwater (cm)

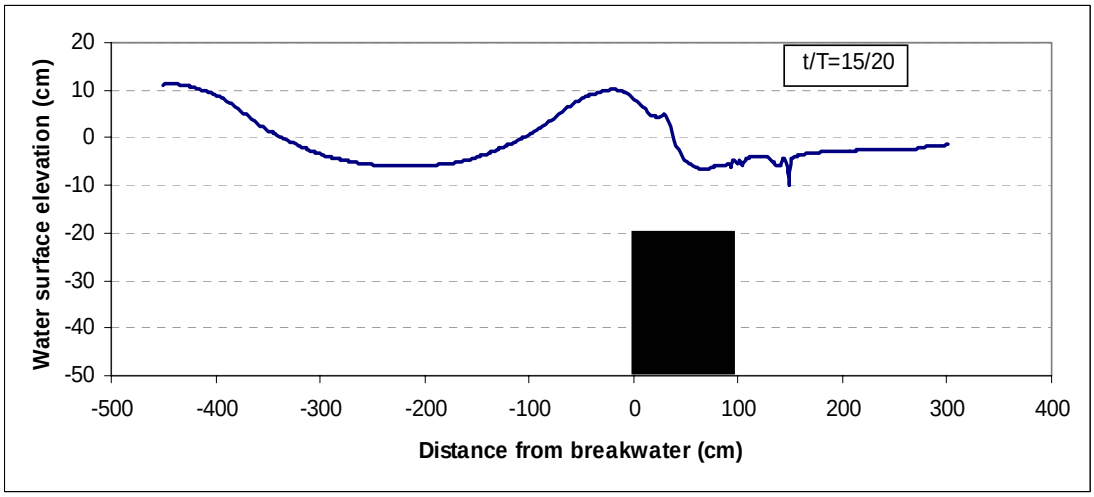
t/T=15/20
Water surface elevation (cm)
20
10
0
-10
-20
-30
-40
-50
-500
-400
-300
-200
-100
0
100
200
300
400
Distance from breakwater (cm)

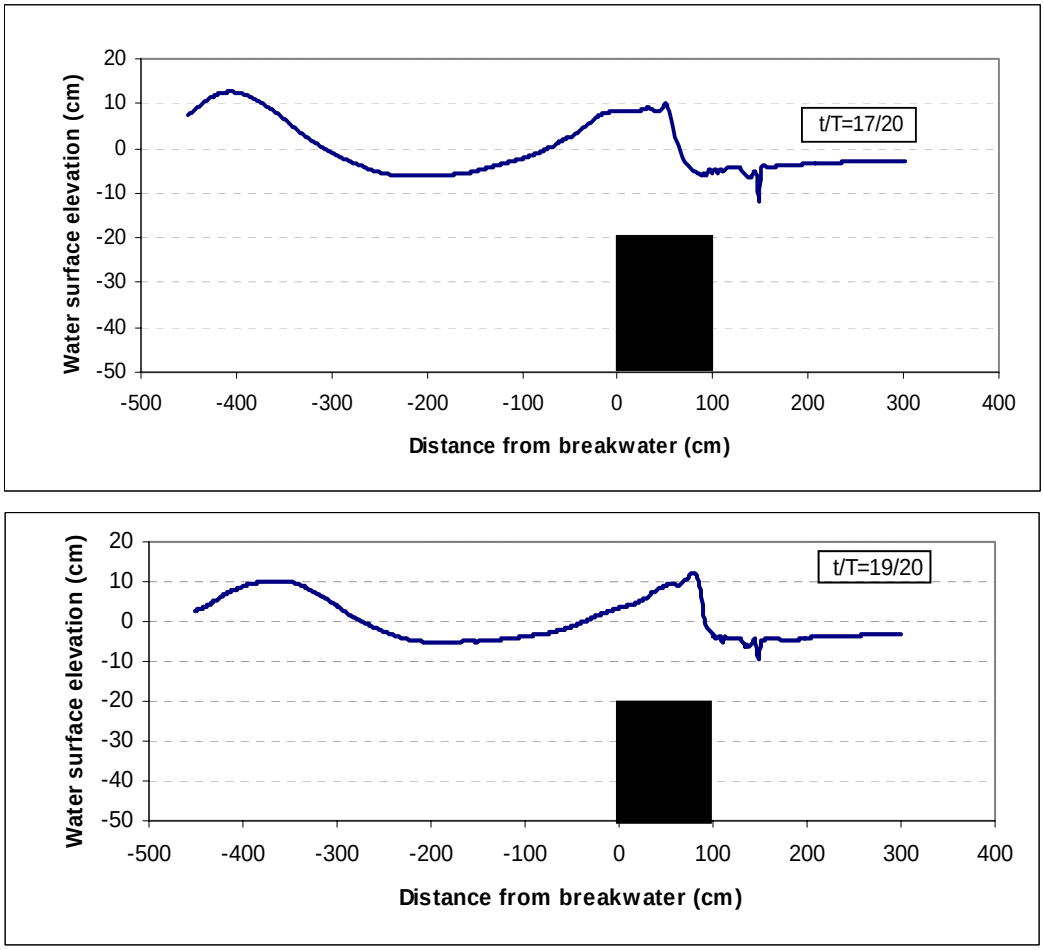

Fig.4.3: Numerical model simulation of time series water surface profiles for a wave cycle (H=15 cm, T=2.0 sec, h=50 cm, h_s=30 cm)

4.5 Numerical model simulation of water particle velocity around the fixed submerged breakwater

The water particle velocity field around the breakwater at the moment of *t*=16.0 second after starting the simulation is shown in Fig. 4.4. The wave height, the wave period and the water depth are considered as 12 cm, 1.6 seconds and 50 cm respectively. The details of numerical simulation of the water particle velocity field around the breakwater for different stages of a wave cycle are shown. The breaking of wave just behind the breakwater is clearly understood from the figure.

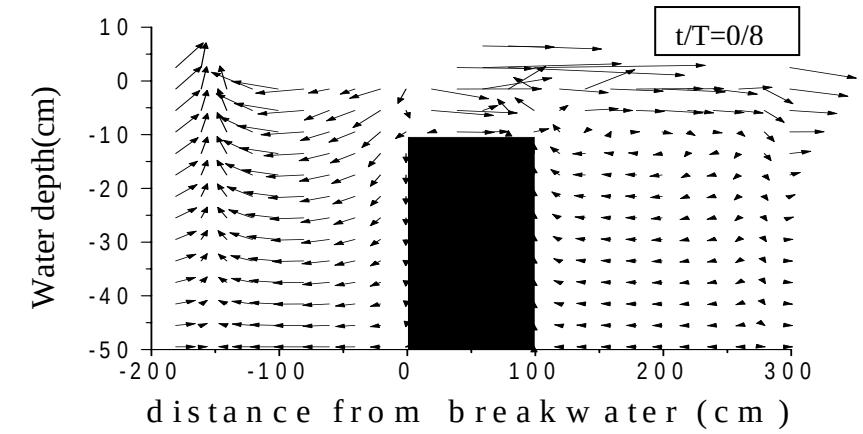
t/T=0/8
Water depth(cm)
10
0
-10
-20
-30
-40
-50
-200
-100
0
100
200
300
distance from breakwater (cm)

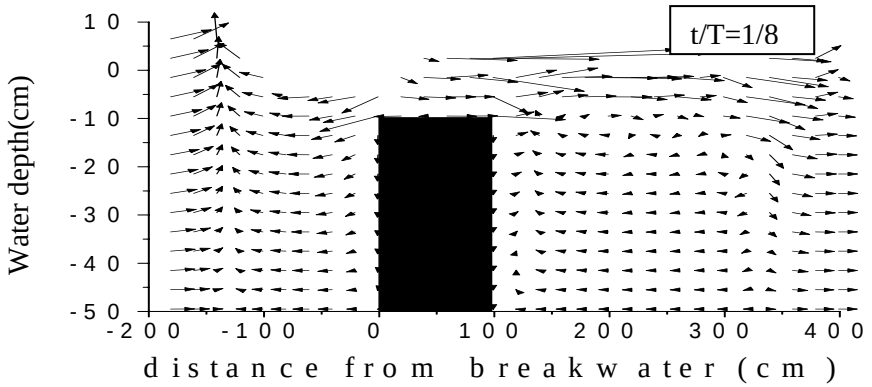
t/T=1/8
Water depth(cm)
10
0
-10
-20
-30
-40
-50
-200
-100
0
100
200
300
400
distance from breakwater (cm)

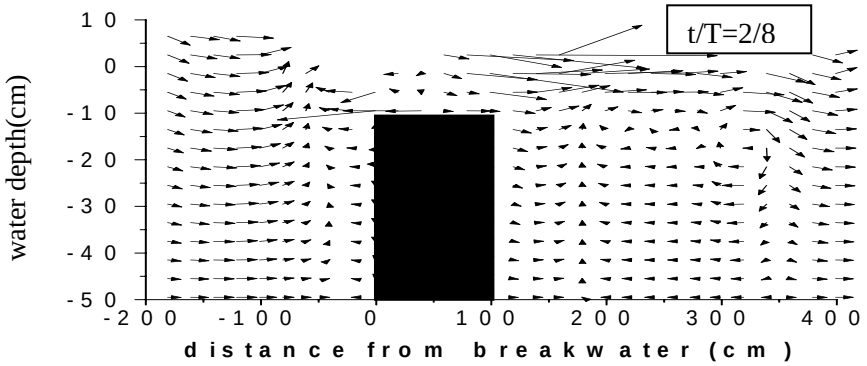
t/T=2/8
water depth(cm)
10
0
-10
-20
-30
-40
-50
-200
-100
0
100
200
300
400
distance from breakwater (cm)

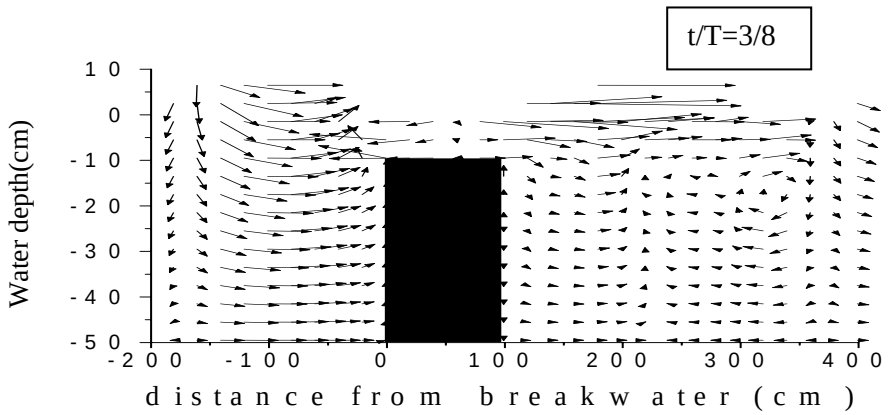
t/T=3/8
Water depth(cm)
10
0
-10
-20
-30
-40
-50
-200
-100
0
100
200
300
400
distance from breakwater (cm)

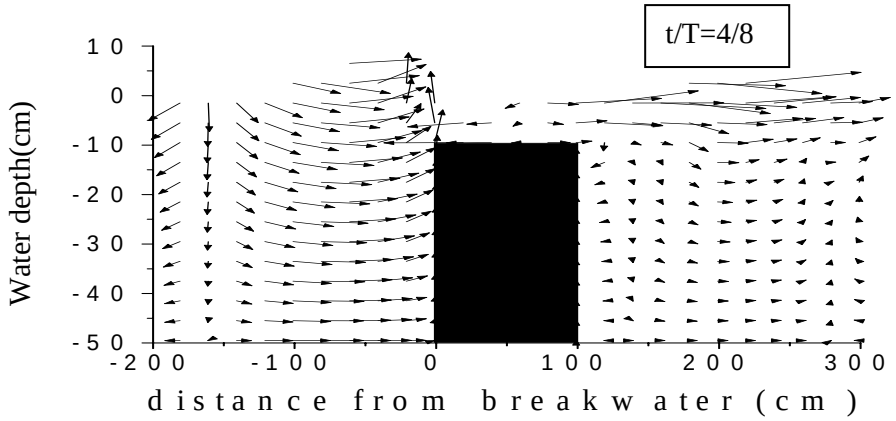
t/T=4/8
Water depth(cm)
10
0
-10
-20
-30
-40
-50
-200
-100
0
100
200
300
distance from breakwater (cm)

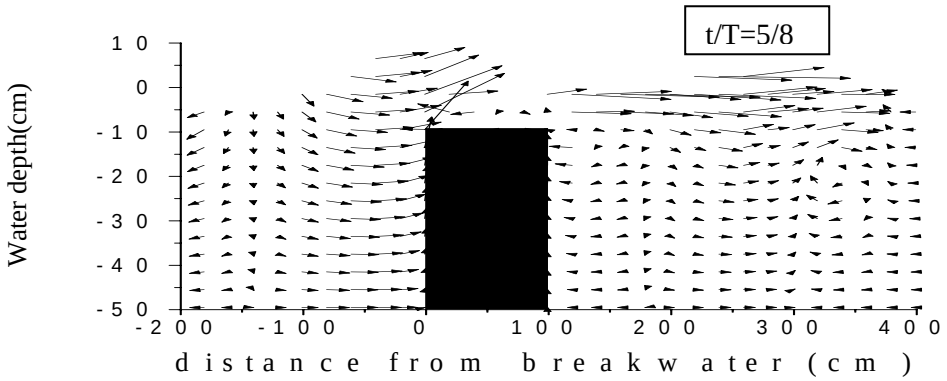
t/T=5/8
Water depth(cm)
10
0
-10
-20
-30
-40
-50
-200
-100
0
100
200
300
400
distance from breakwater (cm)

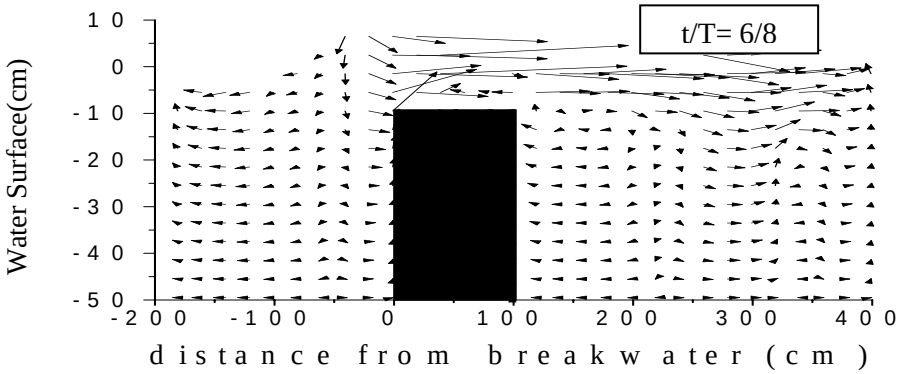
t/T= 6/8
Water Surface(cm)
10
0
-10
-20
-30
-40
-50
-200
-100
0
100
200
300
400
distance from breakwater (cm)

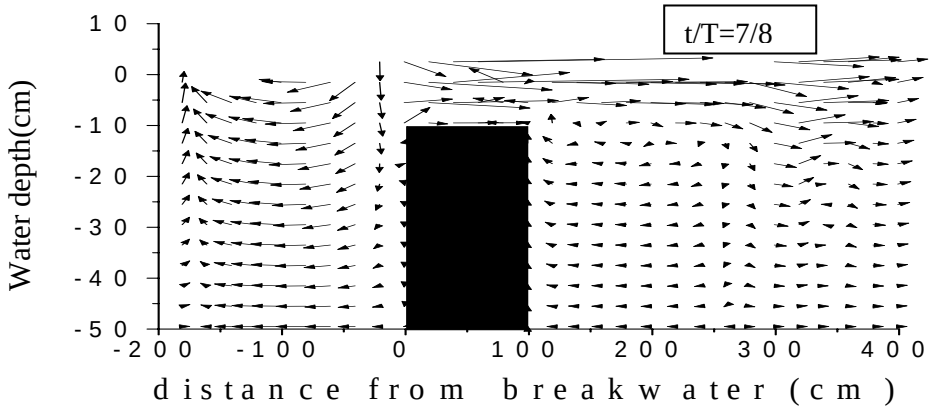
t/T=7/8
Water depth(cm)
10
0
-10
-20
-30
-40
-50
-200
-100
0
100
200
300
400
distance from breakwater (cm)

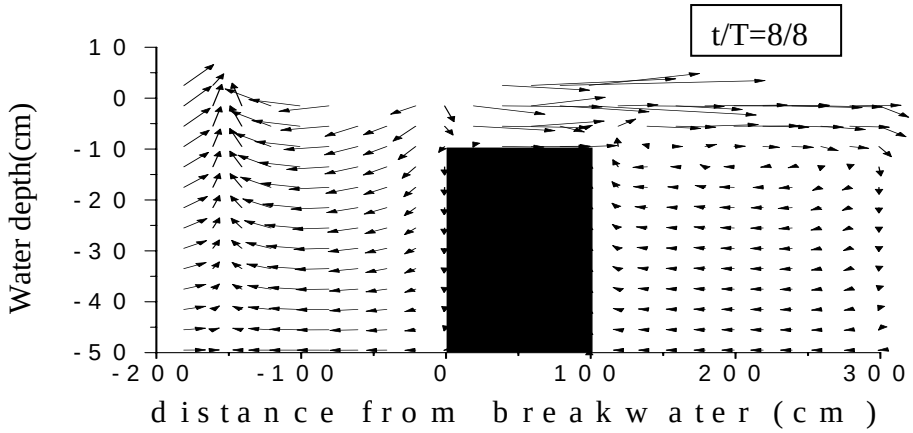

Fig. 4.4: Numerical model simulation of time series water particle velocity around the fixed submerged breakwater for a wave cycle (H=12 cm, T=1.6 sec, h=50 cm, h_s=40cm)

The result at *t/T*=0/8 reveals that the progressive wave collides with the offshore return flow from the offshore face of the breakwater and the direction of the water particle velocity abruptly changes from horizontally to upward. As the wave start to break at *t/T*=2/8 a vortex is seen to appear at the downstream of the submerged body, which continues up to *t/T*=5/8.

In the figure, it is seen that the vortexes are generating after the breakwater and the wave passing over the breakwater breaks with an overturning wave front. The length of arrow of the vector represents the magnitude of the velocity. Furthermore, this figure illustrates that the higher magnitude of the water particle velocity in the offshore side of the breakwater decreases in the onshore side due to the wave energy dissipation through wave breaking by the breakwater.

4.6 VOF function F around the Breakwater

From the experimental video clips, it is seen that most of the wave breaking occurs when the wave front passes over the top surface of the breakwater and its immediate onshore side. Fig. 4.4 shows the numerical simulation of the contour map of the VOF function F, which ranges from 0 to 1 at 15 sec after starting the simulation. The wave height, the wave period and the water depth are considered as 10 cm, 1.5 seconds and 50 cm respectively.

The solid portion in the middle of this figure represents the breakwater containing the obstacle cell having F=0. The deep gray color around the breakwater represents the water containing the fluid cells having F=1. The F value of the top surface of the water surface profile is seen less than 1 (F<1), that represents the surface cells. On the right side of the top surface of the breakwater, it is seen that the wave front becomes light gray color having F<1. It shows that the breaking of wave occurs here and the air-bubble entrained in the corresponding numerical mesh cells due to wave breaking reduces the water volume less than the full volume of a fluid cell. For this reason the numerical model calculates F value of these cells less than 1. Also, the cells having F<1 are seen in both offshore and onshore side of the breakwater. This may happen due to the reason that the higher water particle velocity in vertically downward direction at the onshore face of the breakwater may cause partial void at some cells near the onshore face bottom corner forming vortex in this zone, which can be seen in Fig. 4.5.

Fig. 4.5 (i) shows the contour map of VOF function F with installation of submerged breakwater of 20 cm height in a still water depth of 50 cm. This figure shows smooth distribution of F value as no breaking occurs as the wave passes over the breakwater. At a distance from the breakwater the value of F is 1 at deep water zone because in these regions the computational cells are completely filled by the fluid. The F value is less than 1 in the surface cells partially occupied by water and partially filled by air. Again just at the offshore end of the breakwater, over the breakwater and at the onshore end of the breakwater the value of F is less than 1 because of the presence of bubble and eddies in these cells some air is entrapped there. Fig. 4.5 (ii) shows the effect of installing a 30 cm submerged body in 50 cm depth of water. In this case the variation in the value ofF is almost similar. In Fig. 4.5 (iii), changes in the value of F as a result of breaking of wave by 40 cm submerged body are shown. Here as the waves break overtopping the breakwater the variation in the value of F can be clearly understood.

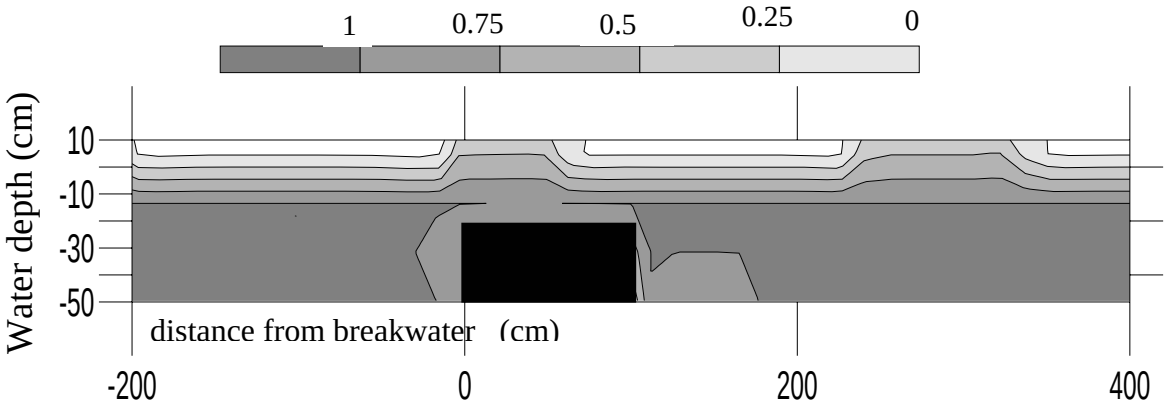

Fig. 4.5 (i): Numerical model results of contour map VOF function value F around the submerged body with height 20 cm(H=10cm, T=1.5sec,h=50cm)

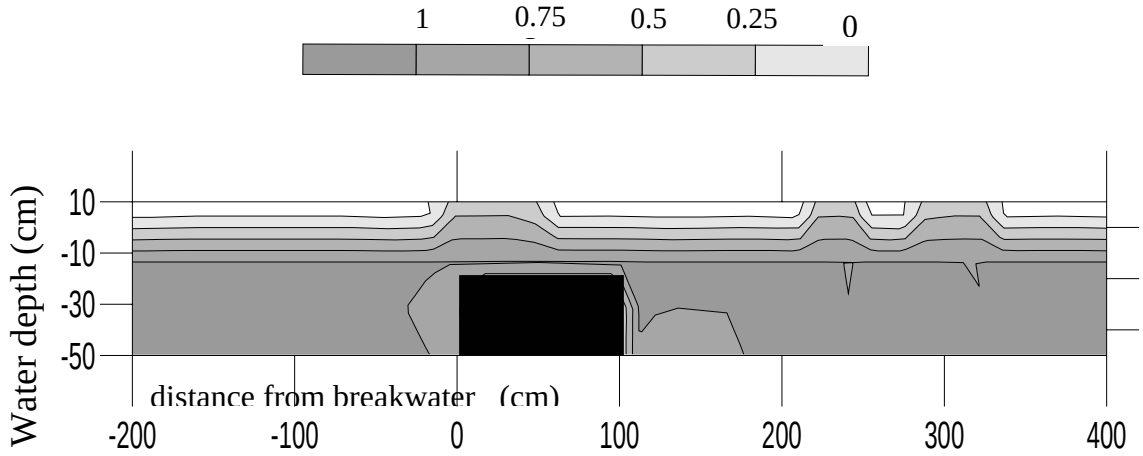

Fig. 4.5(ii): Numerical model results of contour map VOF function value F around the submerged body with height 30 cm(H=10cm, T=1.5sec,h=50cm)

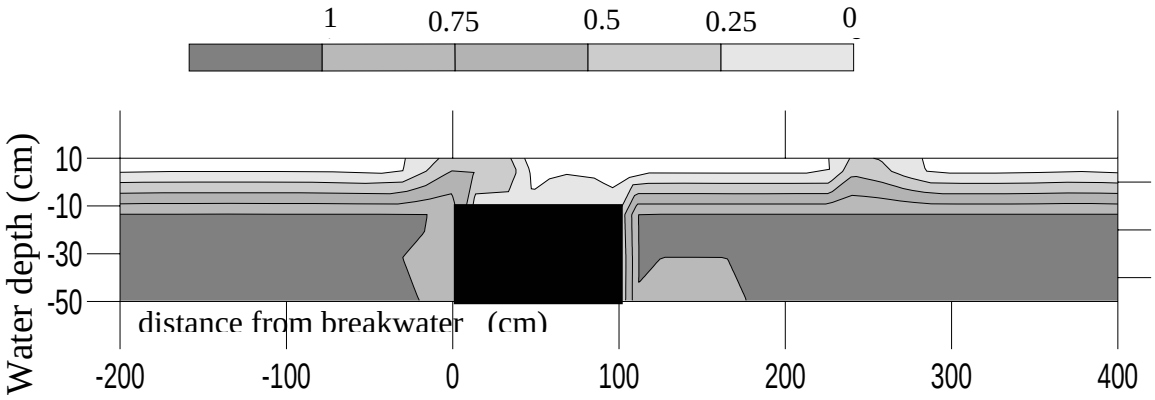

Fig. 4.5 (iii): Numerical model results of contour map VOF function value F around the submerged body with height 40 cm(H=10cm, T=1.5sec,h=50cm)

4.7 Pressure distribution around the breakwater

Fig. 4.6 shows the numerical simulation of the pressure distribution at 20 sec after starting the simulation in dyne/cm^2 unit. The wave height, the wave period and the water depth are considered as 15 cm, 2 seconds and 50 cm respectively. The solid portion in the middle of this figure represents the breakwater. The changes in the pressure distribution for installing fixed submerged body are analyzed here. Pressure distribution around the breakwater changes as the wave breaks because of installing fixed submerged breakwater. From the results of the previous analyses, it is seen that for five different wave periods as 1.5 sec, 1.6 sec, 1.7 sec, 1.8 sec and 2.0 sec the incident wave breaks above the ratio of $h_s/h=0.4$ i.e. by installing a fixed submerged breakwater of height greater than 20 cm in a still water depth 50 cm the incident wave usually breaks for the given wave periods. From the experimental investigations it is seen that most of the wave breaking occurs when the wave front passes over the top surface of the breakwater and its immediate onshore side. This is also evident fom the numerical simulation results.

In this figure it is clear that there is no abrupt change in the pressure distribution around 20 cm breakwater in 50 cm depth of water. As the incident wave does not break because of installing breakwater of $h_s/h=0.4$, the pressure distribution is almost similar around 20 cm submerged body. As a result of providing a 30 cm breakwater in same depth of still water, mild changes occur in the pressure distribution around the breakwater. In this case, the pressure becomes very close to 0 just behind the breakwater. When a breakwater of height 40 cm having $h_s/h=0.8$ is set , the pressure just behind the breakwater becomes very low. The changes in pressure distribution occur because of existence of vortex in that zone which is also seen in the water particle velocity distribution around the breakwater. The water pressure distribution becomes almost linear behind the breakwater whereas, in front of breakwater this distribution is curved.

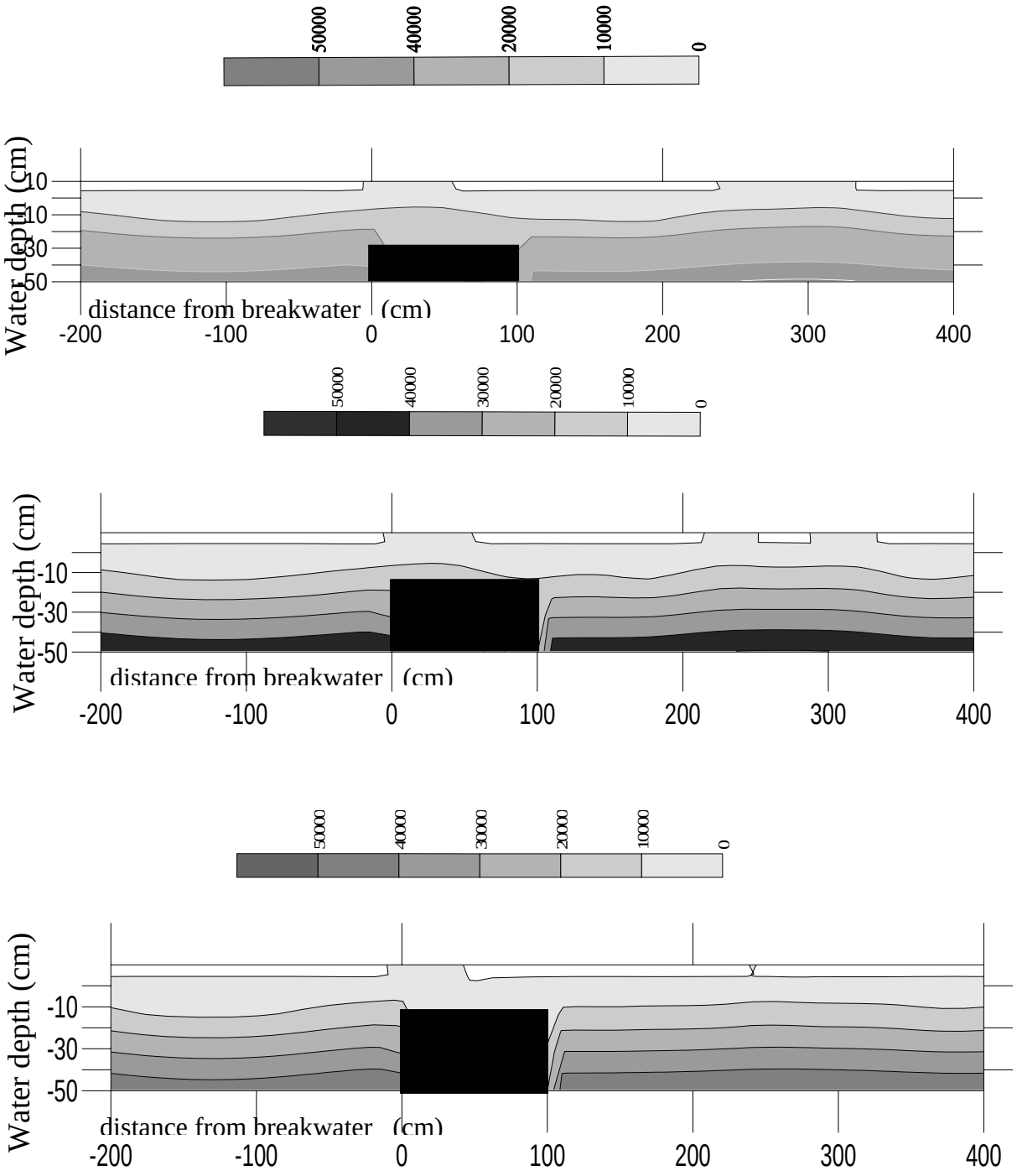

Fig. 4.6: Numerical model results of pressure distribution around the submerged body of three different heights of 20 cm, 30 cm and 40 cm respectively (H=10cm, T=1.5sec,h=50cm)

4.8 Comparison between numerical and experimental results

The performance of the developed two-dimensional numerical model has been verified by comparing the model simulated results with experimentally measured data. The model simulated water surface profiles for all 15 laboratory run conditions are compared with the experimentally measured data for the respective run condition and are shown in Fig. 4.7. In the figure, the experimentally measured data of water surface profile show good agreement with the water surface profiles generated by the developed numerical model. The data collected from the experimental investigations shows the maximum of ± 20% variations with the numerical model data.

Wave breaking positions measured by the laboratory experiments are also presented in this figure. The measured breaking positions in the laboratory experiments show small differences from the locations of breaking indicated by the numerical model simulation marked by the larger circles. In the model simulated water surface profiles the breaking position is considered at the point where the wave collapse.

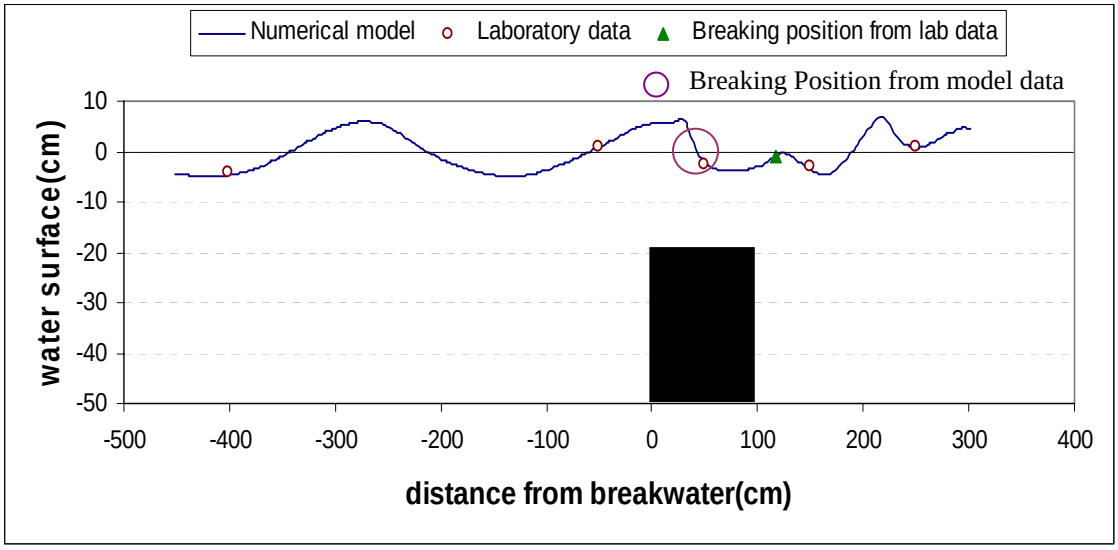

Run 1: T= 1.5 sec, Hi= 10 cm, h=50cm,

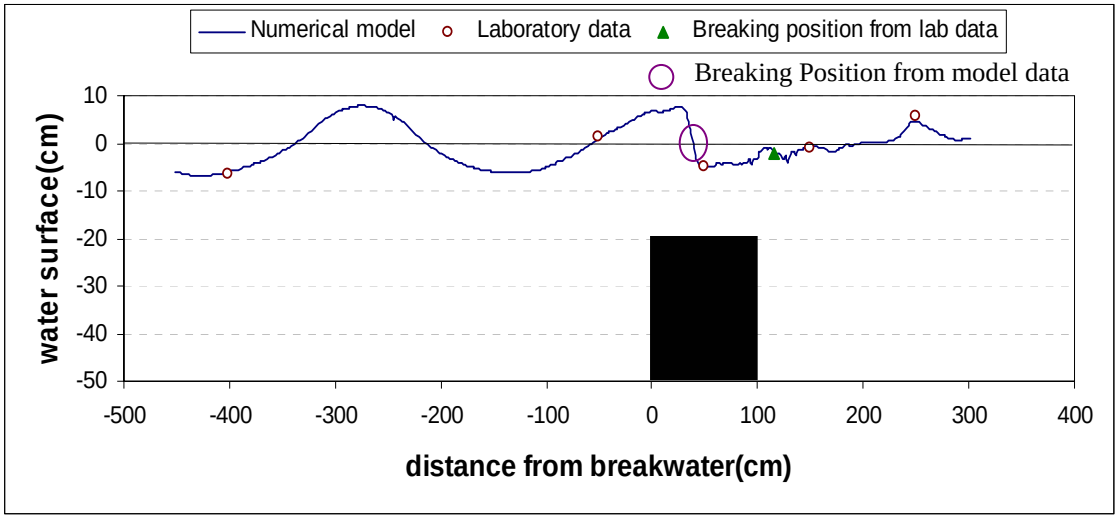

Run 2: T= 1.6 sec, Hi= 12 cm, h=50cm,

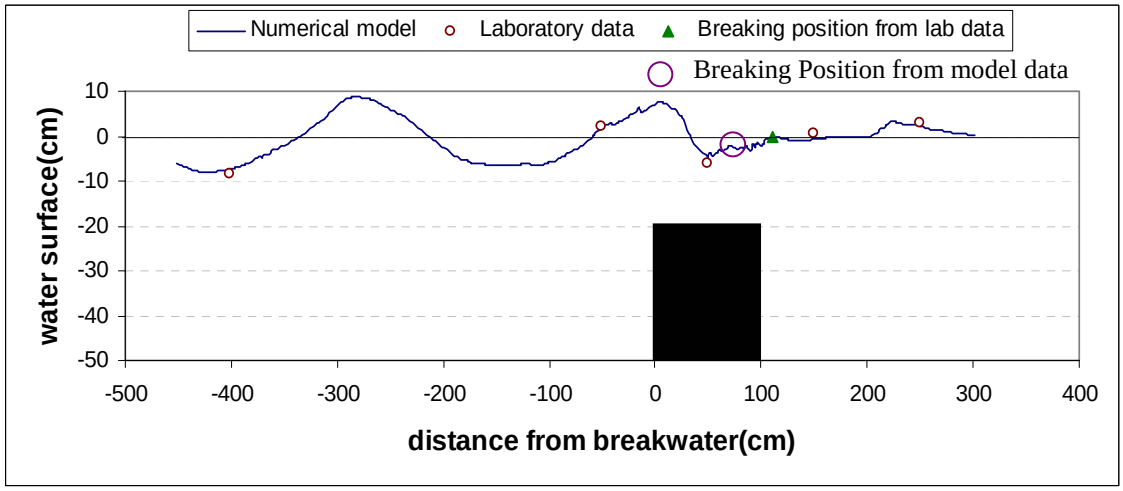

Run 3: T= 1.7 sec, Hi= 13 cm, h=50cm, h_s=30cm

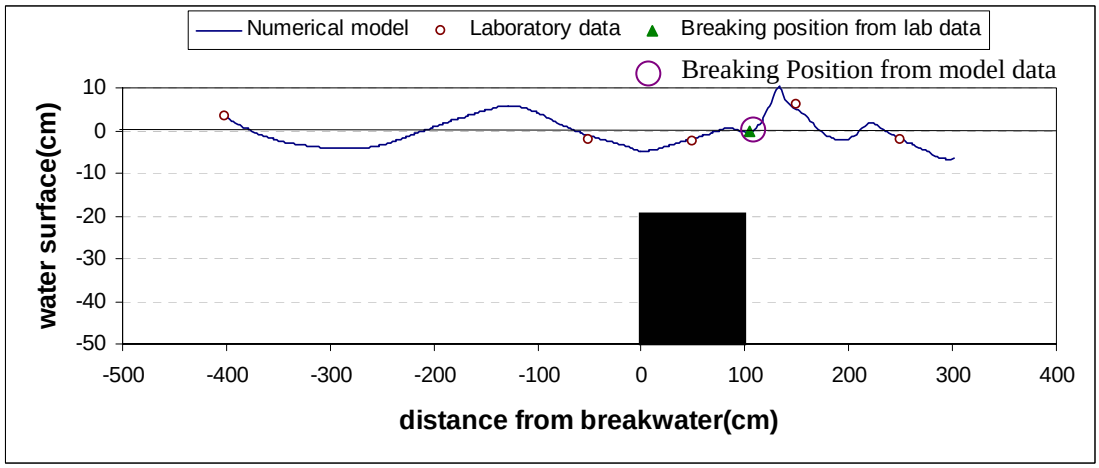

Run 4: T= 1.8 sec, Hi= 14 cm, h=50cm, h_s=30cm

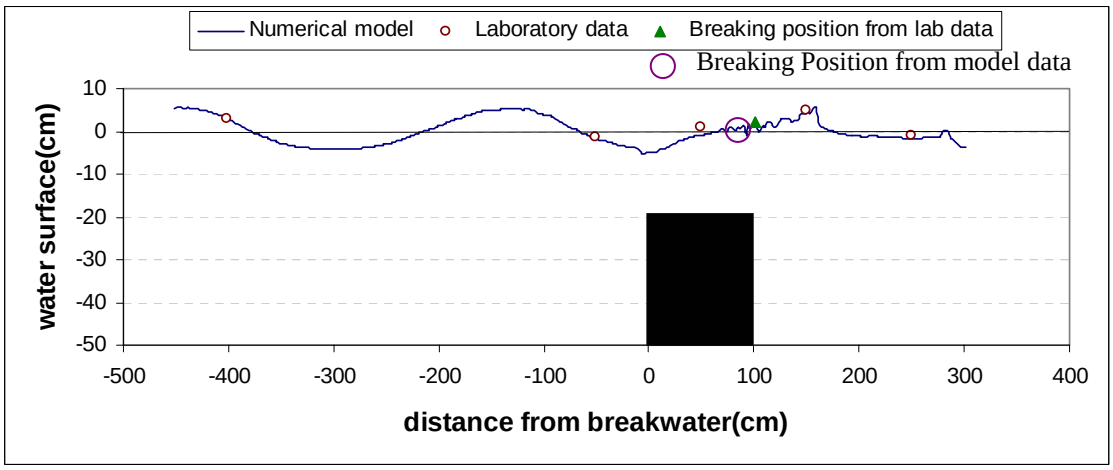

Run 5: T= 2 sec, Hi= 15 cm, h=50cm, h_s=30cm

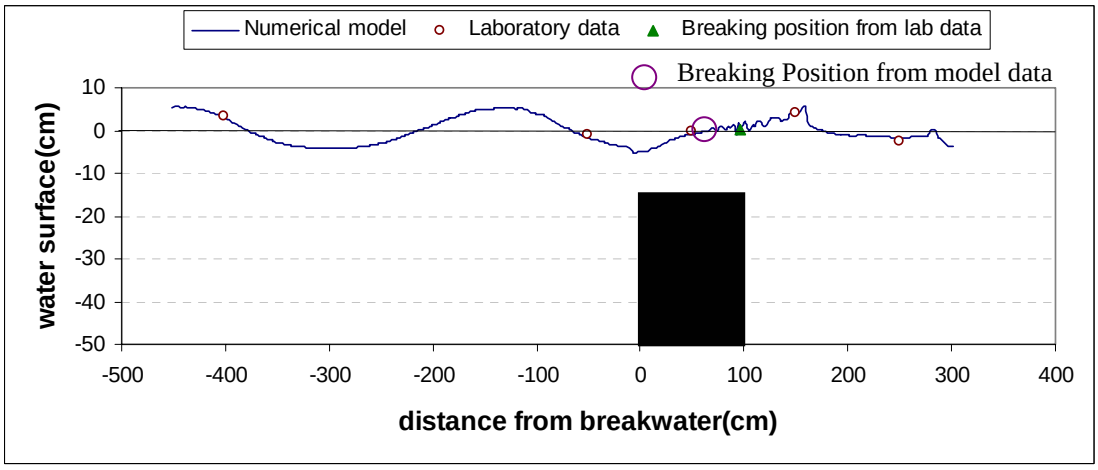

Run 6: T= 1.5 sec, Hi= 10 cm, h=50cm, h_s=35cm

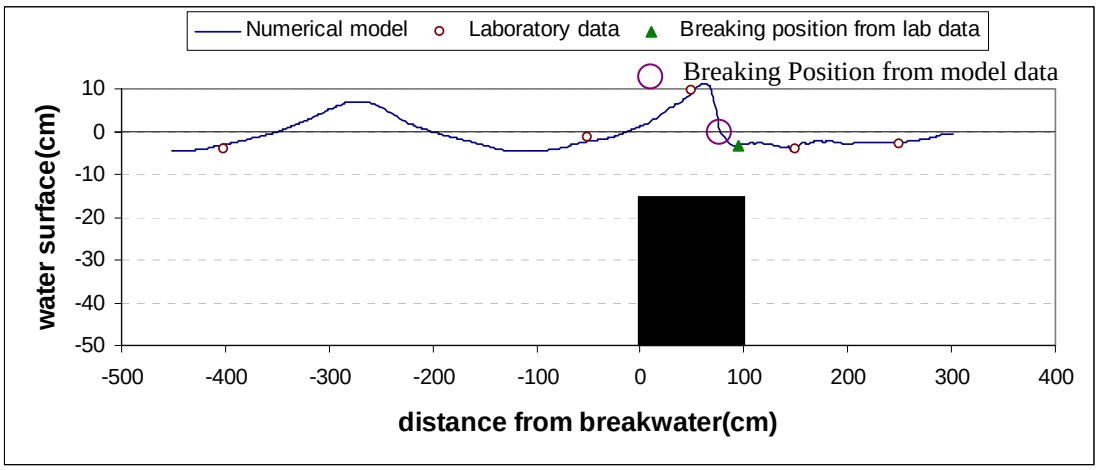

Run 7: T= 1.6 sec, Hi= 12 cm, h=50cm, h_s=35cm

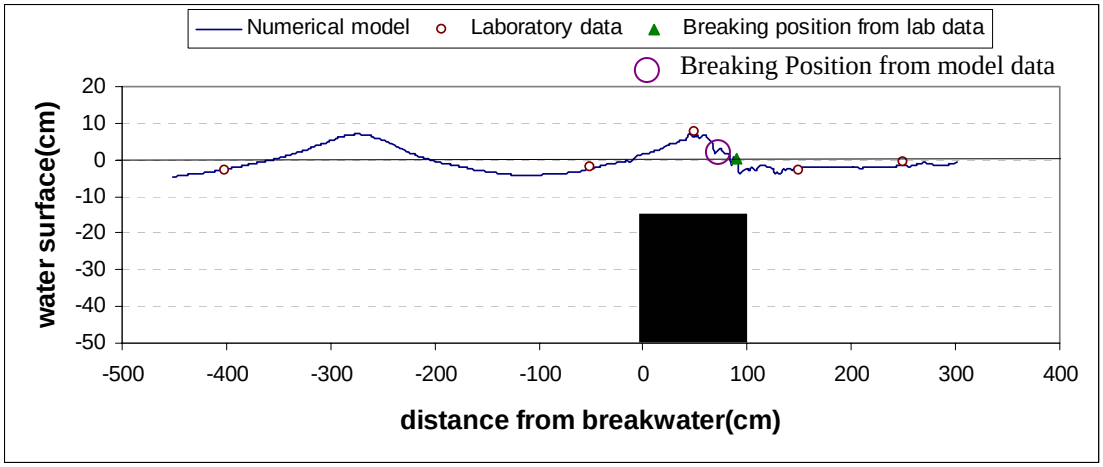

Run 8: T=1.7 sec, Hi= 13 cm, h=50cm, h_s=35cm

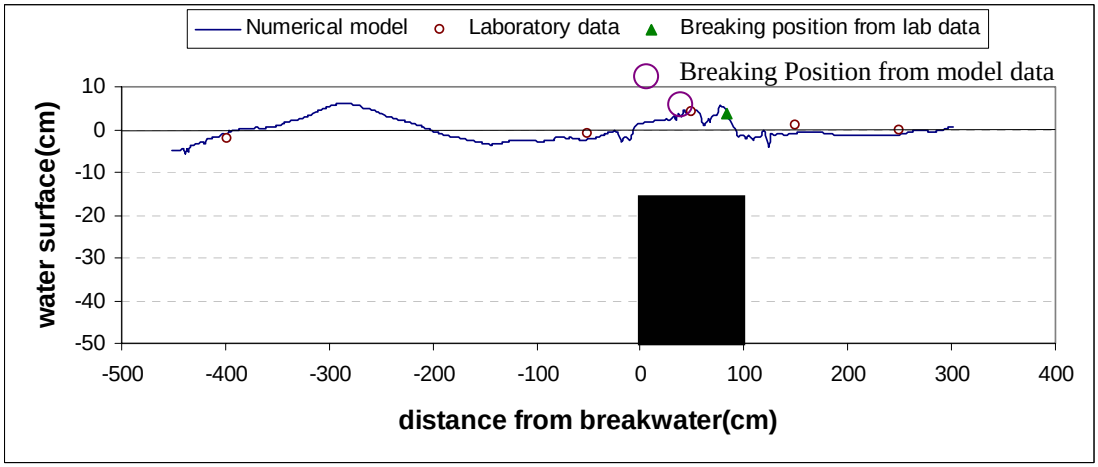

Run 9: T=1.8 sec, Hi= 14 cm, h=50cm, h_s=35cm

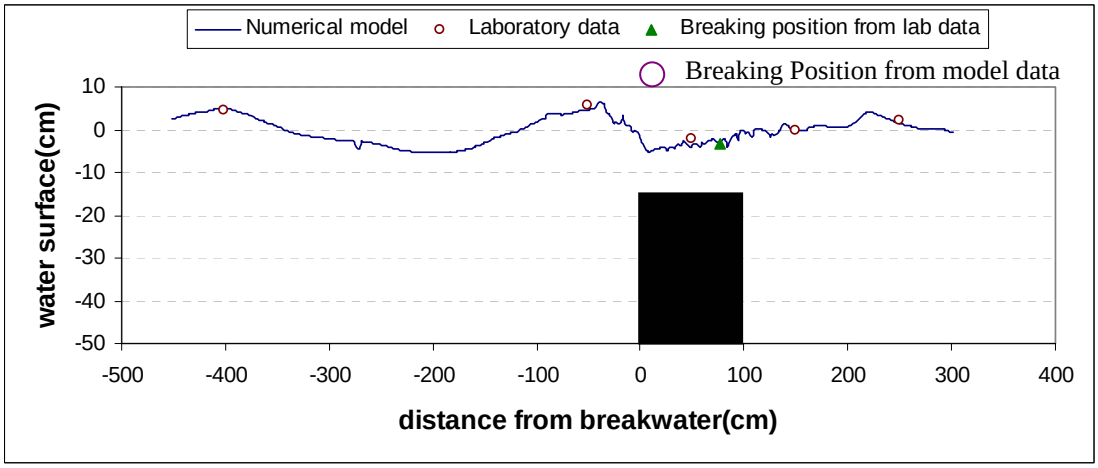

Run 10: T= 2.0 sec, Hi= 15 cm, h=50cm, h_s=35cm

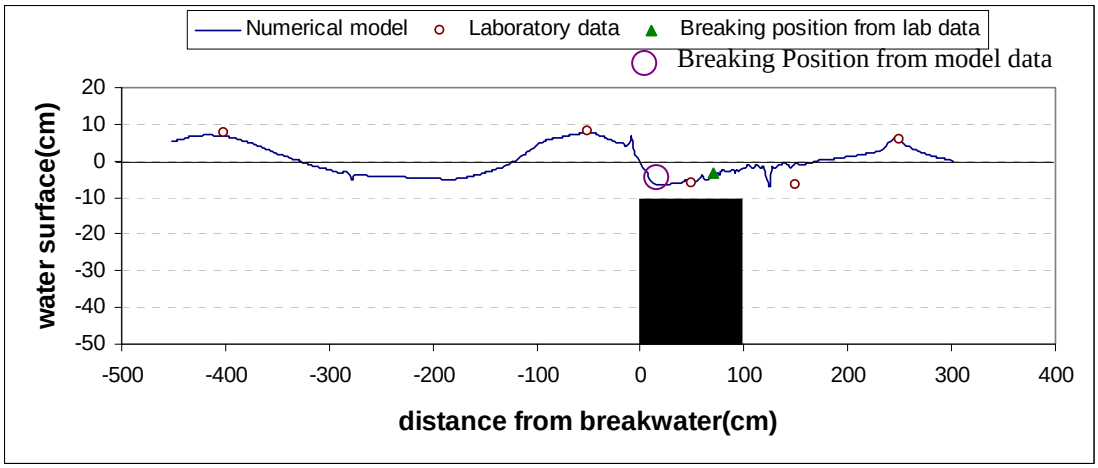

Run 11: T= 1.5 sec, Hi= 10 cm, h=50cm, h_s=40cm

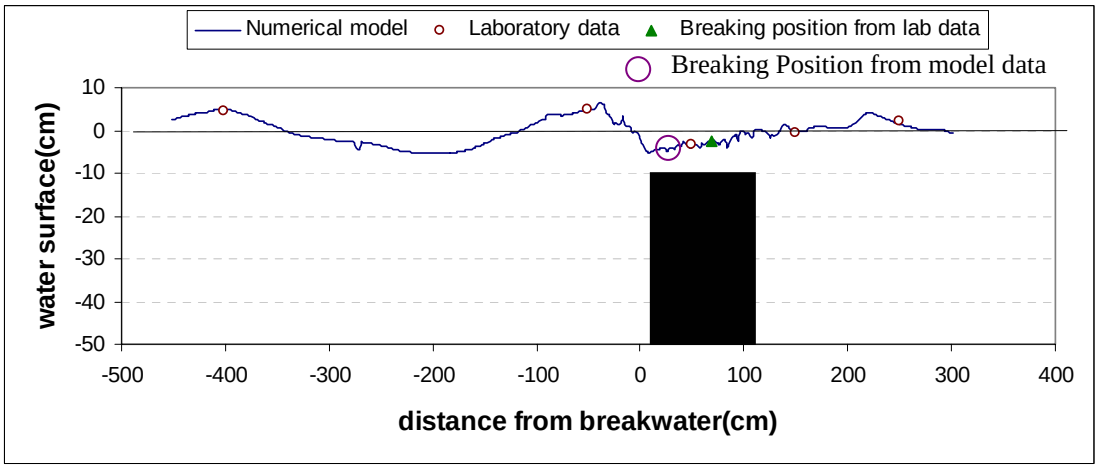

Run 12: T=1.6 sec, Hi= 12 cm, h=50cm, h_s=40cm

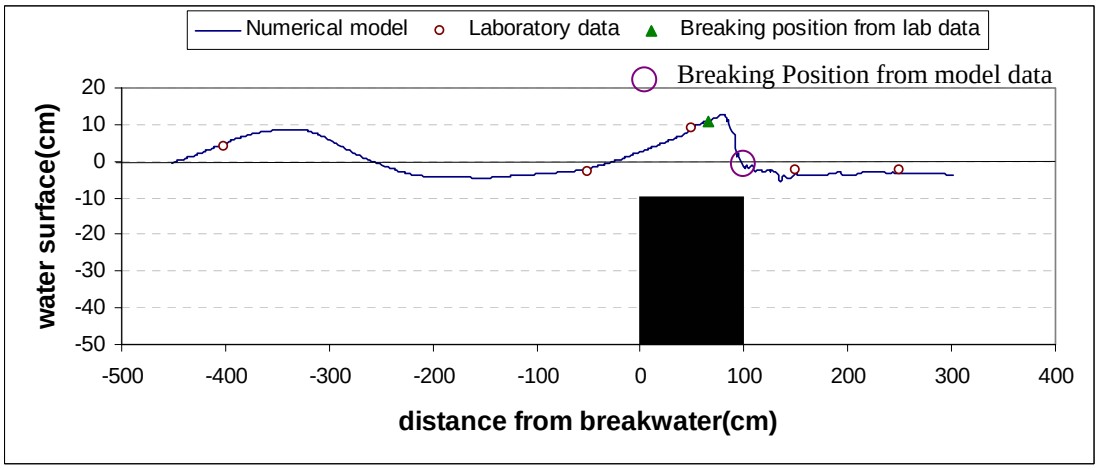

Run 13: T= 1.7 sec, Hi= 13 cm, h=50cm, h_s=40cm

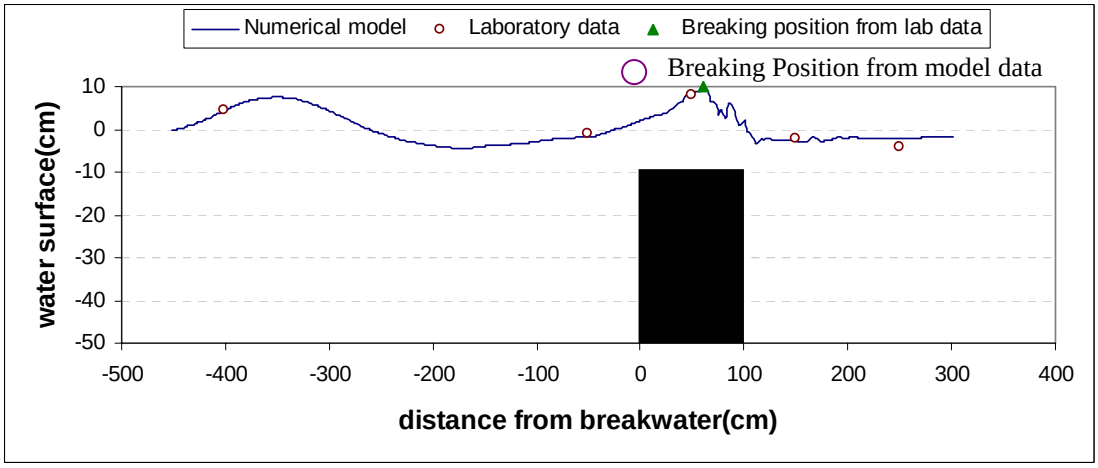

Run 14: T= 1.8 sec, Hi= 14 cm, h=50cm, h_s=40cm

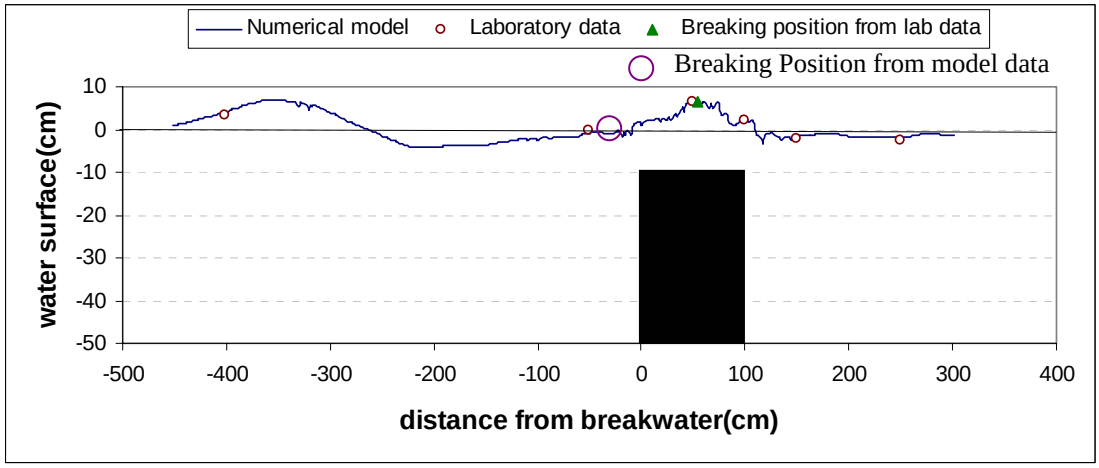

Run 15: T= 2.0 sec, Hi= 15 cm, h=50cm, h_s=40cm

Fig. 4.7 : Comparisons between numerical and experimental results for different runs

CHAPTER 5: CONCLUSIONS AND RECOMMENDATIONS

5.1 Conclusions

Submerged breakwater is a nature-conscious coastal protection work that prevents beach erosion and provides a safe and agreeable environment in the coastal areas. In this thesis work, the interaction between wave and rectangular fixed submerged breakwater has been investigated both experimentally and numerically to find out the effective size of this protection structure for the reduction of wave height. In a two-dimensional wave flume, fifteen experimental runs have been conducted with solid submerged body of three different relative structure heights (h_s= 30 cm, 35 cm and 40 cm) in constant water depth h=50 cm for five different wave periods as T= 1.5 sec, 1.6 sec, 1.7 sec, 1.8 sec and 2.0 sec respectively. Moreover, a two-dimensional moored floating body-wave interaction model by Rahman (2005) is adapted in this study to simulate the wave interaction with fixed rectangular shaped submerged breakwater. The adapted model can simulate water surface profile, velocity profile, water pressure all through the flume length including wave breaking over and around the breakwater. Finally the experimentally measured water surface profiles and wave breaking positions for each of the fifteen run conditions are compared with the model simulated results. The key findings from this study are as follows.

(i) From the experimental investigations, it is seen that for any particular wave period the relative structure height, h_s/h (h_s= structure height and h= water depth) and the relative structure width B/L (B=structure width along the wave direction and L= wave length) are the important parameters for the reduction of incident wave height as mentioned below.

   (a) As the relative structure height h_s/h increases, the incident wave reduces more due to breaking caused by the breakwater. For B/L

=0.35, when the ratio of h_s/h= 0.8, the reduction of wave height is about 60%, whereas the submerged body with h_s/h= 0.7 and 0.6 can reduce wave height up to 45% and 40% respectively.

(b) As the relative structure width B/L increases, the reduction of wave height also increases. For relative structure height h_s/h =0.6, when B/L= 0.25, reduction of wave height due to breaking is 30%, whereas submerged body with B/L= 0.4 can reduce wave height up to 50%.

(ii) The water surface profiles simulated by the numerical model are in good agreement with wave profiles generated from Stokes 3rd order wave theory which indicates the satisfactory performance of the adapted model for any type of wave generation.

(iii) Analyzing the water surface profiles, velocity profiles, water pressure around the breakwater it is seen that in 50 cm depth of water, 20 cm and 25 cm high breakwater cannot break waves passing over it, whereas for breakwater height 30 cm and over, wave breaking is seen clearly for different wave periods ranging from 1.5 sec to 2.0 sec.

(iv) From the comparison between experimentally measured water surface profiles with that of the model simulated values, it is seen that the measured data agree well with the model results with maximum ±20% deviation at some points.

(v) The comparison between experimentally measured wave breaking positions also agree well with model simulated wave breaking positions. Hence the adapted model can be used for submerged body of different heights exposed to various wave conditions.

5.2 Recommendations

Naturally any coastal protection work is exposed to continuous hitting by multidirectional random waves, where wind is one the most important driving force to control the wave height as well as to create turbulence in the free surface of water. In this study, the effectiveness of a rectangular fixed submerged body exposed to unidirectional regular waves in the reduction of wave height has been investigated both experimentally and numerically, where the contribution of wind force induced turbulence has not been considered. To overcome the limitations of the present study, the followings are recommended:

(i) Multi-directional random waves can be created from different wave generators simultaneously in a large wave basin.

(ii) Wind force induced turbulence can be included as an external force in both the physical model and the numerical model in future study. A turbulence model can be combined with the adapted numerical model to analyze the effect of turbulence from wind–water interaction as well as from breaking caused by the submerged body.

(iii) Artificial ditch in a flat sloped bottom can be modeled in the laboratory set-up to represent the undulated sandy coastline.

(iv) The wave interaction with submerged body of other shape like trapezoidal, stair-like stepped, vertical cylindrical, etc can be investigated.

(v) The wave interaction with porous submerged body can also be investigated by combining the porous body model with the numerical model based on SOLA-VOF scheme.

REFERENCES

- Al-Banna, K. and Liu, P. (2007). "Numerical study on the hydraulic performance of submerged porous breakwater under solitary wave attack". *Journal of Coastal Research*, Vol. 50, pp. 201-205.
- Ashgriz, N. and Poo, J.Y. (1991). "FLAIR: Flux Line-Segment Model for Advection and Interface Reconstruction," *J. Comput. Phys.* 93, pp. 449–468.
- Austin, D.I., Schlueter, R.S., (1982). "A numerical model of wave breaking/breakwater interactions," *Int. Proceedings 18th International Conference on Coastal Engineering*, Vol. 3. Cape Town, Republic of South Africa, pp. 2079–2096.
- Bhuiyan, M.A., Matin, M. A., "Coastal Zone Management", *Lecture notes*, Department of Water Resources Engineering , Bangladesh University of Engineering and Technology, Dhaka, Bangladesh.
- Brorsen, M and Larsen, J. (1987) "Source generation of nonlinear gravity waves with the boundary integral equation method," *Coastal Engineering*, Elsevier, Vol. 11, Amsterdam, pp. 93–113.
- Calabrese M., Buccino.M. and Pasanisi.F. (2007). "Qualitative and quantitative feature of wave breaking over a submerged breakwater and effects on non-linear wave-structure interaction", *Proceedings of 2nd International Conference on Marine Research and Transportation*, ICMRT '07, Italy.
- Cheng, S., Liu, S. and Zheng, Y. (2003) "Application Study on Submerged Breakwaters used for Coastal Protection," *Proceedings of International Conference on Estuaries and Coasts*, China.
- Chopra, A. and Greated, C.A. (1995). "Development and validation of the Volume of Fluid technique for water wave dynamics," *Proceedings of the 6th International symposium on Computational Fluid Dynamics*, NV, USA, pp. 212–217. Dean, R.J. and Dalrymple (2002), Coastal process with engineering applications, Cambridge University Press.

- Dean, R.J. and Dalrymple (2002), Coastal process with engineering applications, Cambridge University Press.
- Dick, T.M. and Brebner, A. (1968), "*Solid and permeable submerged breakwaters*"Proc. 11th. Conf. On Coastal Engineering, ASCE, New York, N.Y., II, 1141-1158.
- Golshani. A., Mizutani. N and Hur. D. S. (2003) "Three-dimensional Analysis of Non-linear Interaction between water waves and Vertical Permeable Breakwater", *Journal of Coastal Engineering*, World Sientific, Vol. 45, pp. 329-3451-28.
- Hales, L.Z. (1981). "Floating Breakwaters: State-of-the Art Literature Review," Technical Report No. 81-1, U.S. Army Corps of Engineers, Coastal Engineering Research Center, Fort Belvoir, Virginia.
- Hiew P.D., Katsutoshi.T. and Ca V.T. (2004). "Numerical simulation of breaking waves using a two-phase model", *Journal of applied Mathematical Modelling*, Elesvier, Vol 28, pp. 983-1005.
- Hinatsu, M. (1992). "Numerical simulation of unsteady viscous non-linear waves using moving grid system fitted on a free surface." *J. Kansai Soc. Naval Arch. Japan* 217: 1-11
- Hirt, C.W. and Nichols, B.D. (1981). "Volume of fluid (VOF) method for the dynamics of free boundaries," *J. Comp. Physics*, Vol. 39, pp. 201–225.
- Hur, D.S. (2004). "Deformation of Multi-directional Random waves passing over an impermeable Submerged Breakwater installed on Sloping bed", *Journal of Ocean Engineering*, Elsevier, Vol. 31, pp. 1295-1311.
- Hur, D.S. and Mizutani, N. (2003). "Numerical estimation of wave forces acting on a three-dimensional body on submerged breakwater", *Journal of Coastal Engineering*, Elsevier, Vol. 47, pp. 329-345.
- Hur, D.S., Kawashima. N. and Iwata. K. (2003). "Experimental study of the Breaking Limit of Multi-directional Random waves passing over an Impermeable Submerged Breakwater", *Journal of Ocean Engineering*, Sciencedirect, Vol. 30, pp. 1923-1940.

- Iwata, K., Kawasaki, K. and Kim, D. (1996). “Breaking limit, breaking and post-breaking wave deformation due to submerged structures” *Proceedings 25th International Conference on Coastal Engineering*, Vol. 3. Orlando, USA, pp. 2338–2351.
- Kawasaki, K., Iwata, K., “Wave breaking-induced dynamic pressure due to submerged breakwater,” Proceedings of the Eleventh (2001) International Offshore and Polar Conference, Stravanger, Norway, Vol. 3., pp. 488-493.
- Kothe, D.B., Ferrell, R.C., Turner, J.A., Mosso, S.J. (1997). “A high resolution finite volume method for efficient parallel simulation of casting processes on unstructured meshes,” Los Alamos National Laboratory Report LA-UR-97-30. In: Proceedings 8th SIAM Conference on Parallel Processing for Scientific Community. Minneapolis, MN, USA.
- Kothe, D.B., Mjolsness, R.C., Torrey, M.D. (1991). “RIPPLE: a computer program for incompressible flow with free surfaces,” Report LA-12007-MS, Los Alamos Scientific Report, Los Alamos, NM, USA.
- Lau, S.L, Ji Z. and Ng C.O., (1990). “Dynamics of Elastically Moored Floating Body by the 3-D Infinite Element Method,” *Journal of Ocean Engineering*, Elsevier Science, Vol. 17, Issue 5, pp. 499-516.
- Lee, C., Shen, M. and Huang, C. (2007). “Transformation of irregular waves propagating over a submerged breakwater”, *Proceedings of the 12th ISOPE Conference*.
- Lemos, C.M. (1992). “Wave breaking, a numerical study,” Lecture Notes in Engineering No. 71. Springer-Verlag, Berlin, Germany.
- Mizutani. M, Mostafa, A. M. and Iwata, K. (1998). “Non-linear Regular wave, Submerged Breakwater and Seabed Dynamic Interaction”, *Journal of Coastal Engineering*, Elsevier, Vol. 33, pp. 177-202.
- Petit, H.A.H., van den Bosch, P. (1992). “SKYLLA: wave motion in and on coastal structures. Numerical analysis of program modifications,” Delft Hydraulics Report H1351. Delft, The Netherlands.

- Ohyama, T. and Nadaoka, K. (1991). “Development of a numerical wave tank for analysis of nonlinear and irregular wave field.” *Fluid Dynamics Research* 8: 231-251
- Rufin, T.M., Mizutani. N. and Iwata. K. (1996) “Estimation method of Stable Weight of Spherical Armor unit of a Submerged Wide-crown Breakwater”, *Journal of Coastal Engineering*, Elsevier, Vol. 28, pp. 183-228.
- Rahman, M.A. (2005)**.** “Nonlinear Interaction and Dynamic Behavior of Moored Submerged Floating Breakwater under Wave Action", *Ph.D. Thesis, Nagoya University, Japan.*
- Sabeur, Z.A., Allsop, N.W.H., Beale, R.G., Dennis, J.M. (1996). “Wave dynamics at coastal structures: development of a numerical model for free surface flow,” *Proceedings 25th International Conference on Coastal Engineering*, Vol. 1. Orlando, USA, pp. 389–402.
- Sakakiyama, T. R. and Kajima, R. (1992). “Numerical simulation of nonlinear wave interacting with permeable breakwaters,” *Proc. 22nd Int. Conference on Coastal Engineering*, ASCE, Venice, pp. 1517–1530.
- Sen, D. (1993). “Numerical Simulation of Motions of Two-Dimensional Floating Bodies”, *Journal of Ship Research*, Vol. 37, No.4, pp. 307-330.
- Shirakura,Y., Tanizawa, K., Naito, S. (2000). “Development of 3-D Fully Nonlinear Wave Tank to Simulate Floating Bodies Interacting with Water Bodies,” *Proc. of the 10th ISOPE Conference*, Vol. III, pp. 253-262.
- Torrey, M.D., Cloutman, L.D., Mjolsness, R.C., Hirt, C.W. (1985). “NASA-VOF2D: a computer program for incompressible flows with free surfaces,” Report LA-10612-MS. Los Alamos Scientific Report, Los Alamos, NM, USA.
- Troch, P. (1997). “VOFbreak^2, a numerical model for simulation of wave interaction with rubble mound breakwaters,” *Proceedings 27th IAHR Congress*, San Francisco, USA, pp. 1366–1371.
- Van der Meer, J.W., Petit, H.A.H., van den Bosch, P., Klopman, G., Broekens, R.D. (1992). “Numerical simulation of wave motion on and in

coastal structures," *Proceedings 23rd International Conference on Coastal Engineering*, Vol. 2. Venice, Italy, pp. 1772–1784.

- Van Gent, M.R.A. (1995). "Wave interaction with permeable coastal structures," *PhD thesis*, Technical University Delft, Delft, The Netherlands. ISBN 90-407-1182-8.
- Van Gent, M.R.A., Tonjes, H.A.H. and van den Bosch, P (1994). "Wave Action on and in Permeable Structure," *Proc 24th ICCE, ASCE*, pp 1739-1753.
- Waller, M.N.H., Christakis N., Allsop N.W.H., Beale R.G., Dennis J.M. (1998). "Development and validation of a numerical model of wave dynamics," *Proceedings 17th International Conference on Offshore Mechanics and Arctic Engineering*, Lisbon, Portugal.
- Welch, J.E., Harlow, F.H., Shannon, J.P. and Daly, B.J. (1966). "The MAC method: a computing technique for solving viscous incompressible, transient fluid flow problems involving free surface," Report LA-3425, Los Alamos Scientific Report, Los Alamos, CA, USA.
- Wu, N. (1994). "Numerical simulation of breaking and non-braking wave kinematics at and on vertical structures," *PhD thesis*, Universität Hannover, Hannover, Germany.